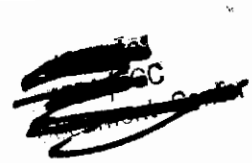

INVESTIGATION OF MEASURING SYSTEM REQUIREMENTS FOR LOW VISIBILITY LANDING

LEE GREGOR HOFMANN
WARREN F. CLEMENT
DUNSTAN GRAHAM
RICHARD E. BLODGETT
KISHOR V. SHAH

FOREWORD

The research reported here was accomplished for the United States Air Force by Systems Technology, Inc., Hawthorne, California, under Contract No. F33615-70-C-1621. The program was sponsored by the Air Force Flight Dynamics Laboratory, Air Force Systems Command, Wright-Patterson Air Force Base, Ohio, under Project No. 404L, Task No. 404L0101.

This research was conducted in support of the Air Force Advanced Landing System Program. This is a follow-on effort to the instrument low visibility approach analysis conducted under Contract No. F33615-69-C-1904 (Ref. 1).

The Air Force project engineer was Major James D. Dillow. Dunstan Graham served as the contractor's technical director and project engineer.

The research was performed during the period from May 1970 to September 1971. The manuscript was released by the authors in December 1971.

This technical report has been reviewed and is approved.

C. B. WESTBROOK
Chief, Control Criteria Branch
Flight Control Division
Air Force Flight Dynamics Laboratory

ABSTRACT

Two methods for determining measuring system requirements for instrument low visibility landing are described. These methods have been applied for analysis of two automatic landing systems using microwave scanning beam landing guidance. Results obtained from these analyses are presented and discussed in detail.

The first method is by means of a detailed time domain simulation which includes the airplane, its control system, the guidance system as well as atmospheric wind, windshear and turbulence inputs, and guidance system fluctuation noise. Application of this method is demonstrated with an automatic landing and rollout system and the DC-8 aircraft for the portion of the approach and landing from the Category II-B decision altitude to a ground rolling velocity of less than 50 ft/sec.

The second method is analytical. A linearized description of the measuring system, kinematics, airplane and its control system is used to investigate the influence of the atmospheric wind, and windshear inputs. Stochastic components of system responses arising from atmospheric turbulence inputs and guidance system fluctuation noise are then added to the deterministic responses to complete the model. Application of this method is demonstrated with a high performance automatic landing system and the CH-53A helicopter. The analysis is carried out in two stages. System performance in terms of delivering the aircraft within the approach "window" at the Category II-B decision altitude is first evaluated. Then the approach and landing from the Category II-B decision altitude is evaluated in terms of the touchdown footprint parameters for a decelerating, one-step flare landing maneuver.

CONTENTS

		Page
I.	INTRODUCTION.	1
	A. Purpose of the Investigation	1
	B. Outline of the Report: A Guide for the Reader	3
II.	TIME DOMAIN SIMULATION OF APPROACH AND LANDING FROM 100 FEET ALTITUDE	6
	A. Description of Automatic Landing System Simulation using the RCTA Recommended Signal Format for the Landing Guidance System	8
	B. DC-8 Aircraft, Landing Control System, and Measuring System Parameters and Initial Conditions	14
	C. Results from the Automatic Landing System Simulation . .	30
III.	ANALYSIS OF LANDING APPROACH TO THE DECISION ALTITUDE FOR A SINGLE ROTOR HELICOPTER REPRESENTATIVE OF A STOL AIRCRAFT . .	46
	A. Description of CH-53A, USAF Advanced Landing System, and Atmospheric Disturbance Models	49
	B. Summary of the Approach Coupler Designs and Performance .	70
	C. Approach Outcome Probabilities and Related Measures of Performance and Safety	92
IV.	ANALYSIS OF LANDING FROM THE DECISION ALTITUDE THROUGH FLARE AND TOUCHDOWN FOR A SINGLE ROTOR HELICOPTER REPRESENTATIVE OF A STOL AIRCRAFT.	96
	A. Description of the Model for the Decelerating Approach and One-Step Flare.	97
	B. Results of Exercising the Analytical Model for the Decelerating Approach and One-Step Flare	105
	C. Addition of Stochastic Input Effects.	123
V.	SUMMARY	130
	A. Positive Results	131
	B. Negative Results	132
	REFERENCES.	133

FIGURES

Page

1. System Analysis Support for Advanced Landing System Preliminary Design. 4
2. Block Diagram of the Digital Simulation Model of the Landing Analysis 9
3. General Siting Plan Configuration. 11
4. Longitudinal Geometry of Terminal Site 21
5. Extrapolation, Smoothing and Damping of Raw Sampled Measurements of Elevation and Azimuth Angles 22
6. Continuous Flare Computer Simulated using Finite Difference Approximation 24
7. Continuous Autothrottle and Thrust Retard Computer Simulated using Finite Difference Approximation 25
8. Continuous Lateral-Directional Coupler and Decrab Computer Simulated using Finite Difference Approximation 26
9. Relative Positions of Touchdown Points for the Worst-Case Combinations Studied 32
10. The Recommended Category II "Window". 50
11. Lateral-Directional SAS Block Diagram 63
12. Assumed Geometry for Measurement System Site (Long-Runway Case). 65
13. Automatic Flight Control System Conceptual Block Diagram for CH-53A Longitudinal Approach Control. 72
14. Actual and Equivalent Representations of Feedbacks to δ_{cc} for Advanced Design 74
15. Conceptual Lateral-Directional Coupler Design. 86
16. AFCS Localizer Coupler Mechanization. 87
17. Frequency Response Function for y/y_c. 89
18. Assumed Geometry of Glide Path and Measurement System Site; Short-Runway Case (All Dimensions Are Feet) 99
19. Modification to the Advanced Longitudinal Coupler for Execution of the Decelerating Approach and One-Step Flare 100
20. Ideal Geometric Approach and Flare Trajectory. 108

Page

21. Actual Approach and Flare Trajectory, Case 0 (Nominal) and Case 2 109

22. Actual Approach and Flare Trajectory, Case 1 (Low, Slow at Window; Decreasing Headwind) 111

23. Actual Approach and Flare Trajectory, Case 3 (High, Fast at Window; Decreasing Tailwind) 113

24. Lateral Approach Trajectory, Case 2 (Left of Runway ℄ at Window; Increasing Crosswind from Right) 114

25. Absolute Altitude Time Responses 117

26. Pitch Attitude Perturbation Response. 118

27. Airspeed Perturbation Response to the Deceleration Command and Wind Shears. 119

28. Absolute Lateral Deviation Response (Case 2) 120

29. Heading Response Exclusive of the Initial Crab Angle (Case 2) . 121

30. Bank Angle Response (Case 2) 122

TABLES

		Page
1.	Problems in Determining Probability Distribution of Parameters Pertinent to Performance at Touchdown	7
2.	Summary of DC-8 Characteristics Used in the Simulation.	15
3.	Equations for Raw Sampled Measurements of Elevation and Azimuth Angles	17
4.	Equations for Raw and Averaged DME Measurements	19
5.	Computations of Linear Glide Slope and Localizer Deviations and Altitude Above Runway.	20
6.	Atmospheric Disturbance Environment	29
7.	Purpose of Different Series of Runs	31
8.	Conditions for Various Cases	32
9.	Data Summary for Series A Runs.	33
10.	Data Summary for Series B Runs.	33
11.	Data Summary for Series C Runs.	34
12.	Data Summary for Series D Runs.	34
13.	Data Summary for Series E Runs.	34
14.	Data Summary for Series F Runs.	35
15.	Data Summary for Rollout End Conditions for Series A Runs.	35
16.	Comparison of Simulated and Computed Touchdown Coordinates, Trim Airspeed Adjusted by One-Half of Wind Speed	37
17.	Touchdown Footprint and Effect of Bug Speed Adjustment for Headwinds on Touchdown Footprint	40
18.	Deviation from Nominal at Touchdown Caused by Winds and Shears	45
19.	Deviation from Nominal at Touchdown Caused by Initial Offsets at the Decision Altitude.	45
20.	Longitudinal Airframe Dynamic Equations of Motion	51
21.	Lateral-Directional Airframe Dynamic Equations of Motion	52
22.	Effective Actuation and Rotor Lag Dynamics.	53

Page

23. SAS and Basic AFCS Transfer Functions Actually Installed on CH-53A. 53

24. CH-53A Longitudinal Dimensional Derivatives 55

25. CH-53A Lateral-Directional Dimensional Derivatives 56

26. CH-53A Longitudinal Manual Control Authorities 57

27. Working Control Authorities and Rate Limits for the CH-53A . . 57

28. Design Target Values for RMS $B_{1_{SAS}}$, $B_{1_{AFCS}}$, $\dot{B}_{1_{AFCS}}$, δ_c, $\dot{\delta}_c$ . . 58

29. CH-53A Longitudinal Transfer Function Factors at 60 Knots for Bare Aircraft plus Effective Actuation and Rotor Lags 60

30. CH-53A Lateral-Directional Transfer Function Factors at 60 Knots for Bare Aircraft plus Effective Actuation and Rotor Lags. . . 61

31. CH-53A Longitudinal Transfer Function at 60 Knots with Pitch SAS and Basic Pitch AFCS plus Effective Actuation and Rotor Lags. . 62

32. Summary of "Severe" Atmospheric Disturbances for Landing Approach 68

33. System Controller Transfer Functions for Straightforward Design. 73

34. System Controller Transfer Functions for Advanced Design . . . 73

35. System Performance in Terms of RMS Values for Straightforward Design. 76

36. Wind and Wind Shear Response for Straightforward Design at the Approach Window. 77

37. System Performance in Terms of RMS Values for Advanced Design . 83

38. Wind and Wind Shear Response for Advanced Design at the Approach Window. 84

39. System Controller Transfer Functions. 85

40. System Performance in Terms of RMS Values for Advanced Design . 90

41. Wind and Wind Shear Response for Advanced Design at the Approach Window. 91

42. Marginal Probabilities for Straightforward Design System . . . 93

43. Marginal Probabilities for Advanced Design System 93

Page

44. Approach Outcome Probabilities and Related Measures of Performance and Safety 95

45. Conditions for Cases Computed, Decelerating One-Step Flare in a Single Rotor Helicopter 106

46. Touchdown Coordinates. 107

47. CH-53A Landing Requirements (Ref. 20) 115

48. Longitudinal Touchdown Dispersions About the Mean 125

49. Joint Event Excess Fraction. 128

SYMBOLS

a	Azimuth angle for scenario in Fig. 12
a_y	Lateral acceleration at the center of gravity
a'_y	Lateral acceleration at a distance ℓ_x, ℓ_z from the c.g., $a'_y = a_y + \ell_x\dot{r} - \ell_z\dot{p}$
a_z	Normal acceleration at the center of gravity
a'_z	Normal acceleration at a distance ℓ_x from the c.g., $a'_z = a_z - \ell_x\dot{q}$
A_1	Lateral cyclic pitch
A^*_{1c}	A_1 command from AFCS
AR	Aspect ratio
AS	Airspeed
ASELIM	Limit on airspeed error feedback
AX	Extrapolated, smoothed and damped azimuth measurement
AZ	Measured azimuth at the time of scan illumination of the aircraft by the azimuth site
b	Wing span
b_{1cc}	Magnitude of input step command, B_{1cc}
B	Baseline distance between elevation site and GPIP in Fig. 12
B_1	Longitudinal cyclic pitch
B_{1cc}	Open-loop longitudinal cyclic pitch command for deceleration
BHLAG	Low-pass filtered absolute altitude derived from elevation site No. 2
c	Mean aerodynamic chord
c.g.	Center of gravity
C	Crosswind velocity
C_2	Complementary filter to G_c/s
CASE	Inertially compensated airspeed error

SYMBOLS (cont'd)

C_D	Drag coefficient, $D/\frac{1}{2}\rho U_o^2 S$
C_{D_α}	Drag coefficient variation with angle of attack, $\partial C_D/\partial\alpha$
$C_{D_{\alpha^2}}$	Drag coefficient variation with (angle of attack)^2, $\partial C_D/\partial\alpha^2$
$C_{D_{\alpha^3}}$	Drag coefficient variation with (angle of attack)^3, $\partial C_D/\partial\alpha^3$
C_{D_q}	Drag coefficient variation with pitch rate, $\partial C_D/\partial\left(\frac{qc}{2U_o}\right)$
C_{D_u}	Non-dimensional variation of C_D with speed; $U_o\partial C_D/2\,\partial U_o$
C_ℓ	Rolling moment coefficient, Roll Moment/$\frac{1}{2}\rho V_{T_o}^2 Sb$
C_{ℓ_β}	Dihedral parameter, variation of rolling moment coefficient with sideslip, $\partial C_\ell/\partial\beta$
$C_{\ell_{A_1}}$	Lateral cyclic pitch rolling effectiveness, $\partial C_\ell/\partial A_1$
$C_{\ell_{\delta_a}}$	Aileron rolling effectiveness, $\partial C_\ell/\partial\delta_a$
$C_{\ell_{\delta_r}}$	Rudder rolling effectiveness, $\partial C_\ell/\partial\delta_r$
$C_{\ell_{\delta_{sp}}}$	Spoiler rolling effectiveness, $\partial C_\ell/\partial\delta_{sp}$
C_{ℓ_p}	Roll damping coefficient $\partial C_\ell/\partial\left(\frac{pb}{2V_{T_o}}\right)$
C_{ℓ_r}	Roll coefficient due to yawing velocity, $\partial C_\ell/\partial\left(\frac{rb}{2V_{T_o}}\right)$
C_L	Lift coefficient, $nW/\frac{1}{2}\rho U_o^2 S$
C_{L_α}	Lift-curve slope, $\partial C_L/\partial\alpha$
$C_{L_{\alpha^2}}$	Lift coefficient variation with (angle of attack)^2, $\partial C_L/\partial\alpha^2$
$C_{L_{\alpha^3}}$	Lift coefficient variation with (angle of attack)^3, $\partial C_L/\partial\alpha^3$

SYMBOLS (cont'd)

$C_{L_{\alpha^4}}$	Lift coefficient variation with (angle of attack)^4, $\partial C_L/\partial\alpha^4$
$C_{L_{\dot{\alpha}}}$	$\partial C_L/\partial(\dot{\alpha}c/2U_o)$; unsteady lift coefficient due to rate of change of angle of attack
$C_{L_{i_H}}$	Horizontal tail incidence lift effectiveness, $\partial C_L/\partial i_H$
C_{L_δ}	Control-surface lift effectiveness, $\partial C_L/\partial\delta$
$C_{L_{B_1}}$	Longitudinal cyclic pitch lift effectiveness, $\partial C_L/\partial_{B_1}$
C_{L_q}	$\partial C_L/\partial(qC/2U_o)$; lift coefficient due to pitching velocity
C_{L_u}	Non-dimensional variation of C_L with speed, $U_o\partial C_L/2\partial U_o$
C_M	Pitching moment coefficient, Pitching Moment/$\frac{1}{2}\rho U_o^2 Sc$
C_{M_α}	Variation of C_M with angle of attack; $\partial C_M/\partial\alpha$
$C_{M_{\alpha^2}}$	$\partial C_M/\partial\alpha^2$
$C_{M_{\dot{\alpha}}}$	$\partial C_M/\partial\left(\frac{\dot{\alpha}c}{2U_o}\right)$; $U_o C_{M_{\dot{w}}}$
$C_{M_{i_H}}$	Horizontal tail incidence pitch effectiveness; $\partial C_M/\partial i_H$
C_{M_δ}	Control-surface pitch effectiveness, $\partial C_M/\partial\delta$
$C_{M_{B_1}}$	Longitudinal cyclic pitch pitch effectiveness, $\partial C_M/\partial B_1$
C_{M_q}	Pitch damping coefficient, $\partial C_M/\partial\left(\frac{qc}{2U_o}\right)$
C_{M_u}	$U_o\partial C_M/2\partial U_o$
C_n	Yawing moment coefficient, Yawing Moment/$\frac{1}{2}\rho V_{T_o}^2 Sb$
C_{n_β}	Static directional stability, $\partial C_n/\partial\beta$

SYMBOLS (cont'd)

$C_{n_{A_1}}$	Lateral cyclic pitch yawing effectiveness, $\partial C_n/\partial A_1$
$C_{n_{\delta_a}}$	Aileron yawing effectiveness, $\partial C_n/\partial \delta_a$
$C_{n_{\delta_r}}$	Rudder yawing effectiveness, $\partial C_n/\partial \delta_r$
$C_{n_{\delta_{sp}}}$	Spoiler yawing effectiveness, $\partial C_n/\partial \delta_{sp}$
C_{n_p}	Yaw coefficient due to rolling velocity, $\partial C_n/\partial\left(\frac{pb}{2V_{T_o}}\right)$
C_{n_r}	$\partial C_n/\partial\left(\frac{rb}{2V_{T_o}}\right)$
C_y	Lateral force coefficient, Lateral Force$/\frac{1}{2}\rho V_{T_o}^2 S$
C_{y_β}	Variation of C_y with sideslip angle, $\partial C_y/\partial \beta$
$C_{y_{A_1}}$	Lateral cyclic pitch side-force effectiveness $\partial C_y/\partial A_1$
$C_{y_{\delta_r}}$	Rudder side-force effectiveness, $\partial C_y/\partial \delta_r$
$C_{y_{\delta_{sp}}}$	Spoiler side-force effectiveness, $\partial C_y/\partial \delta_{sp}$
C_{y_p}	Side-force coefficient due to rolling velocity; $\partial C_y/\partial\left(\frac{pb}{2V_{T_o}}\right)$
C_{y_r}	Side-force coefficient due to yawing velocity; $\partial C_y/\partial\left(\frac{rb}{2V_{T_o}}\right)$
d	Displacement normal to the glide slope in a vertical plane containing the glide slope
d_{cc}	Effective command for following final segment of a two-segment reference glide plane
dt	Time differential
D	Drag

SYMBOLS (cont'd)

DTDB	Normalized total thrust retard increment desired between flare altitude and touchdown
EL(·)	Measured angular elevation at the time of scan illumination of the aircraft by site No. (·)
EL(·)X	Extrapolated, smoothed and damped elevation measurement from site No. (·)
EL1SE	First rearward difference on EL1
EL1SED	Scaled first rearward difference on EL1SE
EL1XS	Value of EL1X at sample (scan illumination) instants
f	Elevation angle as determined from GPIP in Fig. 12
F(Z)	Probability distribution function for Z
g	Gravitational acceleration; elevation angle in Fig. 12
G, G(s)	Controller transfer function, often particularized by a subscript
GSC	Glide slope command, i.e. selected approach path reference angle
GSDE	Inferentially measured linear displacement of the aircraft antenna from the reference glide plane
h	Altitude perturbation; total altitude in sense designated by subscript when present
H	Headwind velocity
HABSE	Inferentially measured absolute altitude of the aircraft antenna above the horizontal plane through site No. 2
i_H	Incidence of horizontal tail
I_x, I_y, I_z	Moments of inertia referred to body axes
I_{xz}	Product of inertia referred to body axes
j	$\sqrt{-1}$
jω	The imaginary portion of the complex variable $s = \sigma \pm j\omega$
k	Gain, often particularized by a subscript
K	Gain, often particularized by a subscript

ℓ_x	Distance along the X axis from the c.g., positive forward
ℓ_z	Distance along the Z axis from the c.g., positive down
L	Rolling acceleration due to externally applied torques; integral scale length of homogeneous isotropic atmospheric turbulence, often particularized by a subscript
LATDE	Inferentially measured linear displacement of the aircraft antenna from the vertical reference plane through the runway centerline
LOC	Localizer
L_β	$\rho S V_{T_o}^2 b\, C_{\ell_\beta}/2I_x$ in dimensional units of $(\text{time})^{-2}$
L_δ	$\rho S V_{T_o}^2 b\, C_{\ell_\delta}/2I_x$ in dimensional units of $(\text{time})^{-2}$
L_p	$\rho S V_{T_o} b^2 C_{\ell_p}/4I_x$ in dimensional units of $(\text{time})^{-1}$
L_{A_1}	$\rho S V_{T_o}^2 b\, C_{\ell_{A_1}}/2I_x$ in dimensional units of $(\text{time})^{-2}$
L_r	$\rho S V_{T_o} b^2 C_{\ell_r}/4I_x$ in dimensional units of $(\text{time})^{-1}$
L_v	L_β/V_{T_o} in dimensional units of $(\text{time})^{-1}(\text{length})^{-1}$
L_i'	$\dfrac{L_i + \dfrac{I_{xz}}{I_x} N_i}{1 - \dfrac{I_{xz}^2}{I_x I_z}}$ where i refers to any motion, or input, quantity
m	Mass
M	Pitching acceleration due to externally applied torques
M_α	$U_o M_w$ in dimensional units of $(\text{time})^{-2}$
$M_{\dot\alpha}$	$U_o M_{\dot w}$ in dimensional units of $(\text{time})^{-1}$
M_δ	$\rho S U_o^2 c\, C_{M_\delta}/2I_y$ in dimensional units of $(\text{time})^{-2}$

SYMBOLS (cont'd)

M_{B_1}	$\rho S U_o^2 c\, C_{M_{B_1}}/2I_y$ in dimensional units of $(\text{time})^{-2}$
M_q	$\rho S U_o c^2 C_{M_q}/4I_y$ in dimensional units of $(\text{time})^{-1}$
M_u	$\rho S U_o c\,(C_M + C_{M_u})/I_y$ in dimensional units of $(\text{time})^{-1}$
M_w	$\rho S U_o c\, C_{M_\alpha}/2I_y$ in dimensional units of $(\text{time})^{-1}(\text{length})^{-1}$
$M_{\dot{w}}$	$\rho S c^2\, C_{M_{\dot\alpha}}/4I_y$ in dimensional units of $(\text{length})^{-1}$
n	Noise input to the measuring system particularized by a subscript; also vertical load factor
N	Yawing acceleration due to externally applied torques
N_{TD}	Expected number of occurrences per second of the joint event; $h_{abs} = 0$, $\dot{h}_{abs} < 0$.
N_β	$\rho S V_{T_o}^2 b\, C_{n_\beta}/2I_z$ in dimensional units of $(\text{time})^{-2}$
N_{A_1}	$\rho S V_{T_o}^2 b\, C_{n_{A_1}}/2I_z$ in dimensional units of $(\text{time})^{-2}$
N_δ	$\rho S V_{T_o}^2 b\, C_{n_\delta}/2I_z$ in dimensional units of $(\text{time})^{-2}$
$N_u^y(s)$	Directly controlled airframe motion quantity, y/control deflection, u, transfer function numerator
$N_{u_1u_2}^{y_1y_2}$	$\left(N_{u_1}^{y_1}N_{u_2}^{y_2} - N_{u_2}^{y_1}N_{u_1}^{y_2}\right)\Delta^{-1}$ important multivariable control identity
N_p	$\rho S V_{T_o} b^2\, C_{n_p}/4I_z$ in dimensional units of $(\text{time})^{-1}$
N_r	$\rho S V_{T_o} b^2\, C_{n_r}/4I_z$ in dimensional units of $(\text{time})^{-1}$
N_v	N_β/V_{T_o} in dimensional units of $(\text{time})^{-1}(\text{length})^{-1}$
N_i'	$\dfrac{N_i + L_i I_{xz}/I_z}{1 - I_{xz}^2/I_x I_z}$, where i refers to any motion, or input, quantity
p	Roll rate, angular velocity about the X axis, positive right wing going down

P_D	Probability of the pilot's making the correct decision to discontinue the approach, given that he did not attain the window
PHDCM	Complementary filtered vertical velocity based on elevation site No. 2, inertial velocity and normal acceleration
P_{MA}	Probability of a missed approach on any given approach
P_W	Probability of <u>not</u> attaining the window on any given approach
q	Pitch rate, angular velocity about the Y axis, positive nose going up; dynamic pressure, $\rho U_o^2/2$ or $\rho V_{T_o}^2/2$
r	Yaw rate, angular velocity about the Z axis, positive nose going right
r*	$r \cos \alpha_G + p \sin \alpha_G$
R	Range or distance, often particularized by a subscript; also wind shear rate with respect to altitude
RM1	Raw measurement of slant range to elevation site No. 1
RM1AV	Averaged DME measurement with respect to site No. 1
RM2	Derived slant range to elevation site No. 2
RMAAV	Averaged DME measurement with respect to the azimuth site
RS1	True slant range to elevation site No. 1 at instant of DME interrogation reply
RSA	Time slant range to azimuth site at instant of DME interrogation reply
s	Laplace operator, $\sigma + j\omega$, a complex variable
S	Wing area; wind increment arising from wind shear
SCAPSI	Nondimensional scale factor used in the rudder steering path at and after decrab
SPHDCM	Unfiltered PHDCM
SYFD	Component of complementary filtered linear lateral deviation rate, $\dot{y}_{fb}$

t	Time; specific times particularized by subscript
$1/T_{(\cdot)}$	Inverse time constant particularized by the subscript, $(\cdot)$
T	Thrust; runway threshold coordinate; time "constant" particularized by a subscript
TAZ	T_{S1}
TCLIM	Limit on thrust increment command
TCRLM	Limit on rate of change of thrust increment command
THCLIM	Limit on pitch attitude command
THCRLM	Limit on rate of change of pitch attitude command
T_I	Lag time "constant" often particularized by a subscript
T_L	Lead time "constant" often particularized by a subscript
T_{S1}	Approximate constant time interval between successive scan illuminations from elevation site No. 1 and from the azimuth site
T_{S2}	Approximate constant time interval between successive scan illuminations from elevation site No. 2
TSU1	T_{S1}
TS2EL	Approximately T_{S2}
u	Linear perturbed velocity along the X axis
U_o	Linear steady state velocity along the X axis
v	Linear perturbed velocity along the Y axis
V_o	Linear steady state velocity along the Y axis
V_T	Total true airspeed
V_{T_o}	Total steady state true airspeed
w	Linear perturbed velocity along the Z axis; also a complex variable
W	Weight

SYMBOLS (cont'd)

W_o	Linear steady state velocity along the Z axis
X	Forward acceleration, along the X axis
X_E	Actual longitudinal touchdown coordinate with respect to nominal point
X_α	$U_o X_w$; $\rho S U_o^2 (C_L - C_{D_\alpha})/2m$ in dimensional units of (length)(time)$^{-2}$
X_{B_1}	$\rho S U_o^2 (-C_{D_{B_1}})/2m$ in dimensional units of (length)(time)$^{-2}$
X_δ	$\rho S U_o^2 (-C_{D_\delta})/2m$ in dimensional units of (length)(time)$^{-2}$
X_q	$\rho S U_o c (-C_{D_q})/4m$ in dimensional units of (length)(time)$^{-1}$
X_{TD}	Longitudinal coordinate of actual touchdown point with respect to nominal touchdown point
X_u	$\rho S U_o (-C_D - C_{D_u})/m$ in dimensional units of (time)$^{-1}$
X_w	$\rho S U_o (C_L - C_{D_\alpha})/2m$ in dimensional units of (time)$^{-1}$
X_{np}	Fuselage station of the neutral point
y	Lateral deviation from a vertical plane through the runway centerline
Y	Side acceleration, along the Y axis
YBKKY	$K\bar{y}/Ky$
Y_β	$V_{T_o} Y_v$ in dimensional units of (length)(time)$^{-2}$
Y_{A_1}	$\rho S V_{T_o}^2 C_{y_{A_1}}/2m$ in dimensional units of (length)(time)$^{-2}$
Y_δ	$\rho S V_{T_o}^2 C_{y_\delta}/2m$ in dimensional units of (length)(time)$^{-2}$
$Y^*_{(\cdot)}$	$Y_{(\cdot)}/V_{T_o}$ in dimensional units of (time)$^{-1}$
Y_p	$\rho S V_{T_o} b\, C_{y_p}/4m$ in dimensional units of (length)(time)$^{-1}$

SYMBOLS (cont'd)

Y_r	$\rho S V_{T_o} b\, C_{y_r}/4m$ in dimensional units of (length)(time)$^{-1}$
Y_v	$\rho S V_{T_o} C_{y_\beta}/2m$ in dimensional units of (time)$^{-1}$
Z_j	Perpendicular distance from the cg to the thrust line (positive for a nose-up pitching moment due to thrust)
Z	Vertical acceleration along the Z axis
Z_α	$U_o Z_w$ in dimensional units of (length)(time)$^{-2}$
Z_{B_1}	$\rho S U_o^2 (-C_{L_{B_1}})/2m$ in dimensional units of (length)(time)$^{-2}$
Z_δ	$\rho S U_o^2 (-C_{L_\delta})/2m$ in dimensional units of (length)(time)$^{-2}$
Z_q	$\rho S U_o c(-C_{L_q})/4m$ in dimensional units of (length)(time)$^{-1}$
Z_u	$\rho S U_o(-C_L - C_{L_u})/m$ in dimensional units of (time)$^{-1}$
Z_w	$\rho S U_o(-C_{L_\alpha} - C_D)/2m$ in dimensional units of (time)$^{-1}$
$Z_{\dot{w}}$	$\rho S c(-C_{L_{\dot{\alpha}}})/4m$, dimensionless
α	Instantaneous angle of attack, w/U_o under no wind conditions
α_G	Gyro tilt angle measured from the X axis in the X-Z plane, positive up.
α_o	Angle of attack of body axis
β	Sideslip angle, v/V_{T_o} under no wind conditions
γ	Perturbed flight path angle, $\theta - \alpha$
γ_o	Steady state flight path angle
Γ_o	Nominal glide slope elevation angle
δ	Control surface deflection, particularized by subscript; also used as an incremental prefix
δ_c	Collective pitch of main rotor
δ^*_{cc}	Collective pitch command upstream of the airspeed crossfeed summing junction

SYMBOLS (cont'd)

δ_F	Flap deflection angle
Δ	Incremental prefix; also $\Delta(s)$
$\Delta(s)$	Demoninator of airframe transfer functions; characteristic equation when set equal to zero
ΔT_c	Limit on thrust increment command
ζ, ζ_i	Damping ratio of linear second order system particularized by the subscript
θ	Pitch angle, $\int q\, dt$ in straight and level flight
θ_o	Steady state pitch angle of the X axis with respect to the horizontal direction
Θ	Total pitch angle
λ	Lateral course angle of the aircraft in the glide slope plane; mixing constant for complementary filtering when particularized by a subscript
μ_{x_o}	Unperturbed advance ratio in X direction
ξ_o	Inclination of the thrust line with respect to the X axis in the plane of symmetry (positive for negative Z force)
ρ	Mass density of air
$\rho(\cdot)$	Probability density function for $(\cdot)$
ρ_o	Mass density of air at sea level
σ	Standard deviation of a stochastic variable, often particularized by a subscript; the real portion of the complex variable $s = \sigma \pm j\omega$
φ	Roll angle, $(\cos \gamma_o \int p\, dt - \sin \gamma_o \int r\, dt)$ in rectilinear flight
Φ	Total bank angle
$\Phi(\omega)$	Power spectral density, often particularized by a subscript
Ψ	Perturbed heading angle of the X axis with respect to its trimmed value

Ψ	Total heading angle with respect to earth-fixed reference
ω_i	Undamped natural frequency of a second order mode; break frequency of a first order mode particularized by the subscript
ω	Circular frequency in dimensions $(\text{rad})(\text{time})^{-1}$
Ω, Ω_1, Ω_2	Reference angles for two-segment approach path in Fig. 18

Subscripts

a	Aileron; accelerometer; actuator
a_y	Lateral acceleration related
a_z	Normal acceleration related
abs	Absolute (altitude)
A	With respect to moving air mass
AFCS	Automatic flight control system
AS	Airspeed
AZ, a	Azimuth measurement related
bar	Barometric
BW	Bandwidth
c	Command value
c_3	Command after passage of decision altitude
ca	Command for aileron channel
cff	Computed feedforward command
cr	Command for rudder channel
CAS	Compensated airspeed related
CL	Command value before limiting
d	Glide slope displacement
D	Decision altitude

SYMBOLS (cont'd)

DC	Decrab
e	Error; effective value; engine thrust related; pitch control, e.g., elevator
E	Referenced to earth-fixed runway oriented coordinates
EL, g, f	Elevation measurement related
f	Feedback
fb, fba	Compensated feedbackto ailerons
fbr	Compensated feedback to rudder
F	Flap, flare altitude, flare related
FL	Flare and landing related
g	Atmospheric gust, when affixed to u, v, w, p, q, r, in particular, denotes corresponding component of air mass velocity
h	Altitude related
I	Integral or lag related
L	Lead related
MAX	Maximum or peak value
o	Unperturbed value
P	MLS receiver antenna station or other body station for inertial sensors
s	Wind shear
SAS	Stability augmentation system
SM	Smoothed value from measuring system
TD	Touchdown
TDC	Touchdown command
w	Wind
wo	Washout
y	Lateral deviation related

θ	Pitch attitude related

Special Notation

Ant	Antenna
AZ	Azimuth
CW	Steady crosswind from left case
CW + S	Increasing crosswind from left case
CW - S	Decreasing crosswind from left case
DME	Distance measuring equipment
EL	Elevation
GPIP	Glide path initial point
GS	Glide slope
$\mathcal{L}[\cdot]$	Inverse Laplace transform of $[\cdot]$
LOC	Localizer
S	Wind velocity component due to shear, positive for tailwind or crosswind from left.
Tx	Transmitter
W_H	Steady headwind case
W_H + S	Decreasing headwind case
W_H - S	Increasing headwind case
W_T	Steady tailwind case
W_T + S	Increasing tailwind case
W_T - S	Decreasing tailwind case
$(\cdot)'$	$(\cdot)$ quantity measured at an off c.g. location; $(\cdot)$ quantity filtered;

Mathematical Symbols

(λ)	Real factor $(s + \lambda)$ of a polynomial in s

$[\zeta; \omega]$	Quadratic factor $[s^2 + 2\zeta\omega s + \omega^2]$ of a polynomial in s
$<$	Less than
$>$	Greater than
$\leq$	Less than or equal to
$\geq$	Greater than or equal to
$<<$	Much less than
$>>$	Much greater than
$\neq$	Not equal to
$\doteq$	Approaches; approximately equal to
$\equiv$	Identically equal to
$\rightarrow$	Fed to; approaches
$\cdot$	(Raised period) d/dt
$\cdot\cdot$	(Dieresis) d^2/dt^2
d	Differential operator
e	Naperian base, 2.71828 ...
E[·]	Expectation operator on [·]
∂	Partial differential operator
$(\cdot)'$	Partial derivative of quantity, (·), with respect to its explicit argument
$\int$	Integration operator
Σ	Summation operator
$\sqrt{\ }$	Square root operator
j,	$\sqrt{-1}$
π	3.14159 ...
lim	limit of ...

SECTION I

INTRODUCTION

This report presents the results of an investigation of measuring system requirements for instrument landing. It demonstrates the application of a general dynamic system model for aircraft landing operations so as to compute mathematical measures of performance, safety, and pilot acceptance which are appropriate to the determination of the requisite characteristics of the measuring system. (As distinct from the control system, the measuring system is here understood to comprise those elements of the landing guidance and control system which determine translational aircraft motion variables in earth-fixed coordinates.)

A. PURPOSE OF THE INVESTIGATION

The United States Air Force has underway a program for the development of an advanced landing system whose ultimate performance goal is to provide guidance information for zero visibility letdown, approach, go-around, flare, touchdown, roll-out, take-off and climb out. The system will ultimately be used for all types of USAF aircraft (from VTOL to large supersonic) and at all types of bases from forward and combat operating bases to main permanent bases. Furthermore, it is intended that the development should be coordinated with national efforts to define a standardized replacement for the existing instrument low-approach system (i.e., the work of the Radio Technical Commission for Aeronautics Special Committee 117).

While there have already been a number of "system" studies of advanced landing systems, these have typically been primarily concerned with the characteristics of the ground-based equipment, and have, by and large, failed to address themselves directly to the question of the requirements and/or limitations which may be imposed on the measuring subsystem by the dynamics of the aircraft and their control subsystems, in response to commands and disturbances. Indeed, the whole question of what constitutes "successful" system performance may be a matter of debate, yet it is precisely at this point where we must

begin, if we wish to distribute the error budget and to rationally determine specifications for subsystem and component performance.

The overall landing system includes many elements: ground-based landing aids; airborne guidance equipment; communication, navigation, and identification channels; the aircraft; the flight control system; pilot (and flight crew); displays, etc. Performance of the overall landing system depends on the interaction among these components. Because of the tremendous variety of aircraft and control system dynamics, piloting techniques, manual or automatic flight operations, environmental conditions, and so forth which may be involved, the overall landing system in which the Air Force advanced landing system is to play a part is enormously complex and varied. Generally, however, we may divide the system into two principal functional parts, the measuring system, and the control system.

The measuring system performs both sensing and guidance functions as needed to determine the course to be followed by the aircraft. The control system utilizes this guidance information to determine, develop, and apply appropriate forces and moments to the aircraft to execute the guidance commands. The measuring system is used to make such outer-loop and/or low frequency measurements as position, altitude, glide path, distance, range rate, and flight path angle, using equipment which may fall into the categories of ground-based landing aids, airborne guidance equipment or ICNI (Integrated Communication Navigation and Identification) gear. In this separation of functions and equipment the control system would include the aircraft, the flight control system, pilot, and displays.

As a practical matter, however, the advanced landing system is essentially the measuring system as defined above. To determine meaningful, detailed performance specifications for the measuring system requires an allotment of the total system errors and a reflection of the overall system performance into the measuring and control subsystems. To accomplish this actually requires a detailed quantitative appreciation of the relationships between subsystem and overall system performance; but this is not presently available. Consequently, a need exists for orderly procedures to analyze subsystem requirements based upon specified overall landing system requirements. This leads to the essential purpose of the investigation reported here.

If this purpose is accomplished, it will be possible to analyze the effects of changes and interplay among the various elements in the total landing system. From the appreciation and understanding gained thereby, requirements can be established for the characteristics of the ground-based signals and their conversion to airborne control commands. This is a key item of system analysis support for preliminary design of an advanced landing system. It is, however, only one element of several leading to the development of performance specifications. As illustrated in Fig. 1, the investigation reported here covers the first block and a portion of the second with respect to the landing process. From the "Landing System and Subsystem Analysis Techniques" development the outputs are "Procedures" and "Measures." The "Procedures" cover system and subsystem analyses leading to estimates of measures for system and subsystem performance, safety, and pilot acceptance.

B. OUTLINE OF THE REPORT: A GUIDE FOR THE READER

At the outset of this investigation, it was thought that very likely believable results with respect to landing system requirements could only be established in the first instance by means of detailed digital simulation. It was further thought that aircraft with a high lift curve slope and/or direct lift control (e.g., STOL aircraft) might present unique requirements for the characteristics of the landing guidance system. Finally, it was recognized that the large costs inherent in the attempt to collect statistics such as the dispersion of touchdown points by running a digital simulation made an analytical approach attractive even if this were only approximate. For these three reasons, as will be made clear, the investigation was organized into three related but distinct tasks. These are described in the next three technical sections which follow.

This report describes the methods of analysis briefly and presents example problems together with some detailed solutions. Conclusions are presented on the basis of these analyses and solutions. Details of the methods used are presented in Refs. 1 and 3.

Section II treats the digital simulation of the landing of a DC8-60 transport aircraft with an advanced automatic flight control system with windproofing features. The main features of the simulation are described, as

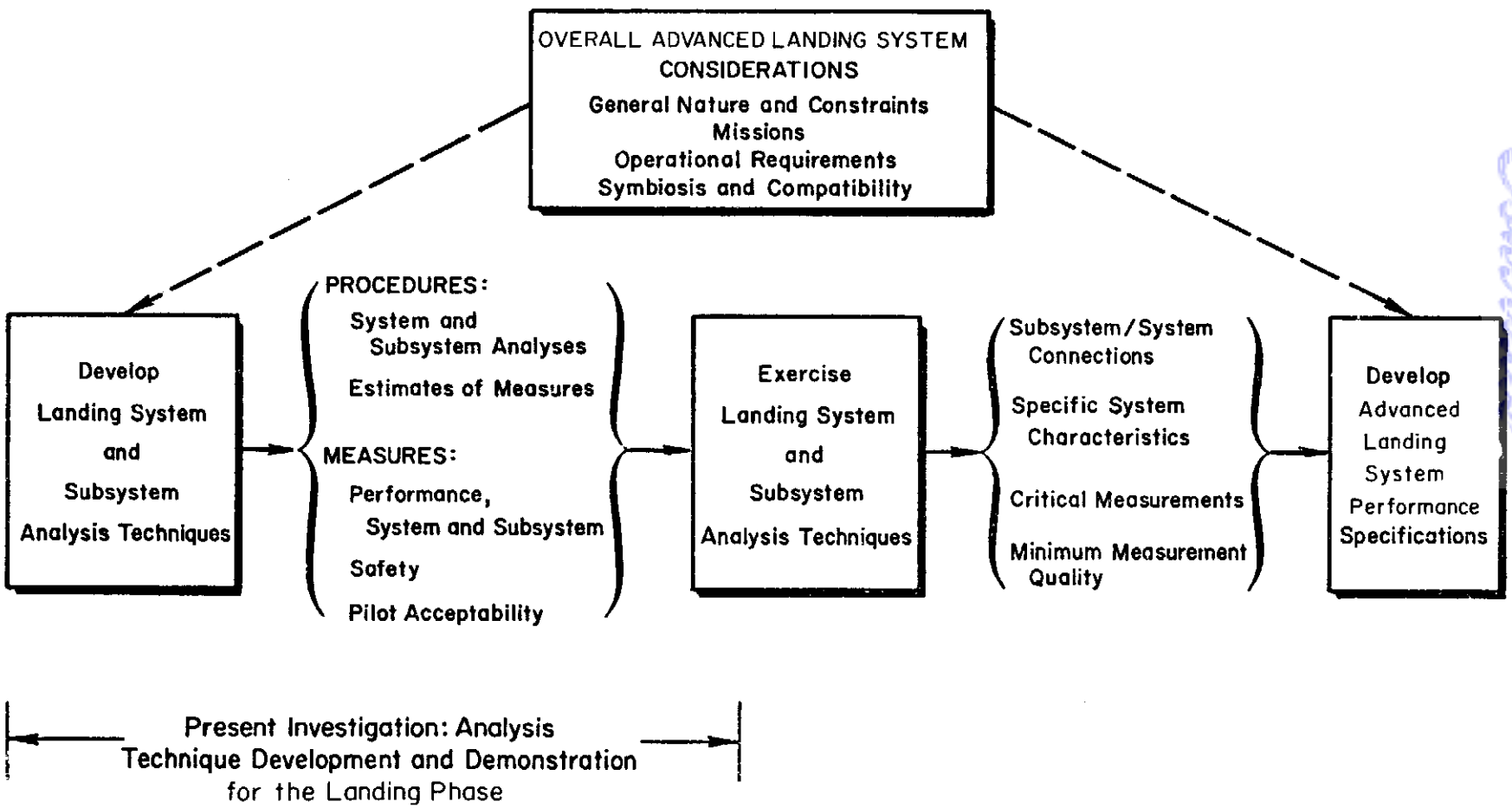

Figure 1. System Analysis Support for Advanced Landing System Preliminary Design

are the aircraft, its control system, and the measuring system. The results of a limited number of simulation runs with systematic variations in the initial conditions at the decision altitude and designed with a view toward displaying the effect of gusts and radio noise are presented to conclude Section II.

The next section, Section III, comprises an analysis of the performance of a single rotor helicopter on an approach to a decision altitude of 100 ft. The analysis here parallels the one presented in Ref. 1, but it is made in connection with an aircraft which has both a high lift curve slope and direct lift control, and which may, therefore, be considered to be representative of a whole class of STOL vehicles.

A third technical section, Section IV, is concerned with the analysis of deceleration, flare, and landing for the same single rotor helicopter treated in Section III. It presents a method which may be used to calculate landing statistics by an approximate method.

Finally, the report is concluded with a brief summary and a statement of both positive and negative results.

SECTION II

TIME DOMAIN SIMULATION OF APPROACH AND LANDING FROM 100 FEET ALTITUDE

The landing process, although more or less continuous, is for purposes of analysis and control usually considered to consist of three separate phases. These include, in chronological order, the approach-glide, the flare, and the ground roll. The terminal conditions of each segment form the initial conditions for the following segment.

A probabilistic method for analyzing the terminal conditions in the approach phase has been developed for the Air Force Flight Dynamics Laboratory in Ref. 1. This method characterizes measures of performance, safety and pilot acceptance in terms of an approach "window" at the Category II-B decision height, 100 ft. Results previously obtained by applying this method of analysis to the approach form initial conditions for investigating measuring system requirements for low visibility (Category III) landing flare, touchdown and ground roll by means of the simulation described here.

Case-by-case simulation in the time domain may be a virtual necessity for any reasonably detailed investigation of the landing flare, touchdown and ground roll processes. This is because of mathematical problems encountered in carrying the approach calculations through to touchdown and rollout when this is attempted directly in terms of a statistical model. The basic cause is that the statistical distributions of the problem variables are not Gaussian, and appropriate distributions are not known. A brief resume of sources contributing to this situation is given in Table 1.

In order to cope with the realities of non-Gaussian probability distributions at touchdown and through the rollout, the flare, touchdown and rollout have been simulated in the time domain. Two user options have been incorporated with the simulation program:

1. Probability estimation may be carried out using the "histograms" of landing metrics after simulation of a sufficiently large number of landings from initial conditions at the Category II-B

TABLE 1

PROBLEMS IN DETERMINING PROBABILITY DISTRIBUTION
OF PARAMETERS PERTINENT TO PERFORMANCE AT TOUCHDOWN

PARAMETER	FACTORS THAT MAKE DISTRIBUTION NON-GAUSSIAN	COMMENTS
$\dot{h}_{TD}$	$\dot{h} > 0$ is impossible at instant of touchdown because runway must be approached from above.	When sink rate is large, then the probability of touchdown occurring is large. A Pearson Type 3 or log Gaussian distribution might be appropriate for this situation.
x_{TD}	x_{TD} is related to gust inputs in a nonlinear manner, producing a skewed distribution of touchdown points. $x_{TD} = f(d)$. PDF(d) is "clipped" at window, producing a flat-topped (platykurtic) PDF(x_{TD}).	Because the nonlinear effects on x_{TD} are smallest for short landings, it may be possible to obtain reasonable approximations in spite of the mathematical complications. Log Gaussian might be appropriate for PDF(x_{TD}).
Total runway used in stopping airplane	x_{TD} is not Gaussian.	"Long landings" depend on x_{TD} and u_{TD}.
y_{TD}	Tails of distribution are "clipped" at window, and time from window to touchdown is insufficient to re-establish full Gaussian distribution. PDF(y_{TD}) is flat-topped (platykurtic)	When distribution at window is combined with dispersions generated after the window it may turn out that even a small σ_y generated after the window will cause a large accident potential.
φ_{TD}	Is probably Gaussian.	
v_{TD}	Is probably Gaussian.	
Minimum distance from runway edge during rollout	Tails of y distribution are clipped at window.	This parameter depends on y_{TD} and ψ_{TD}.

"window" in the presence of stochastic and deterministic atmospheric disturbances and measuring system noise. A reasonably high level of confidence using this first option may, however, require a very large number of simulation runs.

2. Probability estimation may be carried out using inferred distributions of landing metrics after simulation to estimate modes, medians, means, covariances, standard deviations and correlation coefficients. There are two aspects of the second option to be demonstrated.

   a. Simulation of a limited number of landings from initial conditions within the Category II-B window in the presence of only deterministic atmospheric disturbances to estimate modes of the distributions of landing metrics.

   b. Simulation of a limited number of landings from initial conditions on the boundaries of the Category II-B window in the presence of only deterministic atmospheric disturbances to estimate medians of distributions of landing metrics. (In particular, the mean of the two extreme observations is a remarkably better estimate of the median of an unknown probability distribution than the sample median of a collection which is interior with respect to the extreme observations. See Ref. 2.)

The next three subsections proceed, in turn, to present an overall description of the automatic landing system simulation; specific descriptions of the DC-8 aircraft, the terminal site and airborne portions of the measuring system, the landing control subsystem and the winds, windshears and stochastic gusts actually simulated; and a summary of the simulation results which were obtained.

A. DESCRIPTION OF AUTOMATIC LANDING SYSTEM SIMULATION USING THE RCTA RECOMMENDED SIGNAL FORMAT FOR THE LANDING GUIDANCE SYSTEM

The automatic landing system simulation uses a digital computer program prepared in Fortran II. Full consideration has been given to modeling time-varying and nonlinear aspects of system behavior. Complete documentation of this simulation will be contained in a forthcoming companion report, Ref. 3.

Figure 2 shows the main subprograms of the simulation in block diagram form. These consist of the:

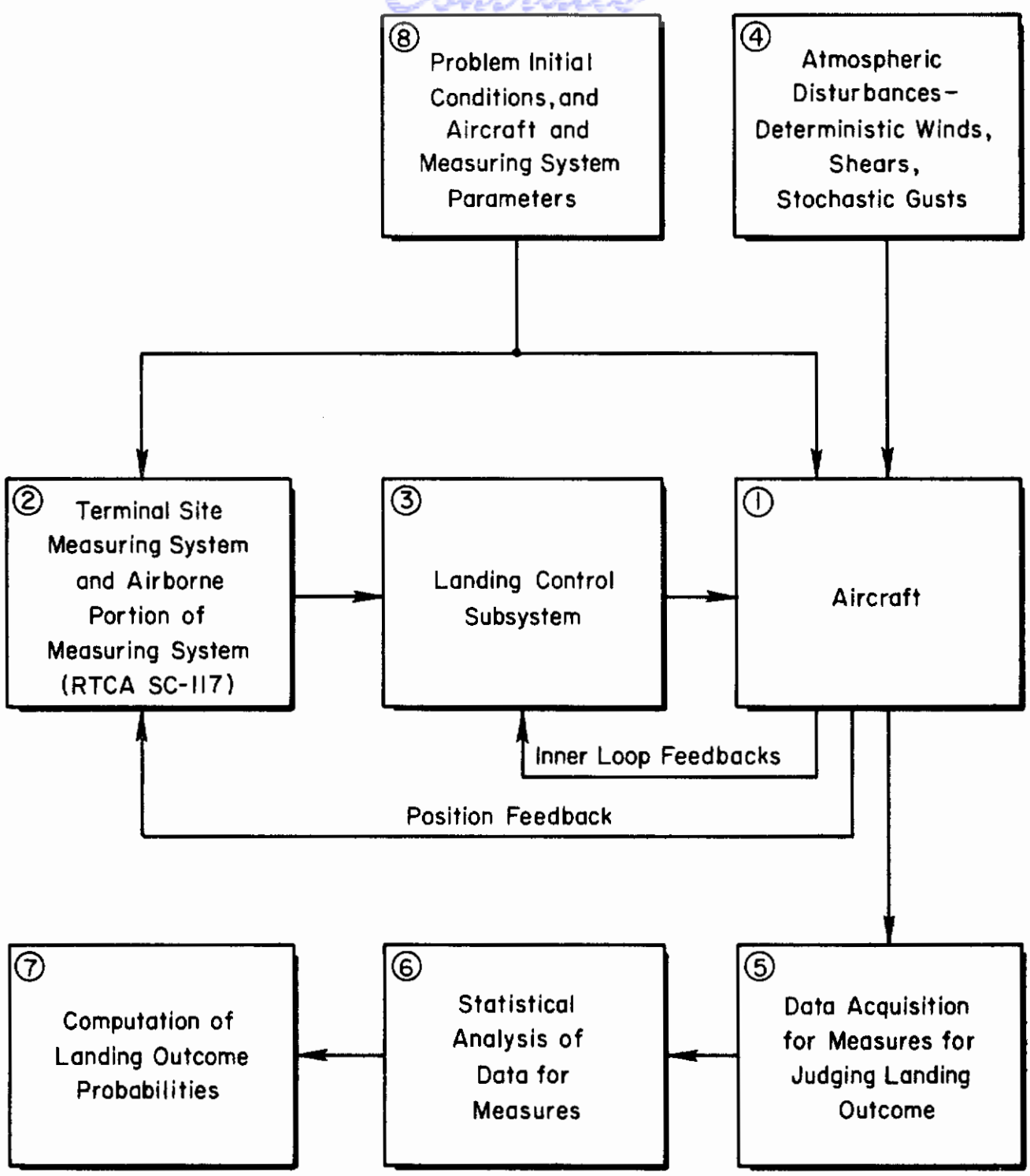

Figure 2. Block Diagram of the Digital Simulation Model of the Landing Analysis

- Aircraft
- Terminal site measuring system and airborne portion of measuring system
- Landing control subsystem
- Atmospheric disturbances, winds, windshears, and stochastic gusts
- Data acquisition for measures for judging landing outcome
- Statistical analysis of data for measures

Two additional blocks, external to the digital program, but part of the systems analysis procedure are:

- Computation of landing outcome probabilities
- Problem initial conditions, and aircraft and measuring system parameters

The scope of each of these several blocks is summarized in the following series of paragraphs.

1. Aircraft

This block contains differential equations of motion which are sufficiently general to simulate CTOL, STOL and VTOL aircraft. Force equations are stated for inertial path axes and the moment equations are stated for body axes. This is the most efficient and accurate axis system in which to numerically integrate the differential equations. All geometric, mass, inertia and stability derivative parameters involved in the dynamic description of the aircraft are entered by means of the input data field so that this subprogram is not specific to any particular aircraft. Provision is made for representing nonlinearities in the aircraft stability derivatives $C_L(\alpha)$, $C_m(\alpha)$ and $C_D(\alpha)$. Ground effect is also included, as are nonlinear landing gear, braking, ground steering, engine thrust and reverse thrust dynamics.

2. Terminal Site Measuring System and Airborne Portion of Measuring System

The measuring system model has been constructed to represent the provisional standard signal format for a conventional microwave scanning beam measuring system reported by the Signal Format Development Team for RTCA Special Committee 117 (Ref. 4).

The terminal site measuring system model includes two elevation transmitting sites and one azimuth transmitting site as shown in Fig. 3. There is provision for two DME transmitting sites. One is co-located with the azimuth site and the second is co-located with elevation site No. 1. Elevation site No. 2 has a scan rate of twice that for site No. 1. The sector coverage in elevation for each of these sites, the scan rate for the No. 1 site, and siting geometry are variable parameters in the model. The azimuth site is similarly described except aximuth coverage may be over a central sector which is scanned at twice the scanning rate used in the edge sectors. The DME interrogators have rate as a variable parameter.

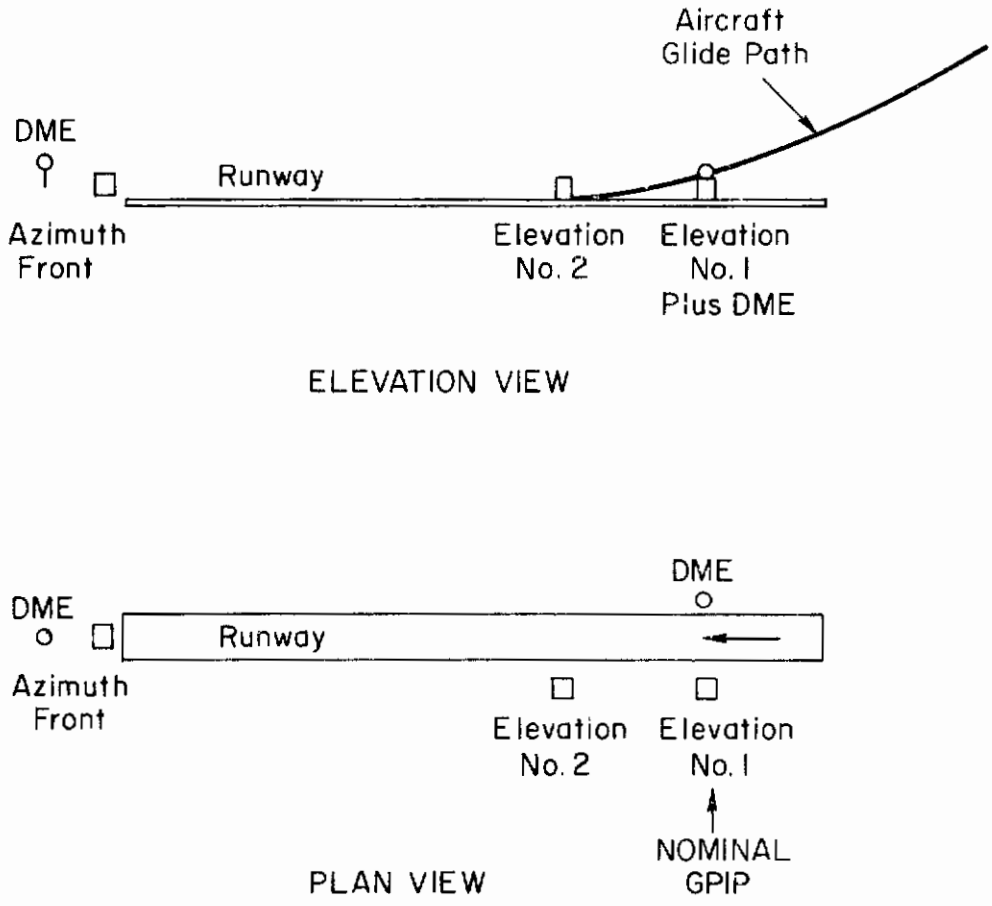

Figure 3. General Siting Plan Configuration

Measuring system noise characteristics are modeled in terms of their effect upon the raw sampled measurements produced at the airborne decoder output. Three different types of noise can be superimposed on the elevation and azimuth outputs. These include sample-to-sample components which are Gaussianly distributed and uniformly distributed, and a Gaussianly distributed component which is sampled at time intervals drawn from an exponential distribution. These may be used, as appropriate, to simulate physical error sources such as multipath reflection anomalies, encoding errors, beam packing errors, etc. DME outputs may have a sample-to-sample component superimposed which is Gaussianly distributed. Provision is made for smoothing, damping and extrapolating the decoded elevation and azimuth samples. DME smoothing and computed distance to elevation site No. 2 is included.

3. Landing Control Subsystem

The longitudinal autopilot of the landing control subsystem provides possible compensated feedbacks of normal acceleration, pitch rate, pitch attitude, airspeed, longitudinal acceleration, sink rate, elevation path deviation rate and elevation path deviation to elevator, power and direct lift controls. The lateral-directional autopilot provides possible feedbacks of lateral acceleration, roll rate, yaw rate, bank angle, heading, azimuth path deviation rate and azimuth path deviation to aileron and rudder.

The landing control system also incorporates the following computers: flare, decrab, thrust retard, thrust reverse, lift dumping, aerodynamic ground steering, nosewheel ground steering and wheel braking.

4. Atmospheric Disturbances

The atmospheric disturbances modeled include steady head- and tailwinds and crosswinds. Crosswind and headwind shear rates are represented in three segments as a function of altitude. Stochastic gusts, including gust gradient effects, are provided in longitudinal, normal, side and effective rolling components.

5. Data Acquisition for Measures for Judging Landing Outcome

Programming has been created for the automatic collection of data which indicate the success or failure of a landing, and, in the case of failure, the primary mode of failure. This subprogram is for large statistical studies. It is not necessary to use this subprogram for deterministic studies. This subprogram is not integrated with the simulation at the present time.

6. Statistical Analysis of Data for Measures

This program uses the data collected in 5, above, to infer probability density functions for the variables indicating the success or failure of landings.

7. Computation of Landing Outcome Probabilities

This is a handbook and manual computation procedure (refer to Section VII of Ref. 1) by which the landing outcome probabilities are computed from the results of 6. The outcome probabilities include, but are not limited to, successful landing and missed approach. Relative measures of landing system capacity and safety are also computed.

8. Problem Initial Conditions, and Aircraft and Measuring System Parameters

This block represents collections of consistent sets of parameters which may be varied to characterize the terminal site measuring system, aircraft, landing control subsystem and atmospheric disturbances. One such collection of data in hand (refer to subsection B, below) and in use is for the landing guidance system signal format for the conventional microwave scanning beam system described in the RTCA Signal Format Development Team Report, the DC-8 transport aircraft, a specially designed high performance landing control subsystem, and a near worst-case atmospheric disturbance environment.

B. DC-8 AIRCRAFT, LANDING CONTROL SYSTEM, AND MEASURING SYSTEM PARAMETERS AND INITIAL CONDITIONS

A limited number of landings were simulated for the DC-8 aircraft to prove the simulation and to show, in a preliminary way, which of the various environmental inputs (winds, windshears, turbulence, measuring system noise, etc.) significantly affect landing system performance. In order to appreciate those results it is necessary to have a specific description of the circumstances which were simulated. This is developed below by means of a series of figures and tables.

The size, nominal inertia and nominal trim condition data for the DC-8 are summarized in Table 2. The longitudinal and lateral-directional dimensionless stability derivatives for the DC-8 are also included in Table 2.

The terminal site measuring system and airborne portion of the measuring system are described in Tables 3 through 5 and Figs. 4 and 5.

Figure 4 describes the assumed siting geometry for the measuring system.

Table 3 gives the equations used to simulate the raw measurements of angular elevation from the two elevation site transmitting antennas, and the angular deviation in azimuth from the extended runway centerline with respect to the azimuth site transmitting antenna. Each of these raw measurements includes six independent noise components. These have been used to simulate fluctuation noise, multipath reflection anomalies, encoding errors, and so forth. (Tables 18 and 19 in Ref. 1 contain a complete description of the assumed error sources.)

Figure 5 is a block diagram showing how the raw measurement samples are smoothed, damped and extrapolated in the intersample interval. Figure 5 applied specifically for the elevation site No. 1 signal processing. The signal processing for the azimuth and elevation site No. 2 signals, however, is similar. The signal processing is a first-order hold with partial velocity correction operating upon the error, EL1SE(n), which is the difference between the current elevation measurement sample, EL1(n), and the extrapolated value of the previous measurement sample, EL1XS(n). The current measurement sample, EL1(n) and the first rearward difference estimate of the error derivative, EL1SED(n) are used with the hold and sawtooth

TABLE 2

SUMMARY OF DC-8 CHARACTERISTICS USED IN THE SIMULATION

Size, Inertia and Trim Condition Data

b	= 142.4 ft	I_x	= 3.2×10^6 slug-ft^2
S	= 2758.0 ft^2	I_y	= 3.8×10^6 slug-ft^2
AR	= 7.36	I_z	= 6.6×10^6 slug-ft^2
c	= 22.16 ft	I_{xz}	= 0.0 slug-ft^2
ξ_o	= 0.055 rad		
Z_j	= 4.0 ft		
W	= 180,000.0 lb		
V_{T_o}	= 228.0 ft/sec	X_{cg}/c	= 0.25
α_o	= 0.0108 rad	X_{np}/c	= 0.47
γ_o	= −0.05 rad	δ_F	= 0.873 rad
$\ell_{x_{antenna}}$	= 60.0 ft	i_h	= 0.001884 rad
ρ	= $0.002378\ (1-0.29\times10^{-4}h)$ slug/ft^3		

Longitudinal Dimensionless Stability Derivatives

C_{L_o}	= 0.18	C_{M_o}	= 0.09
C_{L_α}	= 5.3	$(\Delta C_M)_{LG}$	= −0.01
$C_{L_{\alpha^2}}$	= 0.0	$C_{M_{\alpha^2}}$	= 0.0
$C_{L_{\alpha^3}}$	= 0.0	$C_{M_{\delta_e}}$	= −0.923
$C_{L_{\delta_e}}$	= 0.302	$C_{M_{\delta_F}}$	= −0.104
$C_{L_{\delta_F}}$	= 0.939	$C_{M_{iH}}$	= −1.72
$C_{L_{iH}}$	= 0.562	$(\Delta C_M)_{spoilers}$	= 0.045
$(\Delta C_L)_{spoilers}$	= −0.45	C_{M_q}	= −12.3
C_{L_q}	= 7.68	$C_{M_{\dot\alpha}}$	= −4.01
$C_{L_{\dot\alpha}}$	= 1.31		

TABLE 2 (Concluded)

$C_{D_o} = 0.029$

$C_{D_\alpha} = 0.0765$

$C_{D_{\alpha 2}} = 2.0$

$C_{D_{\alpha 3}} = 0.0$

$(C_{D_{\delta_F}})_o = 0.126$

$\partial C_{D_{\delta_F}}/\partial\alpha = 0.473$

$(C_{\ell_\beta})_o = -0.196$

$\partial C_{\ell_\beta}/\partial\alpha = -0.76$

$C_{\ell_{\delta_a}} = 0.140$

$C_{\ell_{\delta_{sp}}} = 0.213$

$C_{\ell_{\delta_r}} = 0.021$

$C_{\ell_p} = -0.44$

$(C_{\ell_r})_o = 0.20$

$\partial C_{\ell_r}/\partial\alpha = 0.76$

$C_{n_\beta} = 0.10$

$C_{n_{\delta_a}} = 0.0$

$C_{n_{\delta_{sp}}} = 0.053$

$C_{n_{\delta_r}} = -0.10$

$(C_{n_p})_o = -0.025$

$\partial C_{n_p}/\partial\alpha = -0.93$

$C_{n_r} = -0.224$

$C_{y_\beta} = -0.512$

$C_{y_{\delta_a}} = 0.0$

$C_{y_{\delta_{sp}}} = 0.0$

$C_{y_{\delta_r}} = 0.23$

$C_{y_p} = 0.0$

$C_{y_r} = 0.265$

TABLE 3

EQUATIONS FOR RAW SAMPLED MEASUREMENTS
OF ELEVATION AND AZIMUTH ANGLES

Elevation Site No. 1

$$EL1 = \sin^{-1}(h_p/RS1) + \sum_{i=1}^{6} n_{1i}$$

EL1 is the measured angular elevation at the time of scan illumination of the aircraft by site No. 1; i.e., at the sample times. The scan rate is 5.0/sec.

h_p is antenna altitude above the runway.

RS1 is true slant range to elevation site No. 1.

n_{11} is a random number drawn from a zero mean Gaussian distribution with a standard deviation, 0.494×10^{-3} rad, at time intervals selected from an exponential distribution having a mean of 10^4 sec.

n_{12} is a random number drawn from a zero mean Gaussian distribution with standard deviation, 0.592×10^{-4} rad, at each sample time.

n_{13} through n_{16} are each weighted, zero mean random numbers uniformly distributed over a unit interval. The numbers are drawn at each sample time. The respective weightings are:

0.136×10^{-3}, 0.136×10^{-3}, 0.273×10^{-3}, and 0.108×10^{-2} rad

Elevation Site No. 2

$$EL2 = \sin^{-1}(h_p/RS2) + \sum_{i=1}^{6} n_{2i}$$

EL2 is the measured angular elevation at the time of scan illumination of the aircraft by site No. 2. The scan rate is 10.0/sec.

TABLE 3 (Concluded)

RS2 is true slant range to elevation site No. 2.

n_{21} through n_{26} are characterized by the same statistical parameters as are the noise components n_{11} through n_{16}, respectively. Noise components $n_{2(\cdot)}$ and $n_{1(\cdot)}$ are statistically independent, however.

Azimuth Site

$$AZ = \sin^{-1}(Y_{EP}/RSA) + \sum_{i=1}^{6} n_{3i}$$

AZ is the measured angular azimuth at the time of scan illumination of the aircraft by the azimuth site. The scan rate is 5.0/sec.

Y_{EP} is antenna deviation from the extended runway centerline.

RSA is true slant range to the azimuth site.

n_{31} is a random number drawn from a zero mean Gaussian distribution with standard deviation, 0.524×10^{-3} rad, at time intervals selected from an exponential distribution having a mean of 10^{4} sec.

n_{32} is a random number drawn from a zero mean Gaussian distribution with standard deviation, 0.444×10^{-4} rad, at each sample time.

n_{33} through n_{36} are each weighted, zero mean random numbers uniformly distributed over a unit interval. The numbers are drawn at each sample time. The respective weightings are:

$$0.198 \times 10^{-4}, 0.198 \times 10^{-4}, 0.198 \times 10^{-4}, 0.768 \times 10^{-3} \text{ rad}$$

TABLE 4

EQUATIONS FOR RAW AND AVERAGED DME MEASUREMENTS

$$RM1 = RS1 + n_{41}$$

RM1 is the raw measurement of slant range to site No. 1.

n_{41} is a random number drawn from a zero-mean Gaussian distribution with standard deviation, 20.0 ft, at the DME interrogation rate for site No. 1, 10.0/sec.

RM1AV is one-half the sum of the last two samples of RM1. RM1AV is the averaged DME measurement with respect to site No. 1.

RM2 is the derived slant range to site No. 2.

$$RM2 = 2500 \cos EL2X + RM1AV \cos \left\{ \sin^{-1} \left[\frac{2500}{RM1AV} \sin EL2X \right] \right\}$$

EL2X is the smoothed, extrapolated and damped measurement of elevation from site No. 2.

$$RMA = RSA + n_{51}$$

RMA is the raw measurement of slant range to the azimuth site.

n_{51} is a random number drawn from a zero-mean Gaussian distribution with standard deviation, 20.0 ft, at the DME interrogation rate for the azimuth site, 10.0/sec.

RMAAV is one-half the sum of the last two samples of RMA. RMAAV is the averaged DME measurement with respect to the azimuth site.

TABLE 5

COMPUTATIONS OF LINEAR GLIDE SLOPE AND LOCALIZER DEVIATIONS AND ALTITUDE ABOVE RUNWAY

$$GSDE = RM1AV(EL1X - 0.05)$$

GSDE is the inferentially measured linear displacement of the aircraft antenna from the reference glide plane. Here the reference glide plane is inclined to the horizon at 0.05 rad (2.87 deg).

$$LATDE = RMAAV \sin(AX)$$

LATDE is the inferentially measured linear displacement of the aircraft antenna from a vertical reference plane through the runway centerline.

$$HABSE = RM2 \sin(EL2X)$$

HABSE is the inferentially measured absolute altitude of the aircraft antenna above the horizontal plane through site No. 2.

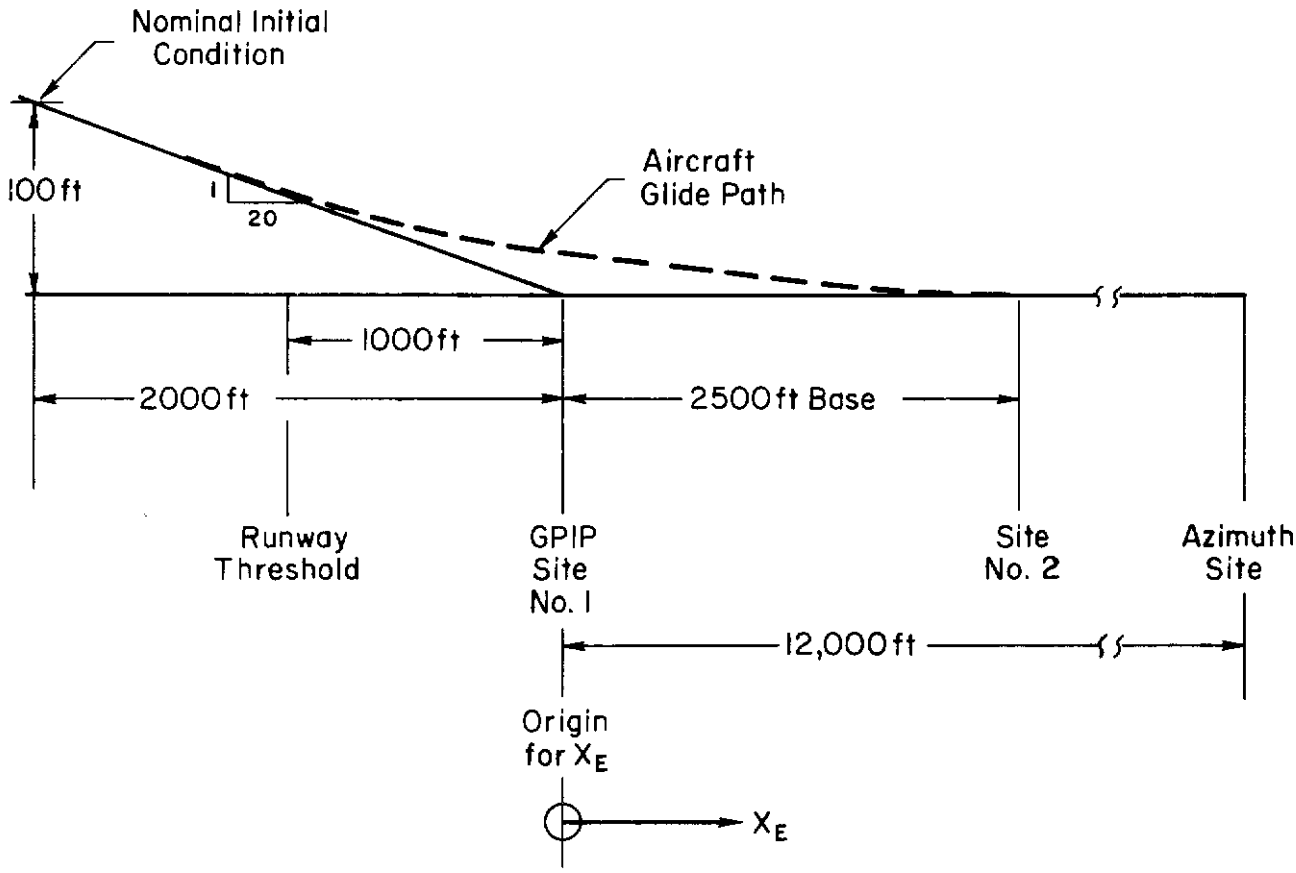

Initial conditions altitude h = 100 ft (nominal)

Longitudinal distance of aircraft c.g. from runway GPIP $X_E = -2000$ ft

Longitudinal distance of glideslope receiver antenna from runway GPIP $X'_E = -1940$ ft since the receiving antenna location is 60 ft forward of center of gravity of the aircraft

Figure 4. Longitudinal Geometry of Terminal Site

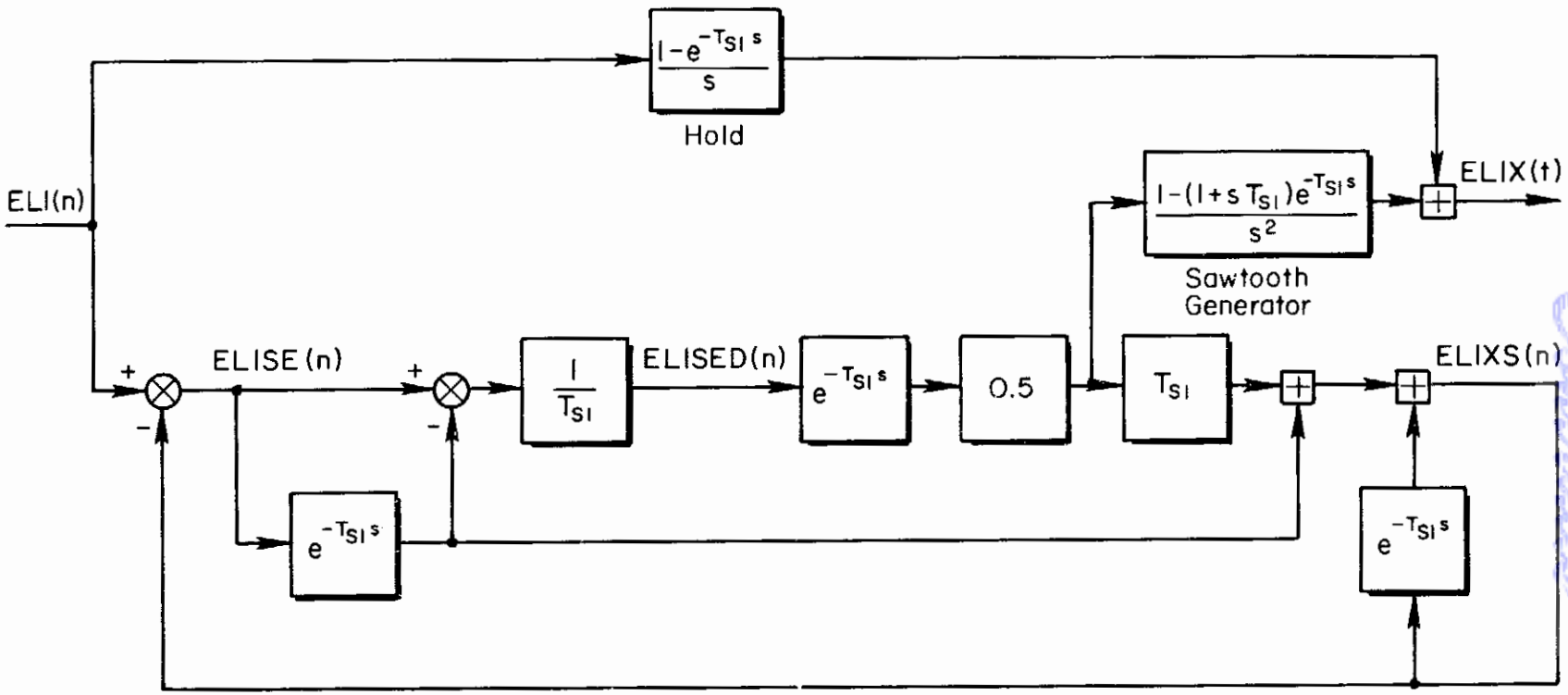

ELIX(t) is extrapolated, smoothed and damped measurement from site No. 1

Signal processing is same for site No. 2 and azimuth site, only differences are in $T_{S(\,)}$ values

Site No. 1	T_{S1} = 0.2 sec	= TSU1
Site No. 2	$T_{S2} \doteq$ 0.1 sec	$\doteq$ TS2EL
Azimuth Site	$T_{S1} \doteq$ 0.2 sec	$\doteq$ TAZ

Figure 5. Extrapolation, Smoothing and Damping of Raw Sampled Measurements of Elevation and Azimuth Angles

generator shown in the figure to generate the continuous time (extrapolated) signal EL1X(t).

Table 4 gives the equations used to simulate the raw DME measurements and the averaged DME measurements with respect to the DME transmitters at elevation site No. 1 and the azimuth site. Each of these raw measurements includes a noise component. Averaged measurements are computed by averaging the last two measurements. The distance between the approaching aircraft and elevation site No. 2 is derived using the averaged DME measurement from elevation site No. 1 and the smoothed elevation measurement from elevation site No. 2.

Table 5 gives the equations by which the linear deviations from the reference glide slope and localizer are computed. The equation for computing the absolute altitude of the approaching aircraft above the horizon plane through elevation site No. 2 transmitting antenna is also given in Table 5. These computations are performed using the extrapolated outputs from the signal processing filters (e.g., EL2X(t) corresponding to EL1X(t) in Fig. 5) and the averaged DME measurements from Table 4.

Figures 6 through 8 describe the landing control subsystem for the interval of flight between passage of the decision altitude, h_D, and touchdown. These figures contain block diagrams which imply that the landing control subsystem is a continuous or analog system. In actual fact, the simulation used finite difference representations of these block diagrams. The two representations are equivalent in the sense that if a staircase approximation with interval equal to the sampling interval be made to the continuous input functions, then the responses of both the continuous system and the finite difference representation to the staircase inputs are equivalent at the sampling instants. (A convenient table of continuous system transfer functions and their finite difference representations is given on pages 45 through 47 of Ref. 5.)

Figure 6 shows the flare computer. At the time of passage of the decision altitude, h_D, an altitude at which to initiate the flare, h_F, is computed. During the interval between passage of the decision altitude and passage of flare initiation altitude a constant rate of descent is commanded. This rate of descent depends upon the selected reference

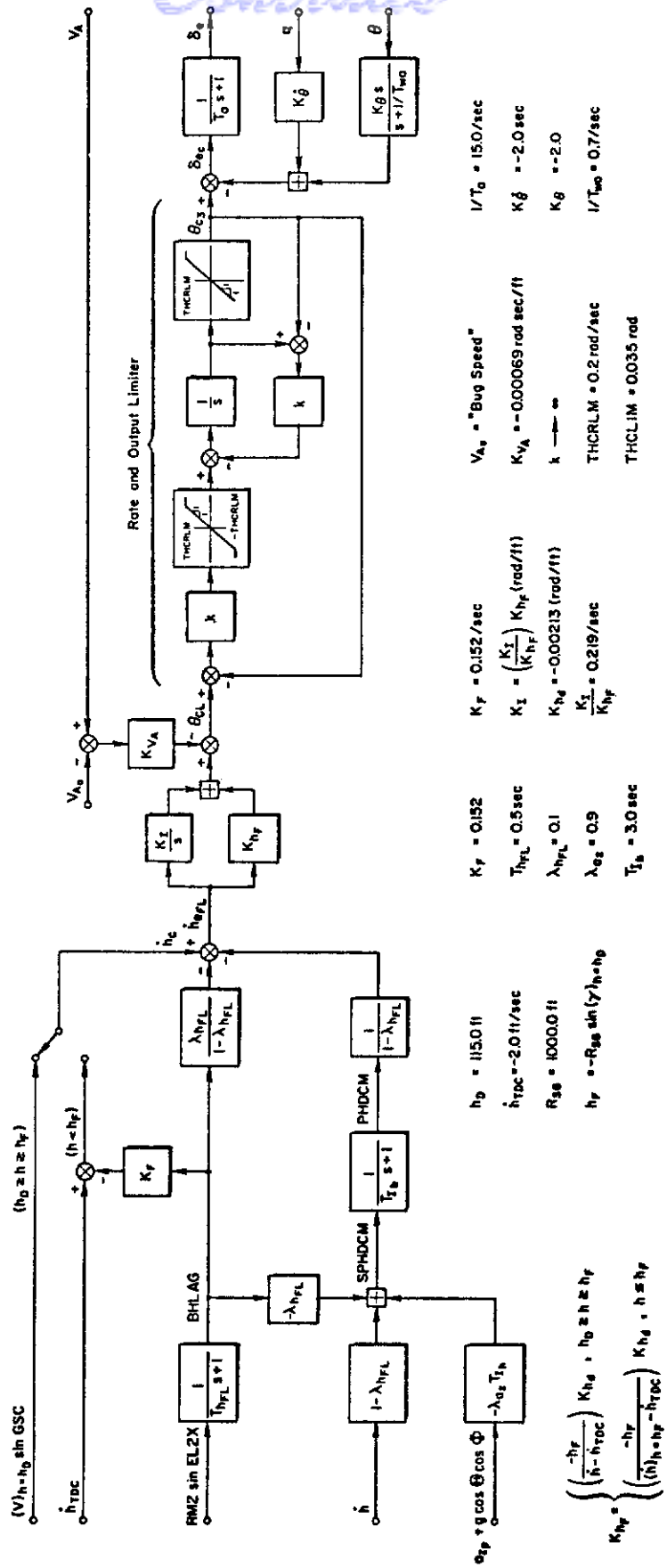

Figure 6. Continuous Flare Computer Simulated using Finite Difference Approximation

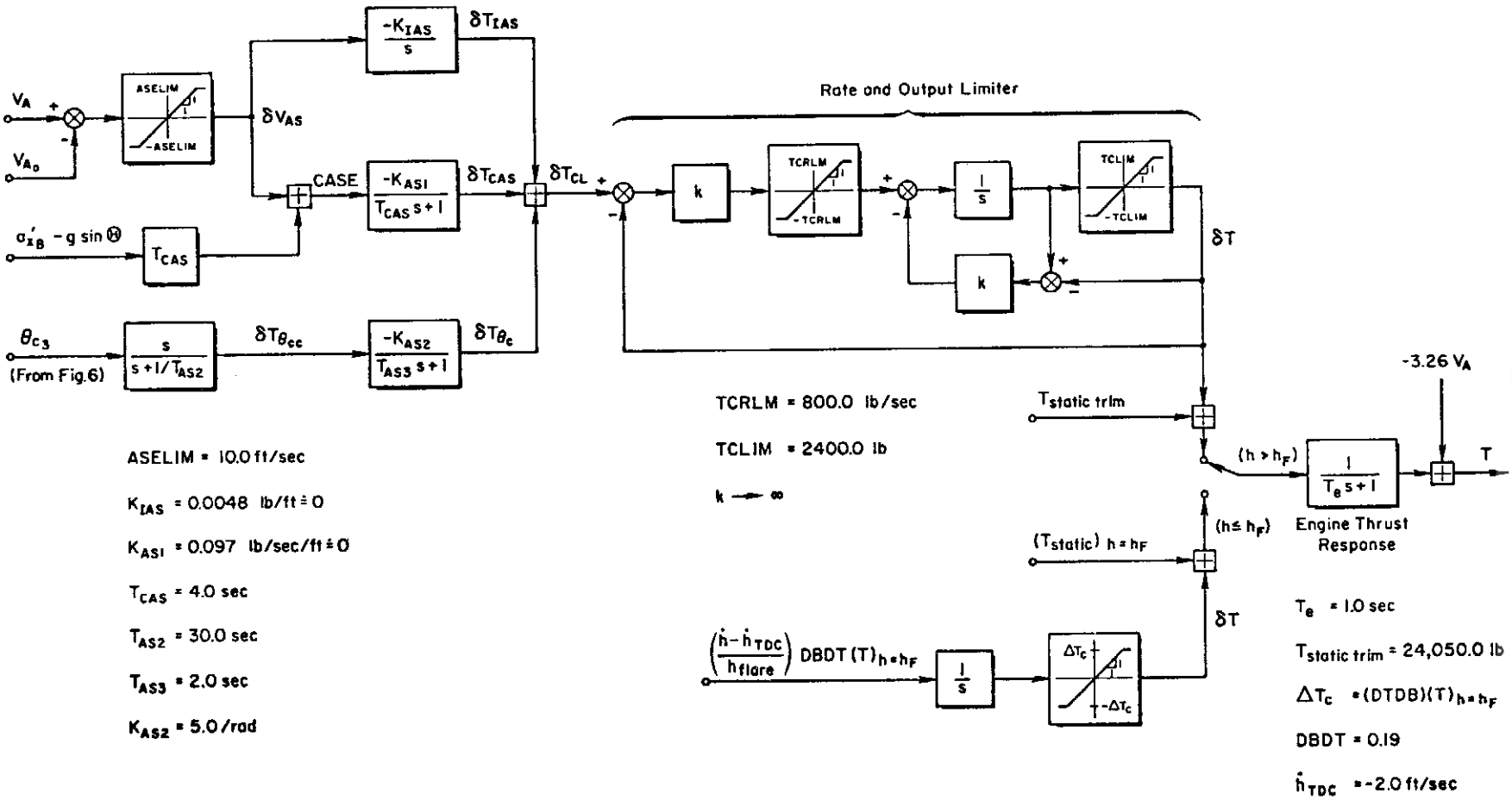

Figure 7. Continuous Autothrottle and Thrust Retard Computer Simulated using Finite Difference Approximation

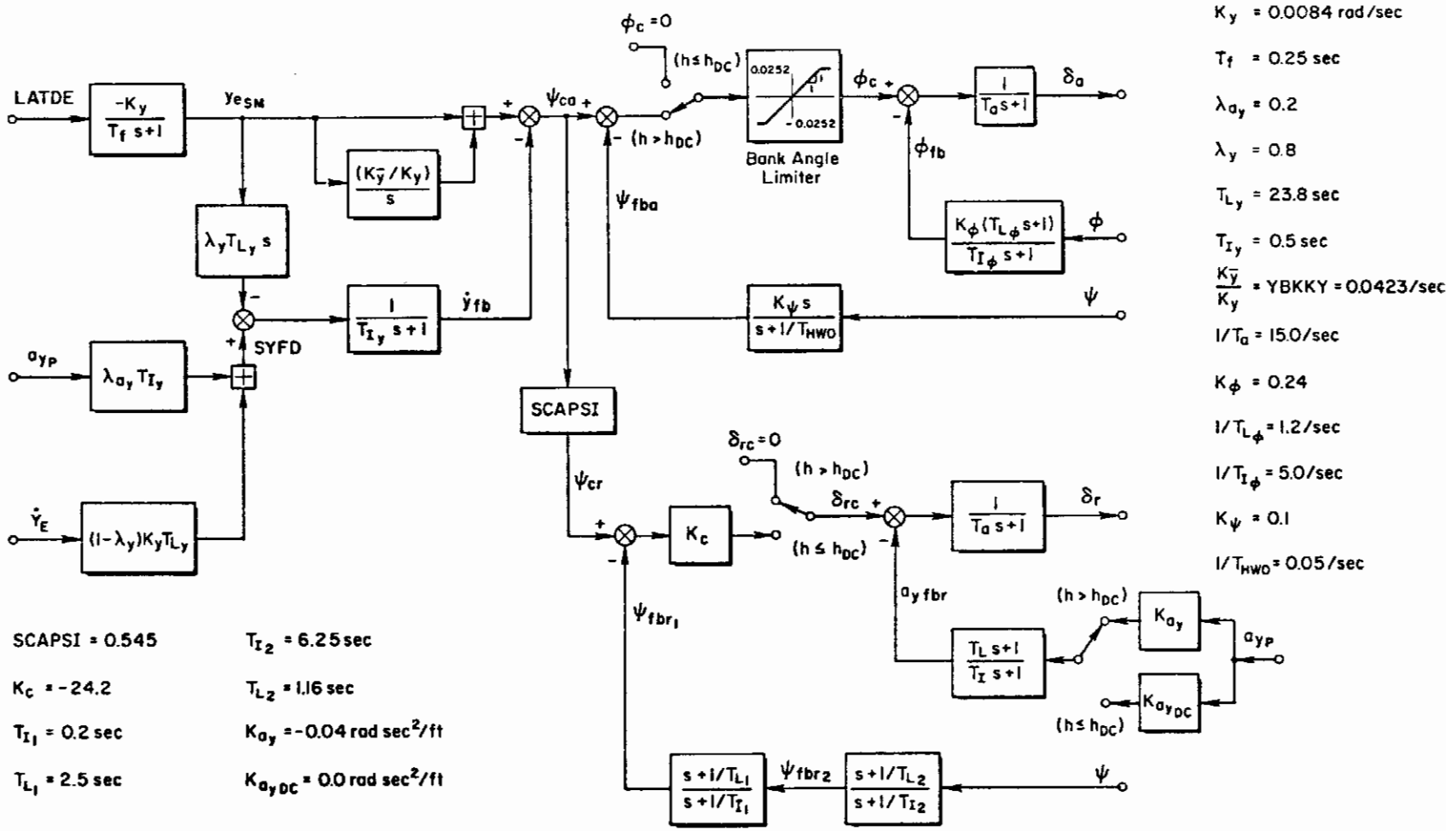

Figure 8. Continuous Lateral-Directional Coupler and Decrab Computer Simulated using Finite Difference Approximation

glide path angle (here GSC = −0.05 rad) and the aircraft ground speed at the time of passage of the decision altitude. After passage of the flare initiation altitude, h_F, the rate of descent command, $\dot{h}_c$, is given by:

$$\dot{h}_c = \dot{h}_{TDC} - K_F BHLAG \doteq -2.0 - 0.152h$$

This results in a smoothly changing rate of descent command from approximately −9.6 ft/sec at h = 50 ft $\doteq h_F$ to −2.0 ft/sec at h = 0.0 ft.

These rate of descent commands are compared with the measured rate of descent. The difference acts through a proportional-plus-integral controller to command pitch attitude. The pitch attitude command also contains a component proportional to airspeed deviation from the "bug speed" or desired airspeed which tends to adjust angle of attack in such a way as to maintain constant lift in the presence of airspeed changes from the bug speed. This pitch attitude command is then rate limited and magnitude limited in the nose-down direction only and is then used as part of the elevator deflection command signal. Other components of the elevator command signal are pitch rate and washed out pitch attitude. These are the basic inner-loop feedbacks. The washout on pitch attitude is for the purpose of obviating the effect of wind shears (windproofing).

Figure 7 shows the block diagram for the autothrottles and thrust retard computer. Prior to passage of the flare initiation altitude, the autothrottles are configured to hold airspeed to the bug speed. Below this altitude, the throttle setting is retarded at a rate determined by the rate of descent. There is a limit upon the maximum throttle change of ±DBDT = ±0.19 of the setting existing at the flare initiation altitude, h_F.

The loop structure for the autothrottles prior to passage of the flare initiation altitude is as follows. The airspeed deviation from the bug speed setting is limited to ±ASELIM = 10 ft/sec. This signal is then integrated with a low gain to form the trim portion of the throttle command signal. The limited airspeed error signal is also complemented with longitudinal acceleration independent of pitch, $a_X - g \sin\Theta$, to give a smoothed airspeed error used for the proportional portion of the throttle command. Provision for feedforward of washed out and smoothed pitch

attitude command, θ_{cz}, in order to provide anticipation in the throttle command for angle of attack (drag) change which is imminent. This anticipation compensates for the engine thrust response lag to a considerable extent.

Figure 8 shows the lateral directional approach coupler and decrab computer. The coupler generates the bank angle commands, φ_c, until the preselected decrab altitude, h_{DC}, is reached. At and below the decrab altitude, the bank angle command is zero and the heading error with respect to ψ_{ca} is commanded to zero.

In the coupler, linear lateral deviation, LATDE, is smoothed and proportional and integral components are used to generate the heading command, ψ_{ca}. The heading command may also contain a beam deviation rate signal, $\dot{y}_{fb}$, derived from LATDE and lateral acceleration. This beam deviation rate signal and the washed out heading feedback which is part of the bank angle command signal provide path damping. The bank angle command is magnitude limited to 6 deg. The limited bank angle command and the inner-loop feedbacks of roll rate and bank angle generate the aileron deflection command.

Before the decrab altitude is reached the only rudder deflection command arises because of the sideslip stability augmentor feedback of compensated lateral acceleration, a_{yfbr}. At the decision altitude, the sideslip stability augmentor gain is reduced to zero and the heading error with respect to ψ_{ca} is regulated to zero using the rudder.

The wind, windshear and stochastic gust disturbances simulated are described in Table 6. Three values of headwind and values of crosswind were used to cover no wind and extreme wind conditions. Severe, two-segment headwind shear and a single segment crosswind shear could also be simulated. Digital random number generators were used to simulate stochastic gusts. The equivalent continuous function power spectral densities for these stochastic gusts are given in Table 6. Longitudinal, normal, side and effective rolling components were generated. The gust gradient effects which result in effective pitch rate and effective yaw rate gust components derived from the normal and side gusts were also simulated.

TABLE 6

ATMOSPHERIC DISTURBANCE ENVIRONMENT

Steady Wind

Headwind	42.2 , 0.0 , −16.9 ft/sec
Crosswind	0.0 , −25.4 (pos. from left) ft/sec

Shear as Function of Altitude

Headwind	±0.135/sec 85 > h ≥ 50 ft (±8. kt/100 ft alt)
	±0.422/sec 50 > h ≥ 0 ft (±25. kt/100 ft alt)
Crosswind	−0.254/sec 85 > h ≥ 0 ft (−15. kt/100 ft alt)

Stochastic Gusts

$$\Phi_{u_g}(\omega) = \sigma_u^2 \frac{2L_u}{\pi V_A} \frac{1}{1+(L_u\omega/V_A)^2}$$

$$\Phi_{v_g}(\omega) = \sigma_{v_g}^2 \frac{2\sqrt{3}\,L_v}{\pi V_A} \frac{1}{1+(\sqrt{3}\,L_v\omega/V_A)^2}$$

$$\Phi_{w_g}(\omega) = \sigma_{w_g}^2 \frac{2\sqrt{3}\,L_w}{\pi V_A} \frac{1}{1+(\sqrt{3}\,L_w\omega/V_A)^2}$$

$$\Phi_{p_g}(\omega) = \sigma_{w_g}^2 \frac{(0.8/L_w V_A)(\pi L_w/4b)^{1/3}}{1+(4b\omega/\pi V_A)^2}$$

$$\Phi_{q_g}(\omega) = \frac{(\omega/V_A)^2}{1+(4b\omega/\pi V_A)^2}\,\Phi_{w_g}(\omega)$$

$$\Phi_{r_g}(\omega) = \frac{(\omega/V_A)^2}{1+(3b\omega/\pi V_A)^2}\,\Phi_{v_g}(\omega)$$

where $\sigma^2 \triangleq \int_0^\infty \Phi(\omega)d\omega$

C. RESULTS FROM THE AUTOMATIC LANDING SYSTEM SIMULATION

Exercise of the automatic landing system simulation has produced results which may serve several purposes. For example, certain results may be compared with independently obtained results for verification of the simulation model; the effects of initial conditions at the decision altitude, and winds and shears upon the touchdown footprint may be investigated; the effects of guidance system noise on the touchdown dispersion may be invesitgated, and so forth. The objective here is not to treat any one of these subjects for investigation in depth, but rather to demonstrate the potential value of the simulation program as an investigative tool.

1. Summary of Simulation Results

It is convenient to summarize the data obtained from selected simulation runs for ready reference in subsequent discussion. This will be done in a series of tables. Table 7 summarizes the different series of runs made, and their purpose.

Worst-case combinations of the initial conditions at the decision altitude, winds and wind shears have been formed in order to obtain indications of extreme behavior from the landing system. These combinations are summarized in Table 8. The initial conditions are the maximum off-nominal conditions in airspeed, glide slope and localizer deviations from which it is permissible to continue an approach from the decision altitude. The deterministic wind and wind shear environment is that described in Table 6, and is nearly the same as that used in Ref. 1, Table 17.

The worst-case combinations result in extreme values of the touchdown coordinates which are pictured in Fig. 9. The touchdown footprint shown is rectangular. This is not necessarily the case, but rather it is a plausible shape readily inferred from the data for the several cases which were run.

TABLE 7

PURPOSE OF DIFFERENT SERIES OF RUNS

SERIES	PURPOSE	SPECIAL CONDITIONS
A	● Establish system trajectory in the absence of all disturbances. ● Establish system trajectories in the absence of all stochastic disturbances and noise, but in presence of deterministic wind and wind shear disturbances and initial conditions (error) at the decision altitude. ● Show effect of bug speed adjustment for winds on touchdown coordinates. ● Show representative end of rollout conditions.	● No measuring system noise present. ● No stochastic gusts present.
B	● Show representative effects of measuring system noise upon touchdown coordinates.	● Measuring system noise present. ● No stochastic gusts present.
C	● Show representative effects of measuring system noise together with stochastic gusts upon touchdown coordinates.	● Measuring system noise present. ● Stochastic gusts present.
D	● Show the effects of stochastic gusts upon touchdown coordinates for different stochastic gust sequences.	● No measuring system noise present. ● Different stochastic gust sequences used in each run.
E	● Show effect of measuring system noise upon touchdown coordinates for different noise sequences.	● Different measuring system noise sequences used in each run. ● No stochastic gusts present.
F	● Show the wind and wind shear effects upon touchdown coordinates in the absence of initial conditions (error) at the decision altitude and stochastic disturbances. ● Show the initial condition (error) effect upon the touchdown coordinates in the absence of winds, wind shears and stochastic disturbances.	● No measuring system noise present. ● No stochastic gusts present. ● Initial offsets at decision altitude are zero in first three runs. ● Deterministic winds and wind shears are zero in last two runs.

TABLE 8

CONDITIONS FOR VARIOUS CASES

CASE	WIND AND SHEAR	AT CATEGORY II DECISION HEIGHT		
		ERROR IN AIRSPEED (ft/sec)	GSD ft	LOC ft
0 (Nominal)	No wind or shear	None	None	None
1	Decreasing headwind from 42.2 ft/sec	MaxSlo −8.45	MaxLo −12	None
2	Increasing crosswind from right at 24.5 ft/sec	None	None	MaxLeft −72
3	Decreasing tailwind from 16.9 ft/sec	MaxHi 8.45	MaxHi +12	None

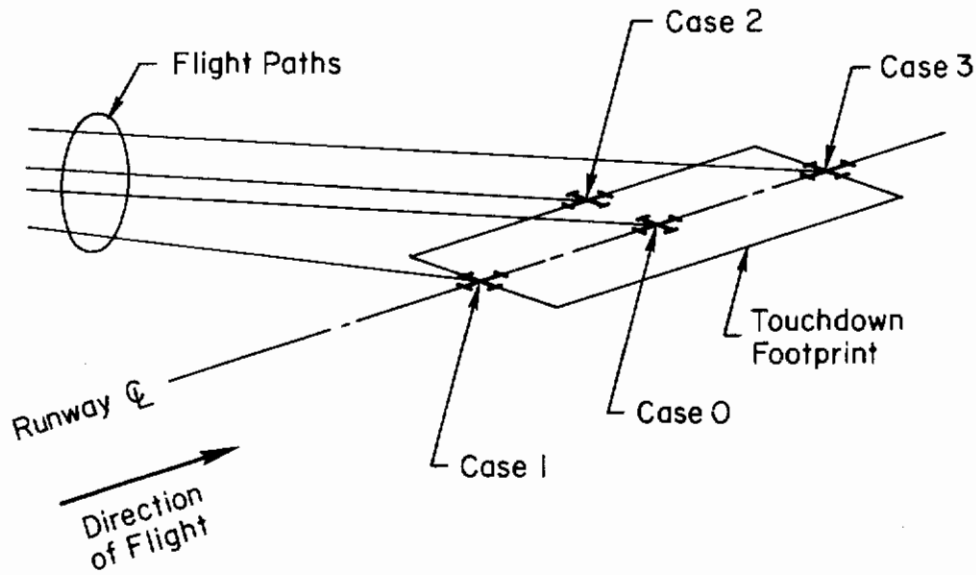

Figure 9. Relative Positions of Touchdown Points for the Worst-Case Combinations Studied

Numerical results obtained from the simulation are summarized in Tables 9 through 15. The variables locating the touchdown coordinates are X_E and Y_E. X_E is the distance in the direction of flight from the glide path intercept point (GPIP). Y_E is distance right of the runway centerline.

TABLE 9

DATA SUMMARY FOR SERIES A RUNS

CASE	X_E (FT)	Y_E (FT)	$\dot{h}$ (TOUCHDOWN) (FT/SEC)
0	1559	-1.76	-2.50
1	-382	-0.44	-7.88
1*	328	-6.57	-4.13
2	1685	-44.1	-2.17
3	5047	-8.32	-0.11
3*	2597	13.1	-0.94

*Indicates runs for which the trim approach airspeed (bug speed) was adjusted by one-half of the longitudinal wind component.

TABLE 10

DATA SUMMARY FOR SERIES B RUNS

CASE	X_E (FT)	Y_E (FT)	$\dot{h}$ (TOUCHDOWN) (FT/SEC)
0	1559	-22.1	-2.41
1	-383	-13.1	-7.93
2	1750	-45.5	-1.73
3	5400	-14.9	-0.10

TABLE 11

DATA SUMMARY FOR SERIES C RUNS

CASE	X_E (FT)	Y_E (FT)	$\dot{h}$ (TOUCHDOWN) (FT/SEC)
0	195	-44.1	-21.7
1	-642	-5.5	-18.7
2	-65	-70.8	-20.3
3	443	-55	-8.1

TABLE 12

DATA SUMMARY FOR SERIES D RUNS

CASE	SEQUENCE	X_E (FT)	Y_E (FT)	$\dot{h}$ (TOUCHDOWN) (FT/SEC)
0	1	195	-44.1	-21.7
0	2	432	61.8	-10.7
0	3	855	71.2	-8.02

TABLE 13

DATA SUMMARY FOR SERIES E RUNS

CASE	SEQUENCE	X_E (FT)	Y_E (FT)	$\dot{h}$ (TOUCHDOWN) (FT/SEC)
0	1	1559	-22.1	-2.41
0	5	1515	-7.17	-2.32
0	2	1515	-7.39	-2.35
0	3	1493	2.10	-2.34
0	4	1559	-15.33	-2.39

TABLE 14

DATA SUMMARY FOR SERIES F RUNS

CASE	X_E (FT)	Y_E (FT)	$\dot{h}$ (TOUCHDOWN) (FT/SEC)
1 NIC	432	-8.9	-4.02
2 NIC	1623	-42.3	-2.05
3 NIC	3598	16.1	-1.25
1 NWS	1214	-9.85	-2.02
3 NWS	1848	-5.84	-2.42

NIC means that initial conditions at the decision altitude given in normal case description of Table 8 have been omitted.

NWS means that the wind and wind shear environment given in the normal case description of Table 8 has been omitted.

TABLE 15

DATA SUMMARY FOR ROLLOUT END CONDITIONS† FOR SERIES A RUNS

CASE	X_E (FT)	Y_E (FT)	ψ (RAD , DEG)	$Y_{E_{MAX}}$ (FT)
0	3757	-5.59	0.0393	-7.02
1	1144	-0.13	0.0111	-5.0
1*	2066	-1.17	-0.0200	-9.67
2	4298	-32.2	0.0806	-133.0
3	7161	-9.06	0.0408	-11.3
3*	4854	3.51	0.0331	15.3

†Rollout is assumed to end when ground speed is reduced below 50.0 ft/sec. The reverse thrust level (when active) is assumed to cause a 0.25g deceleration.

*See footnote, Table 9.

2. Comparison with Related Results (Series A)

Landing simulation results for the DC-8 have been reported in Refs. 5 and 6. These results offer a basis for comparison with results from this simulation.

Comparisons with the results of Ref. 5 must be limited because the landing control subsystem used there was substantially different. In particular, the Ref. 5 system is not windproofed against shears, but contains autothrottles. The present system is windproofed against shears but the autothrottles are inactive (refer to Fig. 7 parameter values for autothrottles). In the absence of winds and windshears, the two systems are comparable because airspeed is not perturbed prior to flare initiation. Table 5(b) in Ref. 5 gives the no-wind longitudinal touchdown coordinate (measured in the direction of flight from the GPIP) as X_E = 1560 ft. The value determined in the present simulation is 1559 ft. The comparable descent rates at touchdown are −2.02 ft/sec for Ref. 5 and −2.50 ft/sec for the present simulation (refer to Case 0, Table 9). This remarkable agreement largely stems from the fact that the important stability derivatives governing aircraft trim conditions and dynamic performance are nearly identical (refer to Table 7 in Ref. 5 and Table 2 here). Further comparison with the Ref. 5 results is not possible because the combined effects of winds and shears and stochastic gusts were there introduced in a different manner than in the present simulation. Furthermore, no attempt was made to investigate off-nominal conditions at the decision altitude in Ref. 5, so there is no basis for comparison in this area.

Further comparisons are possible using the empirical relations between touchdown coordinates and the wind levels, shear rate and off-nominal conditions at the decision altitude. These empirical relationships, which are reported in Ref. 6, were obtained as the result of a six-degree-of-freedom analog simulation of the approach and flare subsequent to passage of the decision altitude. These relationships can be used to produce numbers for comparison with the touchdown coordinates. The conditions under which the empirical relationship were obtained, i.e., with no autothrottles, but using a computed trim airspeed adjustment to the no-wind trim airspeed of one-half the longitudinal windspeed component allow only

limited comparison. Fortunately, however, three runs for the present simulation were made using the same trim airspeed (or bug speed) adjustment rule. Here again, the important stability derivatives and trim conditions are virtually identical. The touchdown coordinates from simulation and from the empirical relationships of Ref. 6 are given in Table 16. The empirical relationship for the longitudinal touchdown point from Ref. 6 is given below in terms of the symbols used in this report.

$$X_E \doteq 1620 + 23u_w/2 + 38\frac{\partial u}{\partial h} - 1.2\left(\frac{\partial u_w}{\partial h}\right)^2 + 43(u_{AS})_{h_D} + 20(d)_{h_D} + 21(\tilde{\dot{h}})_{h_D} \qquad (1)$$

u_w is equal to one-half of the steady wind (tailwinds are +), (kt wind)

$\partial u_w/\partial h$ is the longitudinal wind shear (increasing headwind as you descend is + and is called a headwind shear), (kt wind/100 ft altitude)

$(u_{AS})_{h_D}$ is the error in airspeed (from trim) at the decision altitude ($\doteq$ 100 ft) (increased speed is +), (kt airspeed)

$(d)_{h_D}$ is the deviation from the glide slope beam at the decision altitude altitude (above the beam is +), (ft deviation)

$(\tilde{\dot{h}})_{h_D}$ is the low frequency error in trimmed vertical speed (from nominal) at the decision altitude (decreased sink rate is +), (ft/sec vertical velocity)

TABLE 16

COMPARISON OF SIMULATED AND COMPUTED TOUCHDOWN COORDINATES, TRIM AIRSPEED ADJUSTED BY ONE-HALF OF WIND SPEED

CASE	X_E (FT)		ΔX_E (FT)
	SIMULATION	COMPUTED FROM EQ. 1	
0	1559	1620	+61
1*	328	497	+159
3*	2597	2417	−180

*See footnote, Table 9.

The comparison is reasonably good.

A somewhat similar comparison can be made for the lateral-directional effects of the crosswind and crosswind shear effects upon the lateral touchdown coordinate, Y_E. Y_E for the Case 2 run of Series A is −44.0 ft as the result of a −72.0 ft lateral offset at the decision altitude, a 25.4 ft/sec steady crosswind blowing from right to left across the runway, and a shear component of 15 kt/100 ft alt which acts to increase the wind magnitude as the ground is approached. The flare time (elapsed time from flare initiation until touchdown) is 11.0 sec. Reference 6 gives the following results which may be used for comparison.

$$Y_E \doteq 0.33(y)_{h_D} + 4.6(\dot{y})_{h_D} \qquad (2)$$

$(y)_{h_D}$ is the lateral deviation from the localizer beam at the decision altitude (aircraft to right of beam is +), (ft deviation)

$(\dot{y})_{h_D}$ is the time derivative of y evaluated when $h = h_D$, (ft/sec deviation rate)

Equation 2 applies for a short flare time, 8.7 sec, in the absence of crosswind and crosswind shear. The resulting calculated value of Y_E is −24.0 ft for the initial offset used in the present simulation (refer to Case 2, Table 9). The expression from Ref. 6 which applies for a long flare time, 14.9 sec, and when a 25.4 ft/sec crosswind and a 15.0 kt/100 ft alt crosswind shear is acting is:

$$Y_E = -22 + 0.08(y)_{h_D} + 3.8(\dot{y})_{h_D} \qquad (3)$$

The resulting calculated value of Y_E is −36.4 ft for the initial offset used in the present simulation. This is in qualitative agreement with −44.0 ft value actually obtained. The fact that the actual magnitude is larger is reasonable because the crosswind shear is nearly a factor of 2.0 larger in the simulation than in Ref. 6. However, the actual value of Y_E itself is not a factor of 2.0 larger because of the shorter flare time. Thus, the conclusion of qualitative agreement follows.

3. Effect of Bug Speed Adjustment for the Longitudinal Wind Component on Touchdown Coordinates and Comparison with FAA Limits (Series A)

The landing control system simulated was designed to be particularly effective in compensating for the effects of near worst-case winds and windshears and for compensating for the maximum allowable deviations from the glide slope and localizer prescribed for the FAA Category II decision altitude. These particular conditions were combined into worst-case combinations, and one nominal case to be used for reference in order to evaluate the landing control system effectiveness under the most stringent conditions. Effectiveness was to be determined in terms of the touchdown footprint dimensions. Additionally, the impact on the touchdown footprint of adjusting the trim approach airspeed (bug speed) by one-half of the reported headwind was investigated. (This approximates the United Airlines policy described in Ref. 8.) Numerical results obtained from the simulation are summarized in Table 17. (Data for Table 17 is drawn from Table 9.) The FAA 2σ specification and absolute specification on the touchdown footprint dimensions are also given in Table 17 for relative comparison with the achieved touchdown footprint dimensions. It can be seen that the adjustment of the bug speed is very effective in reducing the longitudinal dimension of the touchdown footprint so it more nearly complies with the FAA specifications in the longitudinal dimension. The lateral dimension of the footprint substantially exceeds the FAA specification. That this is so under these stringent conditions has been previously reported in Ref. 6. It must be mentioned for emphasis here that the particular combination of conditions represented here is considerably less likely than is appropriate for comparison with an acceptable 2σ value. This is particularly so because of the "severe" windshear, and the worst-case combinations used.

TABLE 17

TOUCHDOWN FOOTPRINT AND EFFECT OF BUG SPEED ADJUSTMENT FOR HEADWINDS ON TOUCHDOWN FOOTPRINT

CASE	WITH ADJUSTMENT		WITHOUT ADJUSTMENT	
	X_E (FT)	Y_E (FT)	X_E (FT)	Y_E (FT)
0	+1559	~0	+1559	~0
1*, 1	+328	~0	−382	~0
2	+1559	−44	+1559	−44
3*, 3	+2597	~0	+5047	~0

*See footnote, Table 9.

- FAA 2σ Specification on Footprint Dimensions (Ref. 7)
  Length = 1500 ft ; 1/2 Width = 27 ft

Achieved	With Adjustment	Without Adjustment
Length	2269 ft	5429 ft
1/2 Width	44 ft	44 ft

4. Combined Effect of Measuring System Noise and Stochastic Gusts upon Touchdown Coordinates (Series C, A)

A single set of representative gust and measuring system noise sequences was imposed upon all cases to estimate the significance of these effects upon touchdown dispersion. A comparison of results with and without the stochastic inputs may be had by comparing the results for Cases 0, 1, 2 and 3 in Tables 11 and 9, respectively. The effects of these particular gust and noise sequences are profoundly significant. In fact, X_E, Y_E and $\dot{h}$ at touchdown in virtually every case are outside the limits for an acceptable touchdown. Furthermore, all four cases would result in landing accidents.

The next two subsections will explore the effects of measuring system noise and stochastic gusts individually. It will become clear that the stochastic gusts are the major contributors to the longitudinal touchdown

conditions, and that measuring system noise and stochastic gusts both contribute significantly to lateral touchdown conditions.

5. Effect of Measuring System Noise upon Touchdown Coordinates (Series B, E, A)

A set of representative noise sequences for the measuring system was used for all cases to estimate the significance of this effect upon touchdown dispersion. A comparison of results with and without measuring system noise may be had by comparing the results for Cases 0, 1, 2 and 3 in Tables 10 and 9, respectively. The measuring system noise effect alone upon X_E and $\dot{h}$ at touchdown is almost insignificant. However, the effect upon Y_E may tend to be significant.

The effect of different measuring system noise sequences (all of which have the same infinite length sample statistical parameters) upon the touchdown dispersion for Case 0 may be appreciated from the data in Table 13 and the no-noise data for Case 0 in Table 9. These data, which admittedly are a small sample, indicate that measuring system noise effects upon X_E and $\dot{h}$ at touchdown tend to be insignificant, but the effect upon Y_E at touchdown is indeed very significant.

An additional aspect of the simulation study was to verify that 5.0 scans/sec would be an adequate azimuth scan rate and that 10.0 scans/sec would be an adequate scan rate for elevation No. 2. The 5.0 and 10.0 scans/sec rates do appear to be adequate for the performance of the intended landing maneuver.

6. Effect of Stochastic Gusts upon Touchdown Dispersion (Series D, A)

Different stochastic gust sequences (all of which have the same infinite length sample statistical parameters) were imposed upon Case 0 to investigate the significance of the gusts upon touchdown dispersion. The significance may be appreciated from the data in Table 12, and the no-stochastic gust data for Case 0 in Table 9. All landings are outside the specifications in at least one of the coordinates, X_E, Y_E and $\dot{h}$ at touchdown. All landings might likely result in accidents. (Upper limits upon sink rate $[-\dot{h}]$ are 5 ft/sec for passenger comfort and 12 ft/sec for ultimate landing gear strength.)

The pathology for the three runs in Table 12 was examined using the time histories of the problem variables. Interestingly enough, each of the three excessive sink rates at touchdown arises for a different reason. In order of appearance in Table 12, the reasons are:

- A very large side gust component ($\beta_g \doteq 0.1$ rad) causes a large bank angle ($\varphi \doteq 0.25$ rad) to develop. Since $\cos(0.25 \text{ rad}) \doteq 0.968$, the loss in lift is significant and is not quickly enough compensated for by a change in angle of attack.
- A large tail gust component ($u_g \doteq +16$ ft/sec) is encountered just after flare initiation and persists until touchdown. The initial loss in lift results in a downward acceleration of approximately 4.5 ft/sec^2 and subsequently a high sink rate.
- A large head gust component ($u_g \doteq 12$ ft/sec) is encountered just after passage of the decision altitude. This upsets the stabilized sink rate in a manner which is further excited by the flare sink rate command. The effects combine in an unfortunate way to produce a high sink rate at touchdown.

The latter explanation is also an explanation of a contributory cause to the very high sink rate at touchdown in the first case.

These results raise the question of validity of the atmospheric disturbance environment model which was employed. References 5 and 9, for example, make clear that the characteristic of atmospheric disturbances below 1000 ft altitude are, at best, only incompletely understood and supporting data are very limited. This poses a limitation upon the model validity which is not readily remedied. A second set of limitations upon the validity of the atmospheric disturbance models has been self-imposed.

First, it has been pointed out in private communication from the authors of Ref. 6 that Fig. 8 of Ref. 10 has its ordinate mislabeled as σ_w instead of the correct quantity, σ_u. This means that more appropriate stochastic gust levels would be 68 percent of the values actually used. Furthermore, given an encounter with clear-air turbulence, the probability that the rms gust velocity will equal or exceed the corrected σ_u value is only 0.02 (Ref. 11). Thus, the gust disturbances are "severe" and nearly "worst-case" for approach and landing.

A second factor resulting in increased low- and mid-frequency stochastic gust magnitudes was the decision to use the turbulence scale lengths representative of 100 ft altitude. The model might as well have varied the scale lengths with altitude as recommended in Ref. 10. At lower altitudes this would have caused the half-power frequencies of the gust spectral densities to increase, which, in turn, would have resulted in a reduction in the gust power present at the crucial low- and mid-frequencies.

Other aspects of the atmospheric disturbance environment model which might be questioned involve the finite (short) sample length of the stochastic gust sequences involved in the simulation and the representation of the steady winds and wind shears.

First consider the (deterministic) steady wind and wind shear model. The form of these models seems perfectly adequate from the point of view of intuition and operational experience. The parameter values used in these models were obtained from Ref. 7. They are alleged to represent the limits of acceptable operating conditions. However, the representation may well be from a completely deterministic viewpoint. This viewpoint is a valid one, but it is not clearly stated in Ref. 7. If this is the case, then low frequency gust effects (at those frequencies corresponding to periods longer than the time interval between passage of the decision altitude and touchdown, approximately 15.0 sec in this case) are already represented in the deterministic portion of the atmospheric model and therefore should not be represented again (statistically) in the stochastic portion of the model as was done in this simulation.

That some portion of the steady wind and wind shear components were redundantly simulated is easily appreciated by considering the properties of a relatively short gust sequence which is drawn from an infinite sequence having a specified autocorrelation and a Gaussian probability density function with zero mean and specified variance. A particular short sequence will be characterized by a particular mean value and a mean square about the mean. It could also be characterized by a mean value, a mean linear term in time, and the mean square about the sum of the mean and mean linear term in time. The mean square in the latter case will be equal to or smaller than the mean square in the former case.

This indicates one reason for reducing the mean square stochastic gust component when a deterministic wind shear model is introduced. Another reason arises because of the short sample length properties of the gust sequence itself.

As the sequence length is increased, the expected value of the sequence mean tends to zero, the expected value of the mean linear term in time tends to zero, and the expected value of the mean square tends from zero for a one-point sequence to the variance of the infinite length sequence. Consequently, it is evident that the appropriate variance for the infinite sequence from which the short sequence is drawn should be reduced in a manner appropriate to the sequence length.

The possible conclusion to be drawn is that the combination of the deterministic and stochastic components of the atmospheric disturbances actually simulated do not comprise a valid model of the actual physical process. The development of such a model was, however, beyond the scope of the present effort and remains an important matter for additional research. That this turned out to be the case is not surprising in retrospect. The problem might have been anticipated from the discussion of gust properties of short stochastic gust sequences which appears on pp. 16-17 of Ref. 5, or from the rationale presented on pp. 2-3 of Ref. 6 for ignoring the stochastic gust component. The simulation model of the atmospheric disturbances would seem to be a valid one if either the deterministic wind shear model, or the stochastic gust model (but not both) is used according to one's specific simulation requirements.

7. Effect of Wind and Wind Shear upon Touchdown Coordinates (Series F, A)

To appreciate the significance of the deterministic wind and wind shear disturbances, it is appropriate to compare the first three rows of data in Table 14 with the Case 0 data in Table 9. Comparison places in evidence the profound effect of the winds and shears upon the touchdown coordinates. Sink rate at touchdown, however, is not particularly sensitive to the winds and shears. The deviations from nominal are tabulated in Table 18.

TABLE 18

DEVIATION FROM NOMINAL AT TOUCHDOWN
CAUSED BY WINDS AND SHEARS

CASE*	ΔX_E (FT)	ΔY_E (FT)	$\Delta\dot{h}$ (TOUCHDOWN) (FT/SEC)
1 NIC	-1127	-7.1	-1.52
2 NIC	64	-40.4	0.45
3 NIC	2039	17.9	1.25

8. Effect of Initial Offsets at the Decision Altitude upon Touchdown Coordinates (Series F, A)

The effect of initial offsets at the decision altitude upon the touchdown coordinates and sink rate at touchdown tends to be small. To appreciate this, compare the last two rows of data in Table 14 with the Case 0 data in Table 9. The deviations from nominal are tabulated in Table 19.

This concludes the discussion of the time domain simulation of landing and the representative results which were obtained in exercising the program.

TABLE 19

DEVIATION FROM NOMINAL AT TOUCHDOWN
CAUSED BY INITIAL OFFSETS AT THE DECISION ALTITUDE

CASE†	ΔX_E (FT)	ΔY_E (FT)	$\dot{h}$ (TOUCHDOWN) (FT/SEC)
1 NWS	-345	-8.09	0.48
3 NWS	289	-4.08	0.08

*See footnote to Table 14 for explanation of NIC.

†See footnote to Table 14 for explanation of NWS.

SECTION III

ANALYSIS OF LANDING APPROACH TO THE DECISION ALTITUDE FOR A SINGLE ROTOR HELICOPTER REPRESENTATIVE OF A STOL AIRCRAFT

The work reported in this section is a small part of a continuing program to develop, through the application of systems analysis, recommended ranges for the parameters of the USAF Advanced Landing System. The problem explored here is lateral deviation, altitude and airspeed control for a single articulated rotor helicopter, the CH-53A, along the landing approach path. The tasks at either end of the landing approach (localizer and glide slope acquisition, flare, touchdown and landing roll) are not treated here, although flare and touchdown are considered in the next section. An approach airspeed (60 kt) below the minimum power approach speed (80 kt) is deliberately employed so that use of the power control (in this case, collective pitch) is mandatory. Choice of a helicopter example has been made because this yields an opportunity to study the combined effects of a steep approach (−6 deg), direct lift control and a relatively high value of the Z_w stability derivative.* It turns out that the main effects of the approach angle are upon the minimum power approach speed together with a small augmenting effect upon the Z_w stability derivative. Neither effect is particularly important for landing approach control. The lateral-directional aspects of the problem are quite ordinary except for the high turn rates which are possible at low speeds.

The related matters of direct lift control and a high value of the Z_w stability derivative are of considerable importance, however, because normal gusts, w_g, force the altitude response of the aircraft directly through this derivative. Consequently, the effectiveness of normal gusts in accelerating the aircraft away from the reference flight path is proportional to Z_w. It turns out that the performance levels achievable with the USAF Advanced Landing System will most likely be

*High values of Z_w are characteristic of all aircraft having low wing or disc loadings and are not peculiar to helicopters alone.

limited by the extent to which the aircraft flight control system can compensate for the effects of the aerodynamic disturbance environment. In order to compensate for normal gust disturbances, feedback of instantaneous vertical speed or rate of glide slope deviation or their equivalents to the controls over lift (e.g., collective pitch, elevator, direct lift control spoilers, etc.) are necessary. This, in one way or another, amounts to augmenting the Z_w stability derivative in the characteristic polynomial for the closed-loop longitudinal system. The control system effectiveness in compensating for the normal gust disturbances will be determined by the bandwidth with which lift can be controlled. This bandwidth will be greatest for low inertia controls such as collective pitch which control lift directly and least for high inertia controls which control lift indirectly as in the case of elevator control of angle of attack.

It is also true for the lateral-directional axes that achievable performance levels for the USAF Advanced Landing System will most likely be limited by the extent to which the aircraft flight control system can compensate for the effects of the aerodynamic disturbance environment. There is no realistic prospect for an additional control point for lateral-directional control so that the only improvements in suppressing side and effective rolling gusts must come from increased control bandwidth.

Ordinarily one tends to associate high data rate requirements with high bandwidth requirements. Therefore it might be expected that altitude control using primarily collective pitch control and lateral deviation control using primarily lateral cyclic pitch control for the CH-53A would set upper limits on the absolute altitude and azimuth reference data rate required in the USAF Advanced Landing System for the landing approach. An analysis of the advanced system design developed in the sequel, however, surprisingly enough results in a contrary conclusion. The reason for this somewhat unexpected conclusion is as follows.

Augmentation of Z_w to compensate for the normal gust disturbances requires feedback of plunging velocity, w, altitude rate and pitch attitude, or glide slope deviation rate and pitch attitude. In particular, there is no need for absolute altitude reference feedback information in

the mid- and high frequency regions for the purpose of compensating for the normal gust disturbances. This is very convenient because the absolute altitude reference contains a low-level, but very high bandwidth noise component. We would like to low-pass filter this signal to prevent as much of this noise component as possible from exciting the flight control system actuators. It is possible to introduce this low-pass filtering because relatively noise-free, high bandwidth rate signals needed to compensate for the normal gust disturbances can be obtained from other conventional flight control system sensors.

Analogous reasoning leads to a similar conclusion for the lateral-directional axes. Namely, there is no need for an absolute lateral deviation reference feedback information in the mid- and high frequency regions for the purpose of compensating for the side gust disturbances.

A landing approach control system designed in this fashion is capable of following the glide slope and localizer with high precision in the presence of nearly worst-case disturbances. Furthermore, flight control system authorities, flight control actuator rates and the absolute reference data rate requirements are all minimized. This is at the probable cost of including a conventional normal and lateral accelerometers in the flight control system. This cost will almost always be the favorable trade-off to an alternative requiring more powerful, bulky and faster flight control system actuators.

But what of this alternative? The alternative is represented by the straightforward design for the longitudinal system in the sequel. In this design, the glide slope deviation rate needed to compensate for the normal gusts is a rate which is derived from the absolute altitude reference. This means the data rate for the absolute altitude reference must be significantly higher so that the derived rate will be of high quality out to 2.0 to 3.0 rad/sec. A matter not to be overlooked is the effect of the low-level, very high bandwidth noise component of the absolute altitude reference signal on the quality of the derived rate signal. Its unavoidable effect will be severe. The physical consequences of this effect will be (unnecessary) high frequency excitation of the actuators and the attendant higher stress and wear levels in all downstream mechanical components.

These remarks are made on the basis of a relative comparison of the advanced and straightforward longitudinal system designs examined in detail below. This comparison has been made for system designs which are capable of very nearly the same glide slope following performance. The pilot acceptability is also judged to be the same for the two systems. The design target performance levels are those for which the 3σ levels of glide slope deviation and airspeed deviation at 100 ft attitude coincide with the Recommended Cat II "Window" boundaries shown in Fig. 10 as in Ref. 1.

In the following subsections, the CH-53A, the USAF Advanced Landing System Model and the disturbance environment are described in quantitative detail, the straightforward longitudinal and the advanced longitudinal and lateral-directional flight control system designs are described, and the basic design principles which emerged from the designs are summarized.

A. DESCRIPTION OF CH-53A, USAF ADVANCED LANDING SYSTEM, AND ATMOSPHERIC DISTURBANCE MODELS

1. Aircraft Dynamics

The linearized longitudinal speed and height control dynamics of the CH-53A can be separated from the lateral-directional dynamics because of the weak coupling which exists among most of the degrees of freedom. An exception is the cross-coupled yawing moment response to collective pitch control on the main rotor.

The separated longitudinal and lateral-directional sets of equations are given in Tables 20 and 21, respectively.

The actuation system is a complex assembly of hardware and hydraulic servos, but for analytical purposes a first-order system with a time constant of 0.1 sec is assumed in Ref. 12 to adequately describe the actuation system plus inherent lag of the rotors. Table 22 gives transfer functions for the effective actuation and rotor lag dynamics (Ref. 12). Pitch SAS, basic pitch AFCS and basic altitude AFCS transfer functions are given in Table 23 (Ref. 12).

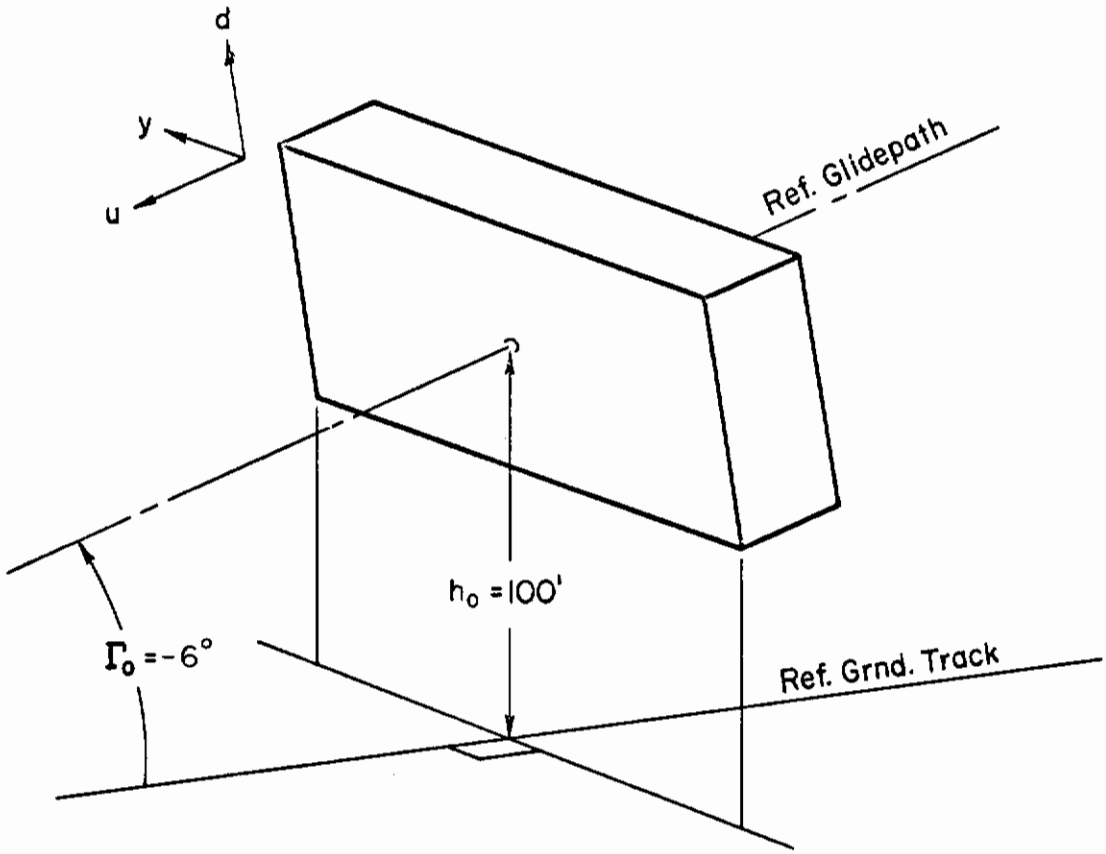

$$\Delta d = \pm 12 \text{ ft}$$

$$\Delta y = \pm 72 \text{ ft}$$

$$\Delta AS = \pm 5 \text{ kts} = \pm 8.45 \text{ ft/sec}$$

Note: d is approximately same as h for the purpose of this study

Figure 10. The Recommended Category II "Window"

TABLE 20

LONGITUDINAL AIRFRAME DYNAMIC EQUATIONS OF MOTION

Longitudinal-Vertical Equations of Motion for Small Disturbances from Trim

$$\begin{bmatrix} s - X_u & -X_w & -X_q s + g - X_\alpha \\ -Z_u & s - Z_w & -Z_q s - Z_\alpha + g \sin\gamma_o \\ -M_u & -M_w^{\cdot} s - M_w & s^2 - (M_q + M_\alpha^{\cdot}) s - M_\alpha \end{bmatrix} \begin{bmatrix} u \\ -sh \\ \theta \end{bmatrix} = \begin{bmatrix} X_{B_1}^{\cdot} s + X_{B_1} & X_{\delta_c} \\ Z_{B_1}^{\cdot} s + Z_{B_1} & Z_{\delta_c} \\ M_{B_1}^{\cdot} s + M_{B_1} & M_{\delta_c} \end{bmatrix} \begin{bmatrix} B_1 \\ \delta_c \end{bmatrix} + \begin{bmatrix} -X_u & -X_w & 0 \\ -Z_u & -Z_w & -Z_q \\ -M_u & -M_w & -M_q \end{bmatrix} \begin{bmatrix} u_g \\ w_g \\ q_g \end{bmatrix}$$

Assumptions

$$X_w^{\cdot} = Z_w^{\cdot} = 0 \ , \quad \theta_o = 0 \ , \quad \text{otherwise negligible cross-coupling}$$

$$-\alpha_o = \gamma_o \doteq 0$$

Equation for Gust Gradient Model For Stochastic Gusts (Ref. 10)

$$(s + U_o \tfrac{\pi}{4b}) q_g = -\tfrac{\pi}{4b} s w_g$$

TABLE 21

LATERAL-DIRECTIONAL AIRFRAME DYNAMIC EQUATIONS OF MOTION

Lateral-Directional Equations of Motion for Small Disturbances from Trim

$$\begin{bmatrix} s-Y_v & -Y_p s-g & -Y_r s+U_o Y_v \\ -L'_v & s^2-L'_p s & -L'_r s+U_o L'_v \\ -N'_v & -N'_p s & s^2-N'_r s+U_o N'_v \end{bmatrix} \begin{bmatrix} sy \\ \varphi \\ \psi \end{bmatrix} = \begin{bmatrix} U_o Y^*_{A_1} & U_o Y^*_{\delta_r} \\ L'_{A_1} & L'_{\delta_r} \\ N'_{A_1} & N'_{\delta_r} \end{bmatrix} \begin{bmatrix} A_1 \\ \delta_r \end{bmatrix} + \begin{bmatrix} -Y_v & -Y_p \\ -L'_v & -L'_p \\ -N'_v & -N'_p \end{bmatrix} \begin{bmatrix} v_g \\ p_g \end{bmatrix} + \begin{bmatrix} -Y_r \\ -(L'_r)_g \\ -(N'_r)_g \end{bmatrix} r_g$$

Assumptions

$Y_{\dot{v}} = L_{\dot{v}} = N_{\dot{v}} = 0$; $\theta_o = \gamma_o = -6.0$ deg ; otherwise negligible cross-coupling

$\alpha_o = 0$; θ_o is a small angle so that $\sin\theta_o \doteq \theta_o$ and $\cos\theta_o \doteq 1$

Definitions

Yawing velocity: $r \doteq s\psi$

Total lateral acceleration at pilot's station:

$$a'_y = s^2 y - g\varphi - (Z' - Z_{cg})s^2\varphi + (X' - X_{cg})s^2\psi$$

Effective yawing gust stability derivatives:

$$(L'_r)_g = (I_{xz}/I_x)N_r/[1 - I^2_{xz}/I_x I_z]$$

$$(N'_r)_g = N_r/(1 - I^2_{xz}/I_x I_z)$$

$$U_o Y(\overset{*}{\cdot}) = Y_{(\cdot)}$$

Equation for gust gradient model for stochastic gusts (Ref. 10)

$$(s + \frac{\pi U_o}{3b})r_g = (\pi/3b)s\ v_g$$

TABLE 22

EFFECTIVE ACTUATION AND ROTOR LAG DYNAMICS

$$B_1/B_{1c} = 10/(s + 10)$$

$$\delta_c/\delta_{cc} = 10/(s + 10)$$

$$A_1/A_{1c} = 10/(s + 10)$$

$$\delta_r/\delta_{r_c} = 10/(s + 10)$$

TABLE 23

TRANSFER FUNCTIONS FOR SAS AND BASIC AFCS ON CH-53A

	ACTUALLY INSTALLED	MODIFIED VALUES USED IN THIS STUDY
Pitch SAS		
	$B_{1c}/\dot{\theta} = 0.4$ sec	Same
Basic Pitch AFCS		
	$B_{1c}/\theta = 0.8$	Same
Basic Altitude AFCS		
	$\delta_{cc}/h = 0.001$ 1/ft	Not Used
Roll SAS		
	$A_{1c}/\dot{\varphi} = -0.1$ sec	-0.04 sec
Yaw SAS		
	$\delta_{rc}/\dot{\psi} = 0.6$ sec	0.1 sec*
Roll AFCS		
	$A_{1c}/\varphi = -0.25$	-0.18
Heading AFCS		
	$A_{1c}/\psi = 0.18$	Not Used

*Variable fed back is $r^* = (\cos 15^\circ)r + (\sin 15^\circ)p$ instead of $\dot{\psi}$

Longitudinal and lateral-directional dimensional stability derivatives for the CH-53A are given in Tables 24 and 25, respectively, along with pertinent trim data, weight, pitch moment of inertia and center of gravity location (Ref. 13).

2. Control Authority

The CH-53A manual control authorities are given in Table 26. This table has been developed from Refs. 14 and 15. SAS and AFCS control authorities and rate limits are in terms of the manual control range. In particular, if the manual control range is taken as 100 percent (100 percent corresponds to 27.0 deg for B_1; 100 percent corresponds to 13.0 deg for δ_c), then the SAS authority is ±10 percent about trim. AFCS authority is the same as the manual control authority except that a rate limit of 10 percent/sec is imposed in the existing CH-53A AFCS systems. This is a particularly niggardly rate limit. Reference 15 indicates that rate limits of 20 percent/sec have been considered for the CH-53A, but have not been flown. The more generous rate limit (20 percent/sec) will be used here.

The trim control setting does not occur in the center of the control range. Therefore, the nearer limit will be used to specify the limits on the control perturbations from trim.

The above considerations lead to a set of working control authorities and rate limits for use in this study. These are summarized in Table 27. The entries in Table 27 can be used to establish design target values for the rms values of $B_{1_{SAS}}$, $B_{1_{AFCS}}$, $\dot{B}_{1_{AFCS}}$, δ_c, $\dot{\delta}_c$, $A_{1_{SAS}}$, $A_{1_{AFCS}}$, $\dot{A}_{1_{AFCS}}$, and $\delta_{r_{SAS}}$. This is done here by choosing the target rms values to be 1/3 of the control authority and rate limit values. If these target values are met, then the limits entered in Table 27 will be encountered less than 0.26 percent of the time. Experience has shown that the effect of such limits on closed-loop system performance under these circumstances is negligible.

However, we shall further reduce the working control authority for δ_c before applying the factor 1/3 to obtain the target rms value. The driect lift control acceleration derivative, Z_{δ_c} in Table 27, is almost −10g/rad (−311 ft/sec^2/rad) at 60 kt. Thus, a δ_c control authority of

TABLE 24

CH-53A LONGITUDINAL DIMENSIONAL DERIVATIVES*

U_o (kt)	Hover	60	90	120	150	170
U_o (ft/sec)		101	152	203	253	287
μ_{x_o}	0	0.146	0.218	0.291	0.364	0.413
X_u	-0.0154	-0.0227	-0.0270	-0.0332	-0.0396	-0.0418
X_w	0	-0.000528	+0.00698	0.0210	0.0301	0.0263
X_α	0	-0.0533	1.06	4.26	7.62	7.55
X_q	1.36†	1.69	1.65†	1.33†	0.790†	0.347†
$X_{\dot{B}_1}$	-1.36†	-1.69	-1.65†	-1.33†	-0.790†	-0.347†
X_{B_1}	33.2	32.3	30.4	27.0	24.3	25.1
X_{δ_c}	0	-3.21	-0.252	+6.36	13.2	14.9
Z_u	0	-0.0893	-0.0257	+0.0240	0.0733	0.106
Z_w	-0.303	-0.694	-0.831	-0.949	-1.08	-1.18
Z_α	0	-70.3	-126	-192	-247	-338
Z_q	0.126†	0.0954	0.158†	0.194†	0.162†	0.0850†
$Z_{\dot{B}_1}$	-0.126†	-0.0954	-0.158†	-0.194†	-0.162†	-0.0850†
Z_{B_1}	0	67.3	115	171	238	292
Z_{δ_c}	-276	-311	-361	-409	-461	-501
M_u	0.00204	0.00322	0.00241	0.00199	0.00165	0.00135
$M_{\dot{w}}$	0	-0.000213	-0.000153†	-0.000127†	-0.000112†	-0.000106†
M_w	0.000746	0.001695	0.00341	0.00492	0.00702	0.00879
M_α	0	0.171	0.519	0.997	1.78	2.52
$(M_q + M_{\dot{\alpha}})$	-0.438	-0.584	-0.638	-0.690	-0.735	-0.762
$M_{\dot{B}_1}$	0.438†	0.441	0.433†	0.443†	0.414†	0.399†
M_{B_1}	-4.32	-4.55	-4.82	-5.28	-6.04	-6.81
M_{δ_c}	0.680	1.95	2.89	3.86	4.95	5.82
M_q	-0.438	-0.562	-0.615	-0.677	-0.724	-0.751
W (lb)	33,500					
c.g. (fus. sta.)	352 (most aft)					
I_y (slug-ft^2)	175,500					

*Trimmed in level flight; sea level pressure altitude.

†Assumed zero in exact factorization of transfer functions.

TABLE 25

CH-53A LATERAL-DIRECTIONAL DIMENSIONAL DERIVATIVES*

U_o (kt)	Hover	60	90	120	150	170
U_o (ft/sec)		101	152	203	253	287
μ_{x_o}	0	0.146	0.218	0.291	0.364	0.413
Y_v	-0.0352	-0.0867	-0.112	-0.134	-0.154	-0.169
U_oY_v	0	-8.757	-17.0	-27.2	-39.0	-48.5
Y_p	-1.43	-1.90	-1.88	-1.63	-1.24	-0.946
Y_r	0.850	2.04	2.70	3.04	3.23	3.32
$U_oY^*_{A_1}$	33.2	32.5	32.0	31.8	32.2	32.8
$U_oY^*_{\delta_r}$	18.9	18.8	22.8	26.3	29.3	31.2
L'_v	-0.0128	-0.0113	-0.0141	-0.0182	-0.0231	-0.0265
$U_oL'_v$	0	-1.141	-2.14	-3.69	-5.85	-7.61
L'_p	-2.31	-2.00	-1.98	-1.90	-1.79	-1.70
L'_r	0.0946	0.227	0.356	0.505	0.654	0.743
L'_{A_1}	22.4	22.2	22.1	22.0	22.1	22.2
L'_{δ_r}	2.18	2.28	3.45	4.90	6.53	7.61
N'_v	0.00531	0.00892	0.0100	0.0105	0.0109	0.0113
$U_oN'_v$	0	0.9009	1.52	2.12	2.706	3.24
N'_p	0.0166	0.0471	0.0709	0.0925	0.115	0.129
N'_r	-0.232	-0.553	-0.709	-0.795	-0.842	-0.867
N'_{A_1}	0.0860	0.0907	0.122	0.163	0.207	0.235
N'_{δ_r}	-5.12	-5.09	-6.21	-7.07	-7.83	-8.33
W (lb)	33,500					
c.g. (fus. sta)	352 (most aft)					
I_x (slug-ft^2)	33,900					
I_z (slug-ft^2)	167,000					

*Trimmed in level flight; sea level pressure altitude.

TABLE 26

CH-53A LONGITUDINAL MANUAL CONTROL AUTHORITIES

CONTROL	CONTROL RANGE FROM ZERO REFERENCE	TRIM CONTROL DEFLECTION FROM ZERO REFERENCE AT 60 KT
B_1	17.0 deg nose-down −10.0 deg nose-up	4.6 deg
δ_c	$5.3 \leq \delta_c \leq 18.3$ deg (δ_c is the main rotor blade pitch angle measured at the cuff)	11.2 deg
A_1	±6.0 deg	−1.3 deg
δ_r	$-2.0 \leq \delta_r \leq 24.0$ deg (δ_r is actually tail rotor collective pitch)	11.4 deg

TABLE 27

WORKING CONTROL AUTHORITIES AND RATE LIMITS FOR THE CH-53A

CONTROL	CONTROL AUTHORITY	RATE LIMITS
$B_{1_{SAS}}$	±2.7 deg (±0.047 rad)	None
$B_{1_{AFCS}}$	±12.4 deg (±0.216 rad)	5.4 deg/sec (0.094 rad/sec)
δ_c	±5.9 deg (±0.103 rad)	2.6 deg/sec (0.0454 rad/sec)
$A_{1_{SAS}}$	±1.2 deg (±0.0209 rad)	None
$A_{1_{AFCS}}$	±4.7 deg (±0.0820 rad)	2.4 deg/sec (0.0418 rad/sec)
$\delta_r = \delta_{r_{SAS}}$	±2.6 deg (±0.0453 rad)	None

±0.103 rad is tantamount to a δ_c-induced normal acceleration authority of ±1.0g. This normal acceleration authority is twice the limit considered to be acceptable to pilots in automatically coupled landing approaches (Ref. 16). Therefore, we shall adopt one-half of the δ_c control authority in Table 27 before applying the factor 1/3, so that 1/6 of the δ_c control authority in Table 27 will be used to obtain a design target value for rms δ_c.

The target rms values are summarized in Table 28.

TABLE 28

DESIGN TARGET VALUES FOR RMS $B_{1_{SAS}}$, $B_{1_{AFCS}}$, $\dot{B}_{1_{AFCS}}$, δ_c, $\dot{\delta}_c$ $A_{1_{SAS}}$, $A_{1_{AFCS}}$, $\dot{A}_{1_{AFCS}}$ AND $\delta_{r_{SAS}}$

VARIABLE	TARGET RMS VALUE
$B_{1_{SAS}}$	0.90 deg (0.0157 rad)
$B_{1_{AFCS}}$	4.1 deg (0.0721 rad)
$\dot{B}_{1_{AFCS}}$	1.8 deg/sec (0.0314 rad/sec)
δ_c	1.0 deg (0.017 rad)
$\dot{\delta}_c$	0.87 deg/sec (0.0151 rad/sec)
$A_{1_{SAS}}$	0.4 deg (0.00696 rad)
$A_{1_{AFCS}}$	1.57 deg (0.0273 rad)
$\dot{A}_{1_{AFCS}}$	0.8 deg/sec (0.0139 rad/sec)
$\delta_r = \delta_{r_{SAS}}$	0.867 deg (0.0151 rad)

3. CH-53A Transfer Functions

Transfer functions for the basic CH-53A are given in Tables 29 and 30. The CH-53 is, in actual practice, always flown with the SAS and basic AFCS systems operative.

The installed SAS and basic AFCS must be considered separately for the longitudinal and lateral-directional systems. This is because the installed $\dot{\theta}$ and θ to B_{1c} loops are appropriate for the longitudinal system, but the remaining installed loops are either inappropriate for automatic landing approach control or have inappropriate gain values for this purpose. This means that the SAS and basic AFCS must be redesigned for the lateral-directional system.

a. **Longitudinal Augmented Transfer Functions.** As mentioned above, the basic AFCS altitude-to-collective pitch loop ($h \rightarrow \delta_{cc}$) is inappropriate for use in landing approach control. It will not be considered further. The remaining SAS and basic AFCS loops ($\dot{\theta} \rightarrow B_{1c}$, $\theta \rightarrow B_{1c}$) are not only appropriate, but necessary for landing approach control. Furthermore, the gains given in Table 23 are quite appropriate. (That this is so is evidenced by the very adequate damping and frequency of the short-period factors of the denominator in Table 31.)

   Transfer functions for the CH-53A plus pitch SAS, basic pitch AFCS, and the effective actuation and rotor lags are given in Table 31.

b. **Lateral-Directional System Augmentation.** The redesigned lateral-directional SAS block diagram is shown in Fig. 11. It features lower roll damping and yaw damping gains than does the installed system. Lowering of these gains is necessary in order to meet both the control rate and deflection budgets and the performance goal for the ultimate automatic coupler design. An additional refinement is the tilting (or effective tilting) of the yaw rate gyro so that some component of roll rate is sensed. This gives better closed-loop damping of the dutch roll than would otherwise result.

   Augmented transfer functions for augmented lateral-directional axes have not been computed. Instead, the SAS loops have been included in the computation at the same time as the automatic coupler and AFCS loops.

TABLE 29

CH-53A LONGITUDINAL TRANSFER FUNCTION FACTORS* AT 60 KNOTS FOR BARE AIRCRAFT PLUS EFFECTIVE ACTUATION AND ROTOR LAGS

Denominator

$$\Delta = (0.4281)(1.102)(1.12)(10.0)^2[-0.324, 0.375]$$

Control Input Numerators

$$N^{\theta}_{B_{1c}} = 4.41(0.00056)(0.668)(1.102)(10.0)(-10.31)$$

$$N^{-sh}_{B_{1c}} = -0.954(-0.0202)(1.102)(10.0)(-706.99)[0.03485, 2.0867]$$

$$N^{u}_{B_{1c}} = -16.9(0.693)(1.102)(10.0)(-19.11)[-0.0343, 2.091]$$

$$N^{-sh}_{\delta_{cc}} = -3110.0(0.466)(1.102)(10.0)[0.159, 0.438]$$

$$N^{\theta}_{\delta_{cc}} = 20.16(0.015)(0.412)(1.102)(10.0)$$

$$N^{u}_{\delta_{cc}} = -32.1(0.412)(1.102)(10.0)[-0.0275, 4.485]$$

$$N^{-sh\,\theta}_{\delta_{cc}\,B_{1c}} = -13696.0(0.00141)(1.102)(-9.363)$$

$$N^{-sh\,u}_{\delta_{cc}\,B_{1c}} = 52528.0(1.102)(-18.71)[0.0343, 2.091]$$

$$N^{\theta\;\;u}_{\delta_{cc}B_{1c}} = -199.18(0.347)(1.102)(-25.44)$$

Gust Input Numerators

$$N^{-sh}_{w_g} = 0.695(1.102)(10.0)^2[-0.0854, 0.2901][0.781, 1.123]$$

$$N^{-sh\,\theta}_{w_g\;\;B_{1c}} = 3.058(0.000557)(1.102)(-8.76)(10.0)(12.54)$$

*Numbers enclosed in parentheses are first-order factors, $(s + a) = (a)$. Quadratic factors are enclosed in brackets, $[s^2 + 2\zeta\omega s + \omega^2] = [\zeta;\omega]$. Other numbers are the transfer function gains.

TABLE 30

CH-53A LATERAL-DIRECTIONAL TRANSFER FUNCTION FACTORS
AT 60 KNOTS FOR BARE AIRCRAFT WITHOUT EFFECTIVE ACTUATION AND ROTOR LAGS

Denominator

$$\Delta = (0.095)(2.07)[0.239 , 0.997]$$

Control Input Numerators

$$N_{A_1}^{p} = 22.2(0.033)[0.306 , 0.965]$$

$$N_{A_1}^{r} = 0.0907(16.6)[0.046 , 2.06]$$

$$N_{A_1}^{a_y} = 32.5(-0.417)(1.79)[0.564 , 1.06]$$

$$N_{A_1}^{\dot{\lambda}} = 0.324[0.294 , 0.954][0.213 , 4.68]$$

$$N_{A_1}^{a_y'} = 32.8(-0.349)(2.092)[0.447 , 1.07]$$

$$N_{\delta_r}^{p} = 2.28(0.033)(-1.30)(1.31)$$

$$N_{\delta_r}^{r} = -5.09(2.04)[-0.006 , 0.341]$$

$$N_{\delta_r}^{a_y} = 16.9(-0.008)(-1.01)(1.67)(1.97)$$

$$N_{\delta_r}^{\dot{\lambda}} = 0.187(-0.971)(1.36)[0.489 , 2.21]$$

$$N_{\delta_r}^{a_y'} = 0.0140(-0.007)(-2.97)(2.06)(702)$$

$$N_{A_1\delta_r}^{\dot{\lambda}\ r} = -1.66(0)[0.225 , 4.66]$$

$$N_{A_1\delta_r}^{\dot{\lambda}\ a_y} = -0.614(-1.03)(1.69)(-11.4)(12.8)$$

$$N_{A_1\delta_r}^{p\ r} = -113(0)(0.043)$$

$$N_{A_1\delta_r}^{p\ a_y} = 301(0.033)(-0.974)(1.69)$$

$$N_{A_1\delta_r}^{p\ a_y'} = -74.6(0.033)[0.552 , 2.58]$$

$$N_{A_1\delta_r}^{\dot{\lambda}\ a_y'} = -6.14[-0.620 , 1.58][0.634 , 3.20]$$

TABLE 31

CH-53A LONGITUDINAL TRANSFER FUNCTION AT 60 KNOTS WITH PITCH SAS AND BASIC PITCH AFCS PLUS EFFECTIVE ACTUATION AND ROTOR LAGS

Denominator

$$\Delta = (0.0284)(0.717)(1.102)(6.48)(10.0)[0.509,2.275]$$

Control Input Numerators

$$N^{\theta}_{B_{1c}} = 4.41(0.00056)(0.668)(1.102)(10.0)(-10.314)$$

$$N^{-sh}_{B_{1c}} = -0.954(-0.0202)(1.102)(10.0)(-706.99) \times [0.0348,2.087]$$

$$N^{u}_{B_{1c}} = -16.9(0.693)(1.102)(10.0)(-19.112) \times [0.0343,2.091]$$

$$N^{-sh}_{\delta_{cc}} = -3110.0(0.0267)(1.102)(6.77)[0.4488,2.279]$$

$$N^{\theta}_{\delta_{cc}} = 20.162(0.01504)(0.4123)(1.102)(10.0)$$

$$N^{u}_{\delta_{cc}} = -32.1(0.4772)(1.102)(15.24)[-0.663,2.312]$$

$$N^{-sh\ \theta}_{\delta_{cc}\ B_{1c}} = -13696.0(0.00141)(1.102)(-9.363)$$

$$N^{-sh\ u}_{\delta_{cc}\ B_{1c}} = 52528.0(1.102)(-18.71)[0.0343,2.091]$$

$$N^{\theta\ u}_{\delta_{cc}\ B_{1c}} = -199.18(0.3472)(1.102)(-25.44)$$

Gust Input Numerators

$$N^{\theta}_{u_g} = -0.00324(0.0)(0.643)(1.102)(10.0)^2$$

$$N^{u}_{u_g} = 0.0227(0.681)(1.102)(9.4)(10.0) \times [0.0351,2.1680]$$

$$N^{-sh}_{u_g} = 0.0893(0.0)(1.102)(7.81)(10.0)[0.228,2.25]$$

$$N^{\theta}_{w_g} = -0.00797(0.0)(0.0224)(0.788)(10.0)^2$$

$$N^{u}_{w_g} = 0.000528(0.0)(0.791)(-0.7076)(10.0) \times (-14.22)(100.58)$$

$$N^{-sh}_{w_g} = 0.695(0.02851)(0.971)(7.032)(10.0) \times [0.4059,2.36]$$

$$N^{-sh\ \theta}_{w_g\ B_{1c}} = 3.058(0.000557)(-8.759)(10.0)(12.54)$$

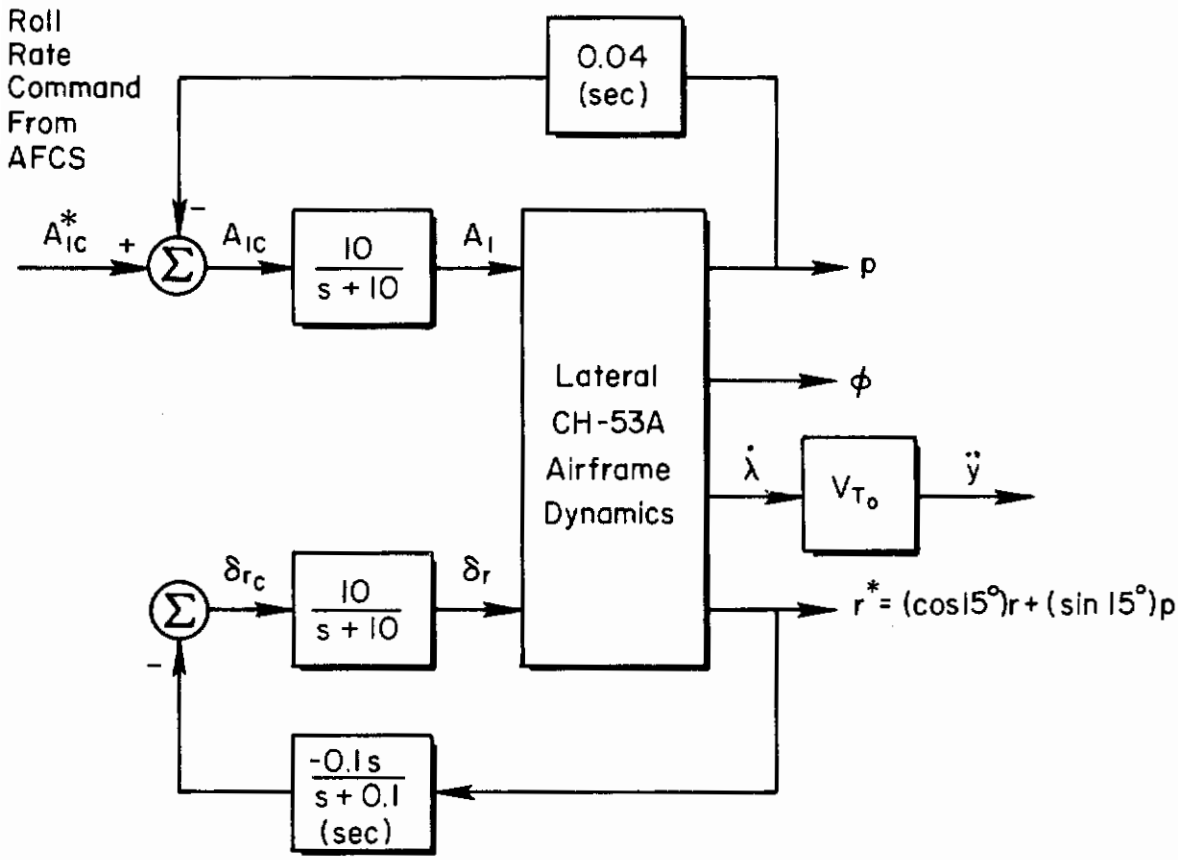

Figure 11. Lateral-Directional SAS Block Diagram

4. USAF Advanced Landing System Guidance Model

Figure 12 describes the vertical plane geometry for landing and the siting of the ground-based portion of the measuring system (Refs. 1 and 17). The reference flight path angle, Γ_o, is pilot selectable. (The value used here, -6 deg, actually exceeds the allowable range for this choice given in Ref. 17. This fact will be disregarded here.) The pilot may also select the glide path intercept point (GPIP) from a fixed set of alternatives. For the "typical" case illustrated in Fig. 12 where the elevation transmitting antenna is 2,500 ft from the runway threshold, the choices are

T − 500 ft
T + 0 ft
T + 500 ft
T + 1,000 ft

where T denotes the runway threshold. The particular choice assumed to be made here is that GPIP = T + 500 ft. This results in a value for B which is 2,000 ft.

The measurements assumed to be available in the USAF Advanced Landing System (refer to Fig. 12) are:

- Angular elevation, g, of aircraft as measured with respect to the elevation antenna site.
- Slant range, R_{DME}, between approaching aircraft and the elevation transmitter antenna site.
- Angular deviation in azimuth from the runway centerline, a, of aircraft as measured with respect to the azimuth antenna site.

The angular elevation, g, and the baseline dimension, B (as determined by the pilot's selection of the GPIP), can be combined to compute the angular elevation, f, of the aircraft with respect to the GPIP. The combination of g, f, B, R_{DME}, and the pilot's selection of a reference flight path angle, Γ_o, enable linear deviation from the reference flight path, d_e*, to be computed. The reference flight path is specified by the

*In the analysis which follows, h_e, which closely approximates d_e for small flight path angles, will be used in place of d_e.

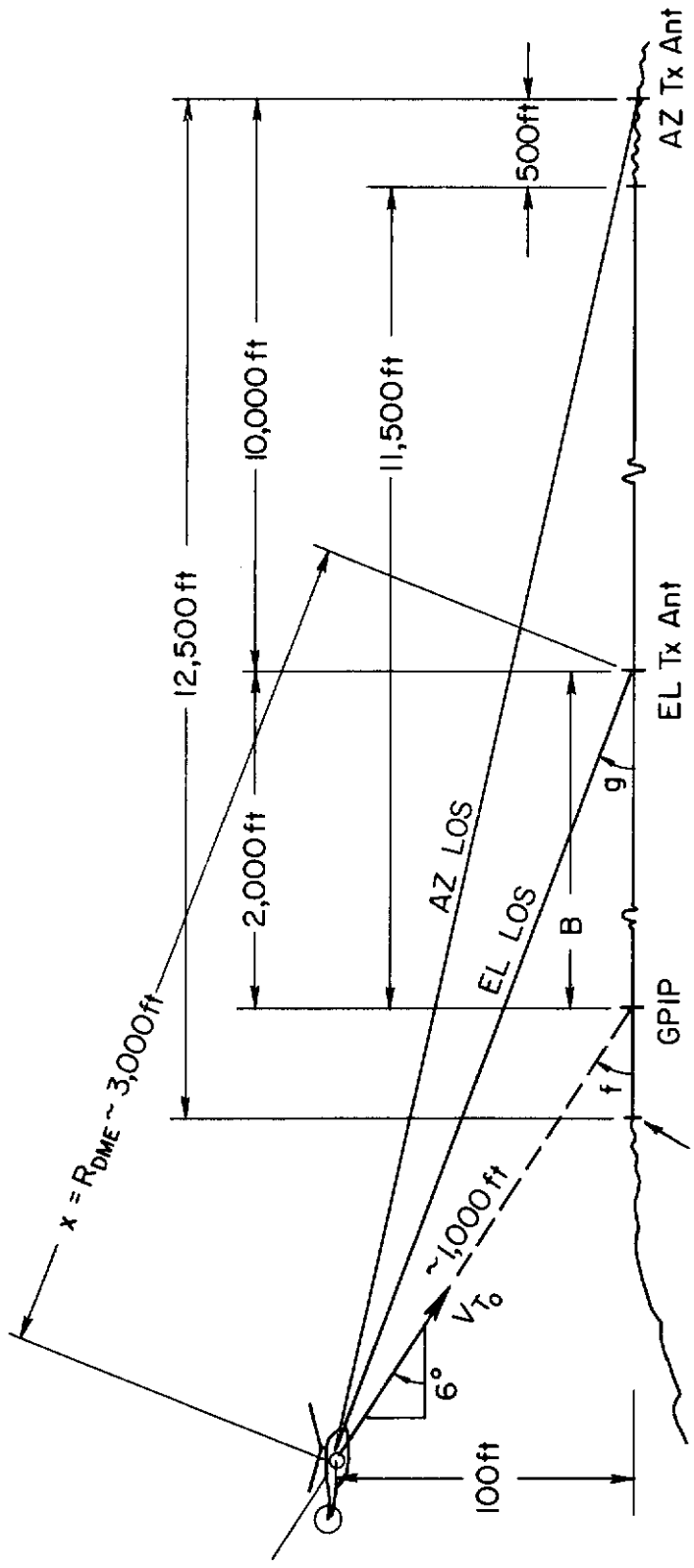

Figure 12. Assumed Geometry for Measurement System Site (Long-Runway Case)

pilot's selection of a reference flight path angle and a GPIP. The rms fluctuation in the elevation reference angle, g, is $\sigma_{EL} = 0.66$ mrad.

The power spectral density for the elevation reference fluctuation is

$$\Phi_g(\omega) = \frac{\sigma_{EL}^2 (0.2122)^2}{1 + \left(\frac{\omega}{14.14}\right)^2} \tag{4}$$

where $$\sigma^2 = \int_0^\infty \Phi(\omega) d\omega$$

In the work which follows, it will be assumed that the fluctuations in the elevation reference angle can be expressed as equivalent linear fluctuations about the ideal geometric reference flight path by merely multiplying by R_{DME}. That is:

$$\Phi_{d_c}(\omega) = R_{DME}^2 \Phi_g(\omega) = \frac{(R_{DME}\sigma_{EL})^2 (0.2122)}{1 + \left(\frac{\omega}{14.14}\right)^2} \tag{5}$$

The product, $R_{DME}\sigma_{EL}$, will be designated σ_{d_c}. The quantity, σ_{d_c}, is then the apparent RMS linear fluctuation of the radio reference flight path about the ideal geometric reference flight path. If R_{DME} = 2,960 ft, σ_{d_c} = 1.95 ft at the 100 ft altitude point depicted in Fig. 12.

The rms fluctuation in the azimuth angular reference is $\sigma_{AZ} = 0.50$ mrad. The power spectral density for the azimuth reference fluctuation is:

$$\Phi_a(\omega) = \frac{\sigma_{AZ}^2 (0.2122)^2}{1 + \left(\frac{\omega}{14.14}\right)^2} \tag{6}$$

Again, it is assumed that equivalent linear measures of the fluctuations are of interest, so that the corresponding power spectral density is:

$$\Phi_{y_c}(\omega) = \frac{[(R_{DME} + R_{WY})\sigma_{AZ}]^2(0.2122)^2}{1 + \left(\frac{\omega}{14.14}\right)^2} \qquad (7)$$

where R_{WY} is the distance between the elevation and azimuth transmitting antennas. Two different runway lengths are considered. For the long-runway case, R_{WY} is 12,000 ft, and for the short-runway case, R_{WY} is 2,000 ft. At an altitude of 100 ft on the approach path, the effective rms value of the fluctuations in linear measure is

$$\sigma_{y_c} = (R_{DME} + R_{WY})\sigma_{AZ} = \begin{matrix} 6.48 \text{ ft (long runway)} \\ 1.65 \text{ ft (short runway)} \end{matrix}$$

5. Atmospheric Disturbances

Overall performance of the system is critically dependent on the atmospheric disturbance environment in which it operates. In particular, it is necessary to examine performance in the presence of an appropriate set of nearly worst-case disturbances. The following types of atmospheric disturbances have been considered.

- Steady winds
- Wind shears
- Stochastic atmospheric gusts

Values for steady wind velocity and shearing gradient are displayed in Table 32 (Ref. 18). The steady winds range from a head-wind velocity of 25 kt to a tail-wind disturbance velocity of 10 kt. The wind shear is 0 kt/100 ft for altitudes greater than 200 ft and increases to 4 kt/100 ft for altitudes between 100 ft and 200 ft. The wind shear below 100 ft altitude does not affect performance at the approach window, the present concern.

The magnitudes given in Table 32 may be considered somewhat arbitrary, but they do represent a consensus of airline pilots as to what near worst-case values should be. It may be noted, however, that much larger shears are not infrequently encountered. In Table 32,

TABLE 32

SUMMARY OF "SEVERE" ATMOSPHERIC DISTURBANCES FOR LANDING APPROACH

TYPE OF DISTURBANCE	COMPONENT	DISTURBANCE VELOCITY		ALTITUDE (h) OR INTEGRAL SCALE (L) OF TURBULENCE (FT)	BREAK FREQUENCIES (DRYDEN FORM)(RAD/SEC)
		KT	FT/SEC		
Steady Wind	Head (H)	25	42.2	(throughout entire approach)	—
	Tail (−H)	10	16.9		—
	Crosswind (C)	−15	−25.4		—
Shear	$\pm dH/dh$ and $\pm\dot{H}$	0	0	$h \geq 200$	—
		4 kt/100 ft	$0.0675\dot{h}_o$ ft/sec^2	$100 \leq h \leq 200$	—
		8 kt/100 ft	$0.135\dot{h}_o$ ft/sec^2	$50 \leq h \leq 100$	—
		25 kt/100 ft	$0.422\dot{h}_o$ ft/sec^2	$0 \leq h \leq 50$	—
Stochastic Turbulence	$\pm dC/dh$ and $\pm\dot{C}$	0	0	$h \geq 200$	
		4 kt/100 ft	$-0.0675\dot{h}_o$ ft/sec^2	$0 \leq h \leq 200$	
		(rms)	(rms)		
	u_g	5.92	10.0	L_u = 672 ft	U_o/L_u
	w_g	3.85	6.5	L_w = 100 ft	$\sqrt{3}\,U_o/L_w$, U_o/L_w
	q_g	longitudinal gradient of w_g	refer to σ_{w_g}	L_w = 100 ft	$U_o\pi/4b$, U_o/L_w , $\sqrt{3}\,U_o/L_w$
	v_g	3.97	6.7	L_v = 100 ft	$U_o/\sqrt{3}\,L_v$, U_o/L_v
	p_g		0.0307 rad/sec		$\pi U_o/4b$

L_u, L_v, L_w = scale length (ft)

U_o = airplane's mean (trim) airspeed (ft/sec)

ω = frequency (rad/sec)

σ = standard deviation

Scale lengths are not well established at low altitudes. The entires in Table 32 are the result of choosing scale lengths appropriate to an altitude of 100 ft. On the other hand, the choice of mean square intensities appropriate to an altitude of 100 ft leads to rms values which were thought to be excessive. For this reason the rms gust velocities were chosen to be the ones from Ref. 10 appropriate to an altitude of 500 ft.

The stochastic gust components are represented as stationary random processes. The response time of a good landing system will be on the order of $3/\omega_c = 10$ sec or less. This indicates that the stochastic gust model parameters should probably be evaluated for a lower altitude where the gust effects will significantly affect performance at the window. A good choice of altitude might be 150 ft (approximately 5 sec before reaching the window), but to be slightly conservative, an altitude of 100 ft is recommended.

Power spectral densities for the gust components are listed below.

$$\Phi_{u_g}(\omega) = \sigma_{u_g}^2 \frac{2L_u}{\pi U_o} \frac{1}{1 + \left(\frac{L_u}{U_o}\omega\right)^2} \tag{8}$$

$$\Phi_{w_g}(s) = \sigma_{w_g}^2 \frac{L_w}{\pi U_o} \frac{1 + \left(\frac{\sqrt{3}\, L_w}{U_o}\omega\right)^2}{\left[1 + \left(\frac{L_w \omega}{U_o}\right)^2\right]^2} \tag{9}$$

$$\Phi_{v_g}(\omega) = \sigma_{v_g}^2 \frac{L_v}{\pi U_o} \frac{1 + 3\left(\frac{L_v}{U_o}\right)^2 \omega^2}{\left[1 + \left(\frac{L_v}{U_o}\right)^2 \omega^2\right]^2} \tag{10}$$

$$\Phi_{p_g}(\omega) = \sigma_{w_g}^2 \frac{\frac{0.8}{L_w U_o}\left(\frac{\pi L_w}{4b}\right)^{1/3}}{1 + \left(\frac{4b}{\pi U_o}\right)^2 \omega^2} \tag{11}$$

where $$\sigma_{(\,)}^2 = \int_o^\infty \Phi_{(\,)}(\omega)\, d\omega \tag{12}$$

The effective pitching gusts are obtained from the normal gust variable, w_g, by using the equation given at the bottom of Table 20. Similarly, the effective yawing gusts are obtained from the side gust variable, v_g, by using the equation given at the bottom of Table 21.

B. SUMMARY OF THE APPROACH COUPLER DESIGNS AND PERFORMANCE

The longitudinal and lateral-directional dynamics for the CH-53A helicopter which have been given in Tables 29 and 30 are typical for a single articulated rotor helicopter. Below, descriptions of the longitudinal and lateral-directional approach coupler systems are given.

1. Longitudinal Approach Coupler

There are two basic ways in which the CH-53A longitudinal approach coupler might be configured for the 60 kt flight condition. These ways involve the following alternative loop closures.

- d or h $\rightarrow B_{1c}$; u, $\theta \rightarrow \delta_{cc}$
- d or h $\rightarrow \delta_{cc}$; u, $\theta \rightarrow B_{1c}$

Both methods can give sufficient damping in the short-period mode and small time constant in a speed subsidence mode. Either glide slope deviation, d, or altitude, h, may be fed back because the effect of speed changes in $\dot{d} = \dot{h} - u \sin \gamma_o$ is small.

In the first alternative, the CH-53A is flown like a conventional aircraft, but it is observed from Table 24 that Z_{B_1} goes to zero as U_o goes to zero. This makes control over altitude impossible by this control technique as airspeed goes to zero.

In the second alternative, the CH-53A is flown like a conventional helicopter in low speed flight. Also, it is observed from Table 24 that Z_{δ_c} is not very sensitive to airspeed, and in particular it does not become zero as airspeed goes to zero. Thus, by this control technique, altitude control is possible at zero airspeed. Pilots would probably find the first alternative more natural to monitor. However, the second alternative in which glide path (altitude) regulation is accomplished through collective pitch has been selected since interest is in advanced system concepts. Advanced systems should be such that approach at very low airspeed is a distinct possibility.

Notice that in the second alternative, pitch angle is used to control airspeed. Therefore, the speed response to u_g gusts is relatively slow when the u, $\theta \rightarrow B_{1_c}$ loop gain is sufficiently low that reasonable pitch angle response results. This means the u_g gusts tend to make the aircraft balloon or fall. This problem can be solved by adding a $u_{AS} \rightarrow \delta_{cc}$ path for high frequency direct lift control.

A block diagram for the CH-53A longitudinal automatic approach control system is given in Fig. 13. Included are feedbacks $h \rightarrow \delta_{cc}$; $u, \theta \rightarrow B_{1c}$; and $u_{AS} \rightarrow \delta_{cc}$. The transfer functions used for the feedback and feedforward blocks are summarized in Table 33 and Table 34 for a straightforward design and an advanced design, respectively. Two different longitudinal designs are presented here in order to place emphasis upon the performance benefits which can accrue from relatively modest design refinements.

The straightforward design may be implemented as indicated in Fig. 13. The advanced design must be implemented in the manner shown at the top of Fig. 14.

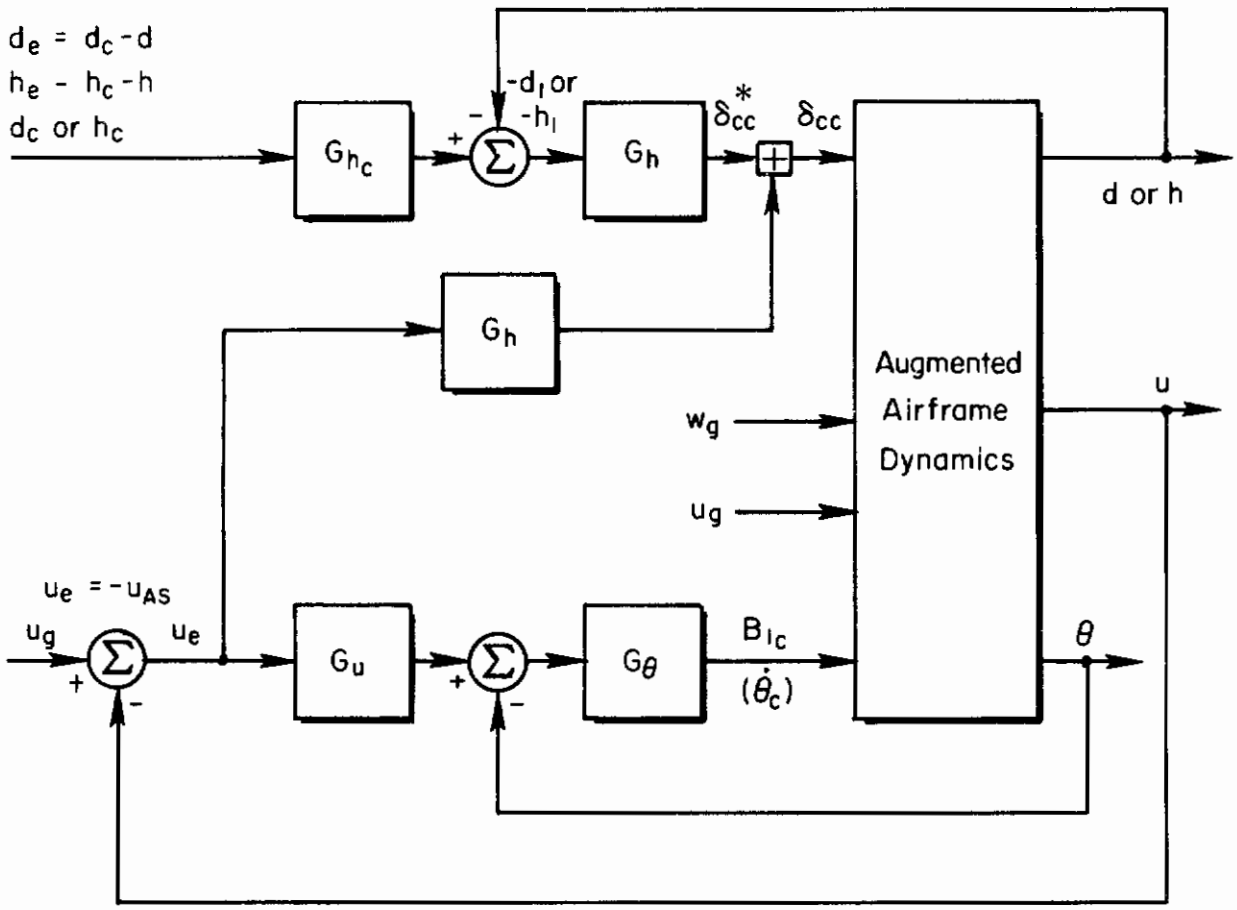

Figure 13. Automatic Flight Control System Conceptual Block Diagram for CH-53A Longitudinal Approach Control

TABLE 33

SYSTEM CONTROLLER TRANSFER FUNCTIONS FOR STRAIGHTFORWARD DESIGN

FEEDFORWARD AND FEEDBACK TERMS		CONTROLLER GAINS SELECTED	
G_θ	k_2	k_2	−0.07
G_u	k_1	k_1	−0.035 rad/ft/sec
G_h	$\frac{10k_h^{\cdot}(s+0.71)}{(s+2)(s+5)}$	$k_h^{\cdot}$	0.004 rad/ft/sec
G_{h_c}	1		—
G_c	k_c	k_c	0.001 rad/ft/sec

TABLE 34

SYSTEM CONTROLLER TRANSFER FUNCTIONS FOR ADVANCED DESIGN

FEEDFORWARD AND FEEDBACK TERMS		CONTROLLER GAINS SELECTED	
G_θ	$\frac{1.5k_2}{s+1.5}$	k_2	−0.07
G_u	k_1	k_1	−0.035 rad/ft/sec
G_h	$\frac{2k_h^{\cdot}(s+0.1)(s+0.71)}{s(s+2)}$	$k_h^{\cdot}$	0.0035 rad/ft/sec
G_{h_c}	$\frac{(0.333)^2}{s^2+2(0.7)(0.333)s+(0.333)^2}$		—
G_c	$\frac{k_c}{s+1}$	k_c	0.001 rad/ft/sec
C_2	$\frac{s+0.470}{s^2+2(0.7)(0.333)s+(0.333)^2}$		—

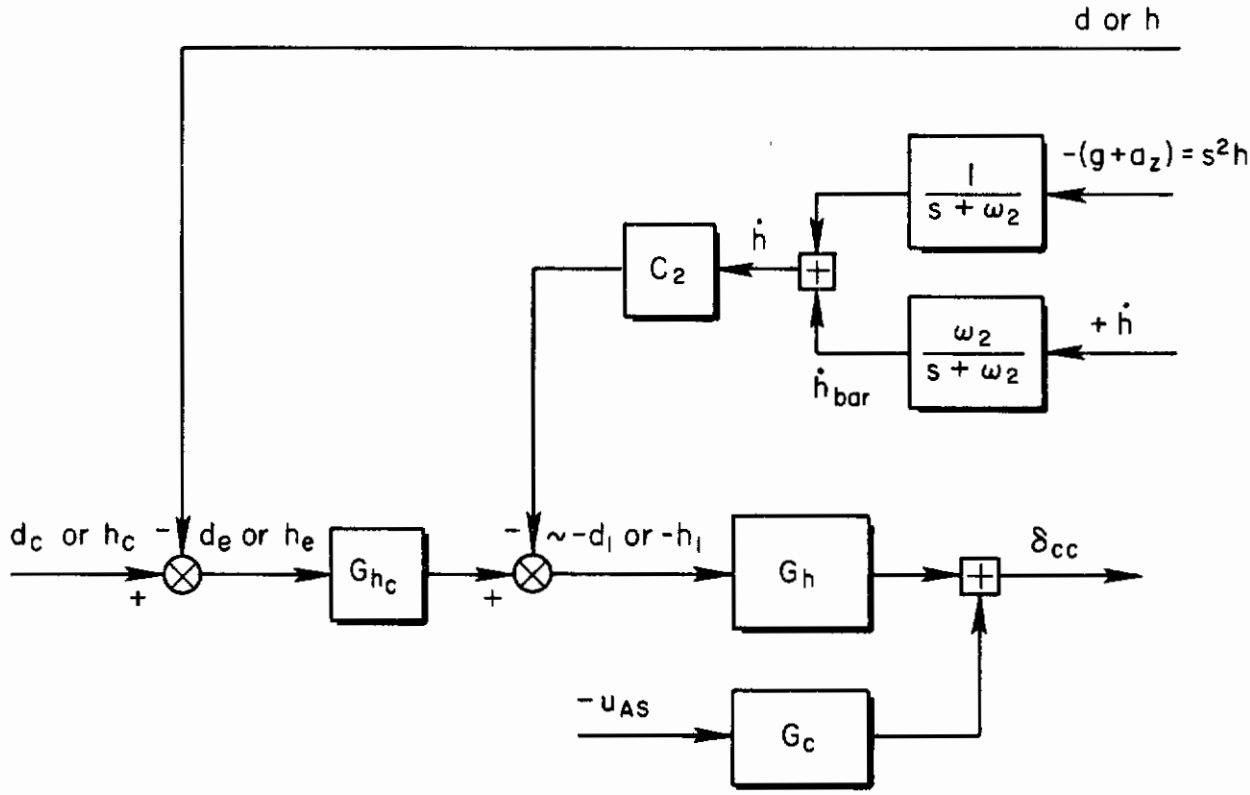

Actual Block Diagram

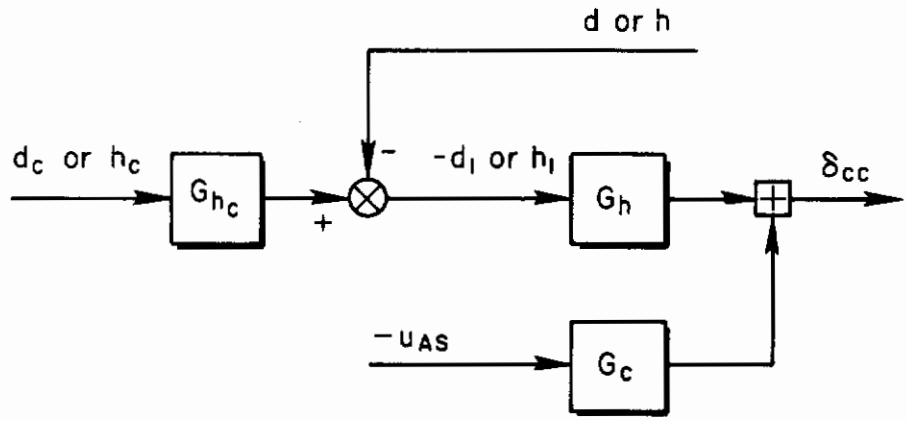

Equivalent Block Diagram

Figure 14. Actual and Equivalent Representations of Feedbacks to δ_{cc} for Advanced Design

The closed-loop transfer function for glide slope tracking is:

$$\frac{d}{d_c} \triangleq \frac{h}{h_c} = \frac{124.4(0.119)(0.71)(1.102)(6.7)[0.426, 2.323]}{(0.119)(0.71)(1.102)(9.65)[0.337,1.383][0.478,2.44][0.997,6.4]} \quad (13)$$

The resulting closed-loop bandwidth for glide slope tracking based upon ±3 dB is 1.03 rad/sec.

Table 35 summarizes system performance in terms of the rms values of key variables in response to the various stochastic command and disturbance inputs. Table 36 summarizes the responses in altitude, altitude rate, airspeed, and pitch attitude to wind and wind shear at the approach window for the straightforward design. It is assumed for the purpose of these computations that the wind shear does not affect the time to go from h = 200 ft to h = 100 ft. The nominal time to descend from 200 ft to 100 ft altitude is 9.47 sec.

In order to have a high probability of flying through the longitudinal approach window on any given approach, the rms values of glide slope deviation and airspeed error should be approximately one-third or less of the longitudinal window dimension given in Fig. 10. One-third of these window dimensions correspond to a 4.0 ft glide slope deviation and to 2.81 ft/sec in airspeed deviation.

The rms value of glide slope deviation is 4.003 ft which is almost precisely equal to the target design value of 4.0 ft for the Cat II "window." The rms value for airspeed error is 7.86 ft/sec. This is somewhat higher than the design target of 2.81 ft/sec. However, if airspeed is smoothed in a manner which likely characterizes a pilot's judgment of airspeed deviation, the rms value is 2.15 ft/sec. (The smoothing used to arrive at this value is a first-order lag having a 20 sec time constant.) If airspeed is smoothed by a first-order lag having a 10 sec time constant, the rms smoothed airspeed error is 3.38 ft/sec. Therefore, the straightforward design offers a high probability of passing through the Cat II window successfully on any one approach in the absence of wind and wind shear.

TABLE 35

SYSTEM PERFORMANCE IN TERMS OF RMS VALUES
FOR STRAIGHTFORWARD DESIGN

VARIABLE	RMS
Glide slope deviation	4.003 ft
Pitch attitude angle	1.701 deg
Longitudinal cyclic pitch	1.010 deg
Longitudinal cyclic pitch rate	2.690 deg/sec
Collective pitch	0.940 deg
Collective pitch rate	2.280 deg/sec
Altitude	3.496 ft
Altitude rate	3.220 ft/sec
Perturbation in longitudinal velocity	6.644 ft/sec
Airspeed perturbation velocity	7.861 ft/sec
Smoothed airspeed (filtered with $0.1/(s+0.1)$)	3.375 ft/sec
Smoothed airspeed (filtered with $0.05/(s+0.05)$)	2.148 ft/sec
Longitudinal cyclic pitch for SAS	0.681 deg
Longitudinal cyclic pitch rate for SAS	1.530 deg/sec
Longitudinal cyclic pitch for automatic flight control system	0.925 deg
Longitudinal cyclic pitch rate for automatic flight control system	2.24 deg/sec

TABLE 36

WIND AND WIND SHEAR RESPONSE FOR STRAIGHTFORWARD DESIGN AT THE APPROACH WINDOW

VARIABLE	WIND SHEAR	TAIL WIND	HEAD WIND	TOTAL RESPONSE TO DETERMINISTIC ATMOSPHERIC DISTURBANCES			
	S	W_T*	W_H*	$W_T + S$	$W_T - S$	$W_H + S$	$W_H - S$
Altitude, h ft	−0.319	1.37	−3.42	1.05	1.69	−3.74	−3.10
Airspeed, u_{AS} ft/sec	−4.27	0.148	−0.370	−4.12	4.41	−4.64	3.90
Pitch Attitude, θ rad	−0.0134 (−0.769 deg)	−0.000729 (−0.0418 deg)	0.00182 (0.104 deg)	−0.014144 (−0.81 deg)	0.01269 (0.727 deg)	−0.0116 (−0.664 deg)	0.01524 (0.8731 deg)
Altitude Rate, $\dot{h}$ ft/sec	−0.0523	0.0	0.0	−0.0523	0.0523	−0.0523	0.0523

*Non-zero steady-state responses to steady head- or tailwinds are due solely to the Z body-axis component of these winds.

The rms value of pitch attitude, 1.70 deg, is somewhat on the high side for pilot acceptability. However, it must be borne in mind that the disturbance environment used here is a nearly worst case. In view of this, the rms pitch attitude is probably acceptable.

Design target values for the rms values of $B_{1_{SAS}}$, $B_{1_{AFCS}}$, $\dot{B}_{1_{AFCS}}$, δ_c, $\dot{\delta}_c$ have been given previously in Table 28. It is observed that the rms value for the AFCS longitudinal cyclic pitch rate and the collective pitch rate are higher than the design target values. The rms values of $B_{1_{SAS}}$, $B_{1_{AFCS}}$, and δ_c are well within the design target values.

Inspection of Table 36 reveals that the response in altitude deviation to deterministic aerodynamic disturbances is mainly the result of steady head wind or tail wind. The response in airspeed error to deterministic aerodynamic disturbances is mainly the result of wind shear. The contribution to airspeed error due to wind shear is -.27 ft/sec. This is probably not crucial for VTOL vehicles such as the CH-53A which are capable of hover. This is because it may be argued that the Cat II window airspeed limits shown in Fig. 10 are not appropriate here since lift changes due to airspeed changes can always be compensated for by using direct lift control. The response in altitude rate due to steady wind is zero. The response in pitch attitude due to steady wind and wind shear is acceptable.

Thus the straightforward design tends to have the following unacceptable features in view of the initial design target values:

- Rate limits required on collective pitch and longitudinal cyclic pitch for the automatic flight control functions are higher than the design target rate limits.
- Response in altitude deviation to steady winds is excessive.

Otherwise, the design is commendable for both its performance and simplicity.

The straightforward system gives acceptable rms altitude response to w_g gusts. This is largely the result of the high gain in the rate path of the δ^*_{cc}/h_e transfer function.

$$\frac{\delta_{cc}^{*}}{h_1} = \frac{\delta_{cc}}{h_e} = \frac{10k_{\dot{h}}^{\cdot}(s+0.71)}{(s+2)(s+5)} \quad ; \quad k_{\dot{h}}^{\cdot} = 0.004 \text{ rad/ft/sec}$$

However, the high gain in the $\dot{h}_c \rightarrow \delta_c$ path produces high collective pitch rates, $\dot{\delta}_c$. This is because h_c has a flat power spectral density out to approximately 14.0 rad/sec.

This suggests that an advanced design concept should strive to lower the gain at high frequencies in the $\dot{h}_c \rightarrow \delta_c$ path while maintaining the gain at all frequencies in $\dot{h} \rightarrow \delta_{cc}$ path. The gain in the $\dot{h} \rightarrow \delta_{cc}$ path is approximately $k_{\dot{h}}^{\cdot}$. Such a feature of the advanced design can be mechanized by means of complementary filtering techniques for the construction of a broadband, low-noise altitude signal. Since the ideal reference flight path is a straight line, the absolute altitude reference, $(h_c - h)$, need be retained only at very low frequencies.

The complementary filtering scheme is as follows. $\dot{h}$ is reconstructed from measurement of barometric rate of climb and normal acceleration measured at or near the vehicle center of gravity. The result is calculated instantaneous vertical speed (IVS) or $\dot{h}$. This is obtained using complementary filtering on $\dot{h}_{bar}$ and $-a_z$. This is shown as a portion of the Actual Block Diagram in Fig. 14 which generates the input to the block C_2. The equations for developing $\dot{h}$ from the two measurements are:

$$\frac{1}{s+\omega_2}(-g-a_z) + \dot{h}_{bar} = \dot{h} \tag{14}$$

where

$$\dot{h}_{bar} = \frac{\omega_2}{s+\omega_2}\dot{h} \tag{15}$$

Clearly, $-(g+a_z) = s\dot{h}$ if normal acceleration is measured at the center of gravity, so that Eq. 14 becomes

$$\left(\frac{s}{s+\omega_2} + \frac{\omega_2}{s+\omega_2}\right)\dot{h} = \dot{h} \tag{16}$$

since

$$\frac{s}{s+\omega_2} + \frac{\omega_2}{s+\omega_2} = 1 \tag{17}$$

In the second stage of complementary filtering, G_{h_c} low-pass filters the signal, h_e, and C_2 filters signal, $\dot{h}$, in such a way that the transfer function from $-h$ to $-h_1$ is unity and the transfer function from h_c to $-h_1$ is G_{h_c}. The equation expressing the first condition is:

$$-G_{h_c}h - shC_2 = -h_1 \tag{18}$$

where

$$G_{h_c} + C_2 s = 1 \tag{19}$$

G_{h_c} should be selected such that C_2 has more poles than zeros. To obtain a relatively sharp cutoff in the h_c path without resorting to the use of high-order filters, we have selected the following transfer function for G_{h_c}.

$$G_{h_c} = \frac{\omega_1^2}{s^2 + 2.0(0.7)\omega_1 s + \omega_1^2} \tag{20}$$

This leads to a transfer function for C_2 which is:

$$C_2 = \frac{s + 1.4\omega_1}{s^2 + 2.0(0.7)\omega_1 s + \omega_1^2} \tag{21}$$

The bandwidth for G_{h_c}, ω_1 has been somewhat arbitrarily selected as 0.333 rad/sec. Other values of ω_1 might be selected, but experience has shown that bandwidth of 0.333 rad/sec for following the reference glide slope is acceptable.

Next consider what additional compensation in the G_h block of Fig. 14 may be appropriate for further improving the straightforward design. The excessive response in altitude deviation in response to steady winds indicates that integral by-pass compensation be used in the $h_1 \rightarrow \delta_{cc}$ path. Furthermore, the high frequency filtering, $5/(s+5)$, is no longer required because h_c has been low-pass filtered by G_{h_c}. This filter is eliminated in the advanced design. The transfer function for G_h then becomes:

$$G_h = \frac{2.0k_{\dot{h}}(s+0.1)(s+0.71)}{s(s+2.0)} \tag{22}$$

Considerable collective pitch rate, $\dot{\delta}_c$, can still result from the $u_{AS} \rightarrow \delta_{cc}$ path of the controller, however. The straightforward design uses a gain in this path. It is self-evident, however, that direct lift control in response to high frequency fluctuations in airspeed is not really essential. Since this control can contribute to high collective pitch rates, it will be helpful to introduce a low-pass filter into the $u_{AS} \rightarrow \delta_{cc}$ path. A first-order filter with a 1.0 rad/sec break frequency is appropriate, since this break frequency is several times the u_g gust disturbance bandwidth, 0.15 rad/sec. The transfer function for G_c then becomes:

$$G_c = \frac{k_c}{s+1.0} \tag{23}$$

Considerations similar to those discussed in connection with the $u_{AS} \rightarrow \delta_{cc}$ path also motivate the introduction of low-pass filtering into the $u, \theta \rightarrow B_{1_c}$ path. This will result in reduction of the AFCS longitudinal cyclic pitch rate, $\dot{B}_{1_{AFCS}}$. The transfer function for G_θ then becomes:

$$G_\theta = \frac{1.5k_2}{s+1.5} \tag{24}$$

The resulting closed-loop transfer function for glide slope beam tracking is:

$$\frac{h}{h_c} = \frac{2.42(0.100)(0.127)(0.710)(1.00)(1.48)(6.79)[0.432, 2.25]}{(0.128)(0.721)(0.975)(1.10)(1.47)(6.55)(10.2)[0.700, 0.333][0.507, 1.39][0.527, 2.31]} \tag{25}$$

The closed-loop glide slope tracking bandwidth based upon ±3 dB is 0.375 rad/sec.

Table 37 summarizes system performance in terms of the rms values of key variables in response to the various stochastic command and disturbance inputs. Table 38 summarizes the responses in altitude, altitude rate, airspeed, and pitch attitude to wind and wind shear at the approach window for the advanced design.

The rms value of glide slope deviation is 3.93 ft, which is less than the target design value of 4.0 ft for the Cat II window. The rms value for airspeed error is 8.14 ft/sec. This is somewhat higher than the design target of 2.81 ft/sec. However, again, if airspeed is smoothed in a manner which likely characterizes a pilot's judgment of airspeed deviation (i.e., with a 20 sec lag), the rms value is 2.21 ft/sec. If airspeed is smoothed by a first-order lag having a 10 sec time constant, the rms smoothed airspeed error is 3.48 ft/sec. Therefore, the advanced design offers a high probability of passing through the Cat II window successfully on any one approach in the absence of wind and wind shear.

The rms value of pitch attitude is still somewhat on the high side for pilot acceptability. However, again, it must be borne in mind that the disturbance environment is nearly worst-case. In view of this, the rms pitch attitude may be acceptable.

Design target values for the rms values of $B_{1_{SAS}}$, $B_{1_{AFCS}}$, $\dot{B}_{1_{AFCS}}$, δ_c, $\dot{\delta}_c$ have been given previously in Table 28. It is observed that the rms values for these control variables are all now within the design target values.

Inspection of Table 38 reveals that the response in altitude deviation to steady wind is zero because of the integral by-pass. The response in airspeed error to deterministic aerodynamic disturbances is mainly the result of wind shear. The contribution in airspeed error due to wind shear is −4.40 ft/sec. Again, this is probably not crucial in VTOL vehicles such as the CH-53A which are capable of hover. The response in altitude rate due to steady wind is zero. The response in pitch attitude due to steady wind and wind shear is acceptable. Thus, the advanced design is fairly satisfactory if one accepts the argument that response in airspeed error to deterministic aerodynamic disturbances is not crucial for vehicles capable of hover.

TABLE 37

SYSTEM PERFORMANCE IN TERMS OF RMS VALUES FOR ADVANCED DESIGN

VARIABLE	RMS
Glide slope deviation	3.932 ft
Pitch attitude angle	1.640 deg
Longitudinal cyclic pitch	0.810 deg
Longitudinal cyclic pitch rate	1.580 deg/sec
Collective pitch	0.793 deg
Collective pitch rate	0.715 deg/sec
Altitude	3.414 ft
Altitude rate	2.827 ft/sec
Perturbation in longitudinal velocity	6.742 ft/sec
Airspeed perturbation velocity	8.142 ft/sec
Smoothed airspeed (filtered with $0.1/(s+0.1)$)	3.483 ft/sec
Smoothed airspeed (filtered with $0.05/(s+0.05)$)	2.205 ft/sec
Longitudinal cyclic pitch for SAS	0.566 deg
Longitudinal cyclic pitch rate for SAS	1.220 deg/sec
Longitudinal cyclic pitch for automatic flight control system	0.708 deg
Longitudinal cyclic pitch rate for automatic flight control system	1.156 deg/sec

TABLE 38

WIND AND WIND SHEAR RESPONSE FOR ADVANCED DESIGN AT THE APPROACH WINDOW

VARIABLE	WIND SHEAR	TAIL WIND	HEAD WIND	TOTAL RESPONSE TO DETERMINISTIC ATMOSPHERIC DISTURBANCES			
	S	W_T*	W_H*	$W_T + S$	$W_T - S$	$W_H + S$	$W_H - S$
Altitude, h ft	−0.300	0.0	0.0	−0.300	0.300	−0.300	0.300
Airspeed, u_{AS} ft/sec	−4.40	0.148	−0.37	−4.25	4.55	−4.77	4.03
Pitch Attitude, θ rad	−0.0134 (−0.767 deg)	−0.000729 (−0.0418 deg)	0.00182 (0.1043 deg)	−0.0141 (−0.809 deg)	0.0127 (0.725 deg)	−0.0116 (−0.663 deg)	0.0152 (0.871 deg)
Altitude Rate, $\dot{h}$ ft/sec	−0.0196	0.0	0.0	−0.0196	0.0196	−0.0196	0.0196

*Non-zero steady-state responses to steady head- or tailwinds are due solely to the Z body-axis component of these winds.

2. Lateral-Directional Approach Coupler

A single advanced configuration lateral-directional coupler for the CH-53A at the 60 kt flight conditions was investigated. A block diagram illustrating the basic control concept is shown in Fig. 15. The feedbacks are $\varphi \rightarrow A_{1c}^{*}$ for bank angle stabilization, $y_e' \rightarrow A_{1c}^{*}$ for path regulation, and $\dot{y} \rightarrow A_{1c}^{*}$ for path damping. The low-pass filter, G_c, is introduced to prevent the broad bandwidth noise on the guidance from exciting the actuators. The transfer functions and gains used in Fig. 15 are given in Table 39.

TABLE 39

SYSTEM CONTROLLER TRANSFER FUNCTIONS

FEEDFORWARD AND FEEDBACK TERMS		CONTROLLER GAINS SELECTED	
$G_{A_{1c}^{*}}$	$\frac{s + 0.24}{s + 0.105}$		
G_c	$\frac{(0.3)^2}{s^2 + 2(0.5)0.3s + (0.3)^2}$		
G_F	$\frac{s + 0.42}{s^2 + 2(0.5)0.3s + (0.3)^2}$		
G_W	$\frac{1}{s + 0.03}$		
G_I	$\frac{s + 0.03}{s}$		
		K_φ	0.18
		$K_{\dot{y}}$	0.0594 sec/ft
		K_y	0.00356/ft

All of the signals used for feedback in Fig. 15 are not directly measurable. In actual practice the controller configuration shown in Fig. 16 would be used. This provides a close approximation to the signals

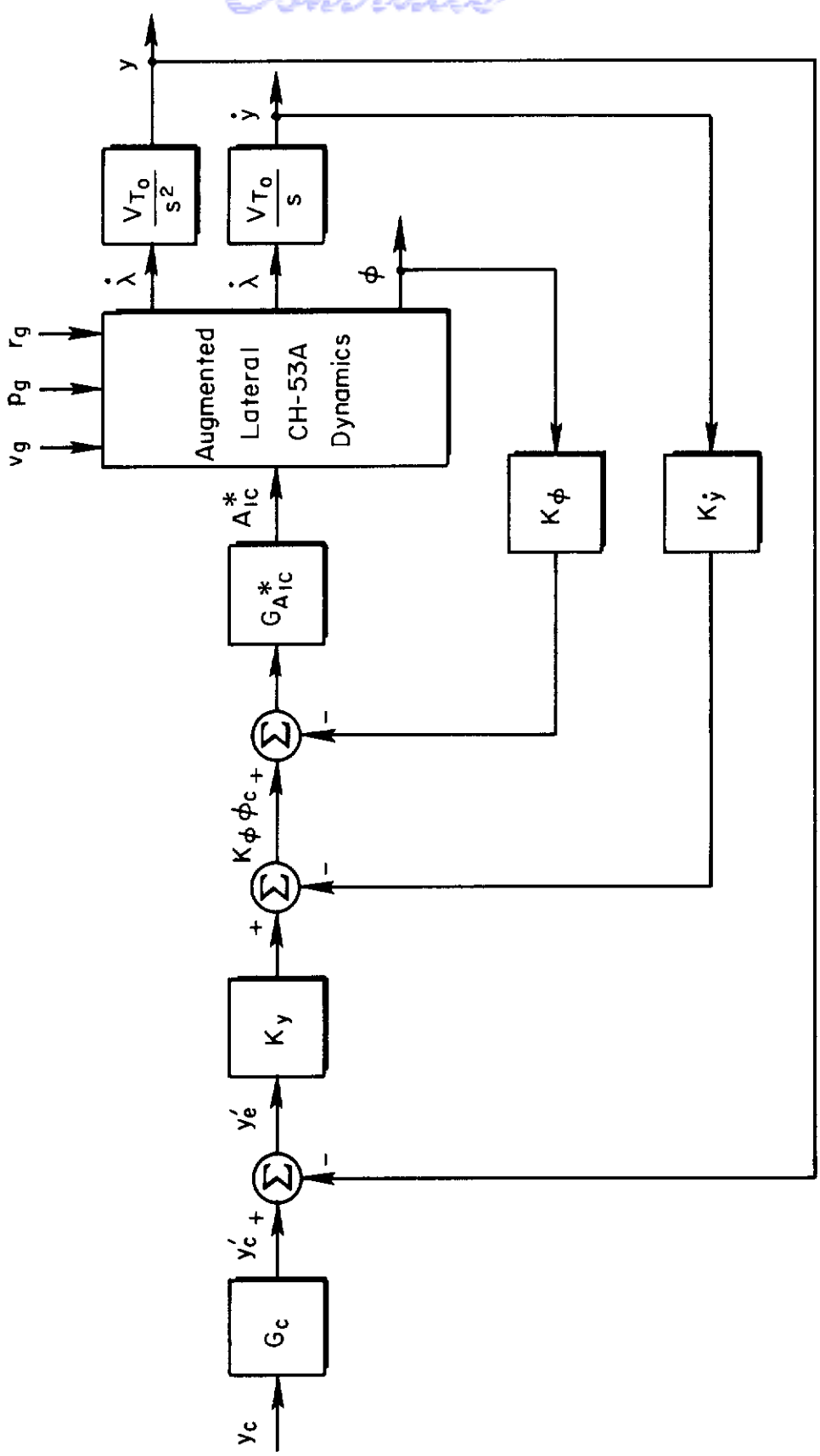

Figure 15. Conceptual Lateral-Directional Coupler Design

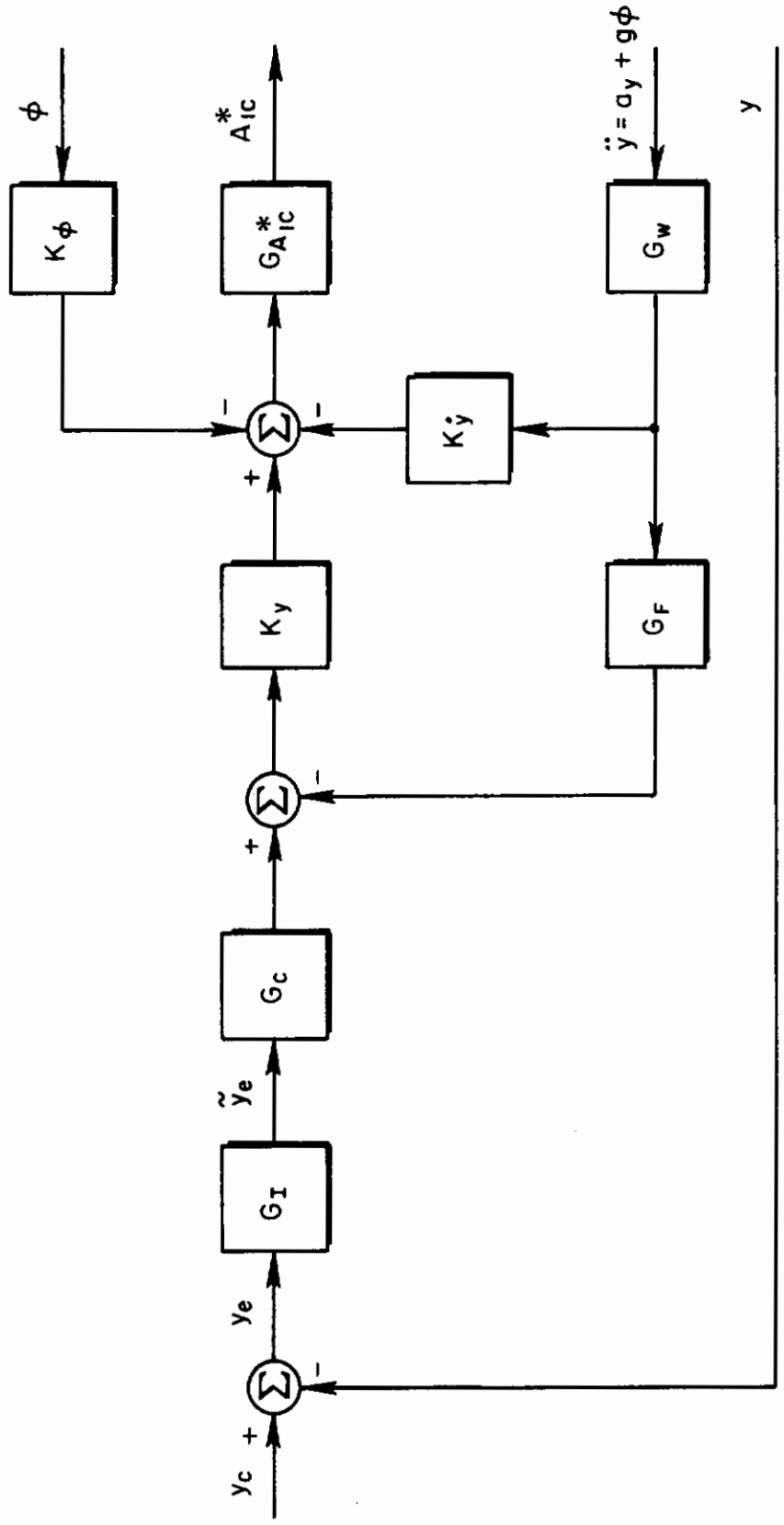

Figure 16. AFCS Localizer Coupler Mechanization

used in Fig. 15. The filter, G_W, is a pseudo-integrator which produces an approximation to $\dot{y}$ at mid- and high frequencies. G_F is a filter which is approximately complementary to G_C so that the y feedback is in effect unfiltered, while the forward path from y_c is low-pass filtered by G_C. Stated another way

$$G_C + sG_F \doteq 1 \tag{26}$$

An integral by-pass, G_I, has been inserted in the y_e feedback to suppress beam standoff errors.

The closed-loop transfer function for localizer tracking is:

$$\frac{y}{y_c} = \frac{0.104(0.0300)^2(0.107)(0.240)(9.15)[0.583, 0.955][0.105, 4.74]}{(0.0220)(0.0876)(0.106)(0.303)(0.595)(1.78)(9.31)^2[0.981, 0.234][0.437, 0.859][0.166, 1.40]} \tag{27}$$

The closed-loop bandwidth for localizer tracking may be determined from Fig. 17. If one neglects the peak of +3.5 dB, then the bandwidth based upon the −3 dB point is 0.350 rad/sec. The peak of +3.5 dB is troublesome as transient responses in the next section will show. Subsequent investigation has shown that the peak may be reduced by locating the integral by-pass in the path preceding K_y in Fig. 16 instead of in the path preceding G_C.

Table 40 summarizes system performance in terms of the rms values of key variables in response to the various stochastic command and disturbance inputs. Table 41 summarizes the responses in lateral deviation, lateral deviation rate, sideslip angle, yaw attitude, and bank angle to wind and wind shear at the approach window for the advanced design.

The rms value of localizer deviation is 1.95 ft for the short-runway case and 6.64 ft for the long-runway case. These figures are both far less than the design target, 24.0 ft. Therefore, this design offers a high probability of passing through the Cat II window successfully on any one approach in the absence of wind and wind shear.

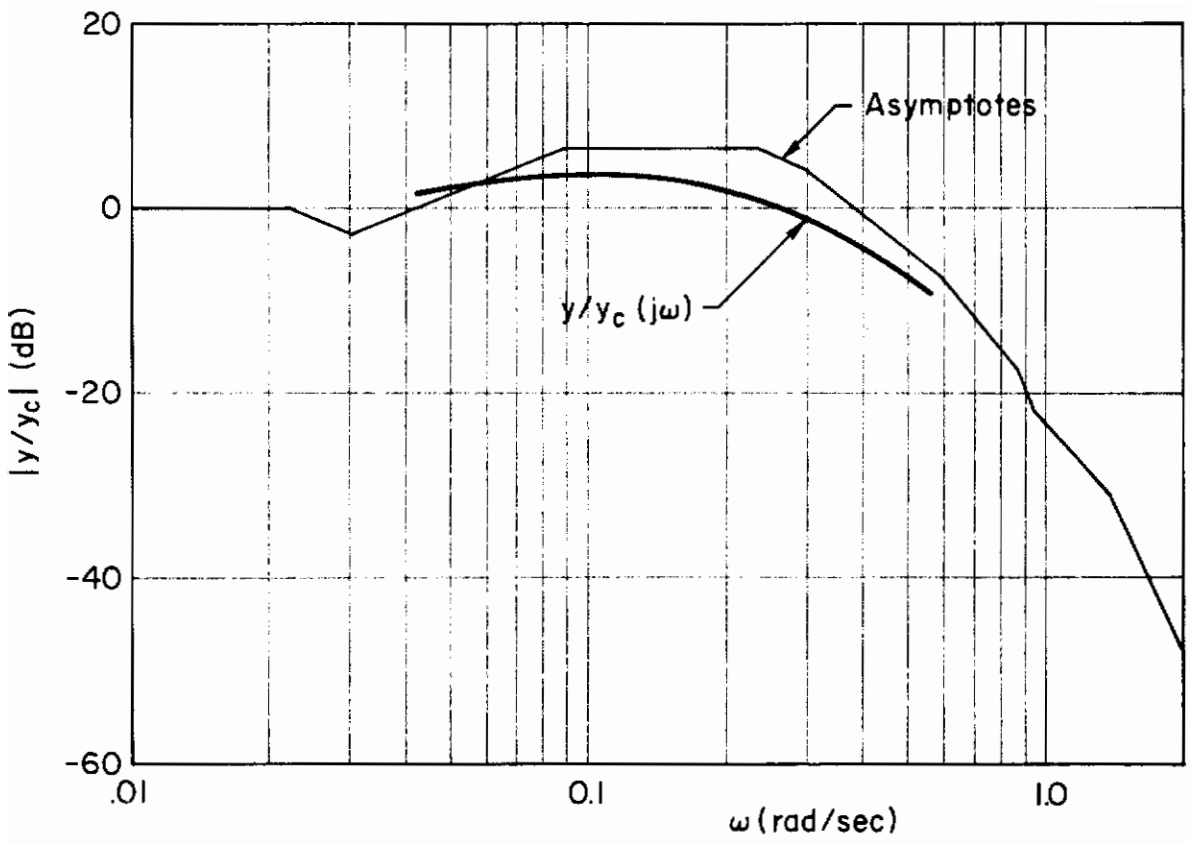

Figure 17. Frequency Response Function for y/y_c

TABLE 40

SYSTEM PERFORMANCE IN TERMS OF RMS VALUES FOR ADVANCED DESIGN

VARIABLE	RMS A*	RMS B*
Localizer deviation, y_e ft	1.952	6.643
Roll attitude angle, φ deg	1.873	1.905
Roll rate, p deg/sec	2.508	2.533
Heading angle, ψ deg	1.610	1.620
Yaw rate, $\dot{\psi}$ deg/sec	0.8715	0.8778
Sideslip angle, β deg	1.703	1.710
Sideslip rate, $\dot{\beta}$ deg/sec	1.196	1.204
Lateral cyclic pitch, $A_{1_{AFCS}}$ deg	0.3172	0.3203
Lateral cyclic pitch rate, $\dot{A}_{1_{AFCS}}$ deg/sec	0.403	0.408
Tail rotor collective pitch, δ_r deg	0.0985	0.09884
Tail rotor collective pitch rate, $\dot{\delta}_r$ deg/sec	0.1316	0.1318
Lateral cyclic pitch, $A_{1_{SAS}}$ deg	0.0974	0.0985
Lateral cyclic pitch rate, $\dot{A}_{1_{SAS}}$ deg/sec	0.1593	0.1604
Total lateral cyclic pitch, A_1 deg	0.3151	0.3169
Total lateral cyclic pitch rate, $\dot{A}_1$ deg/sec	0.4102	0.4130
Lateral deviation from the ideal geometric reference, y ft	1.043	1.462
Lateral rate of deviation from the ideal geometric reference, $\dot{y}$ ft/sec	0.5780	0.6409

*A = short-runway case. B = long-runway case.

TABLE 41

WIND AND WIND SHEAR RESPONSE FOR ADVANCED DESIGN AT THE APPROACH WINDOW

OUTPUT VARIABLE at t = 9.47 sec	CROSSWIND SHEAR	CROSSWIND STEADY-STATE RESPONSE	TOTAL RESPONSE TO DETERMINISTIC WIND DISTURBANCE	
	$S = \int \dot{C} dt$	CW	CW + S	CW − S
Roll Attitude, φ rad (deg)	−0.007724 (−0.4426)	0	−0.007724 (−0.4426)	0.007724 (0.4426)
Yaw Attitude, ψ rad (deg)	−0.02563 (−1.469)	−0.2515 (−14.41)	−0.27713 (−15.876)	−0.2259 (−12.94)
Sideslip Angle, β rad (deg)	0.02629 (1.506)	0.2515 (14.41)	0.2778 (15.91)	0.2252 (12.90)
Lateral Deviation Rate, $\dot{y}$ ft/sec	0.06622	0	0.06622	−0.06622
Lateral Deviation, y ft	0.6247	0	0.6247	−0.6247

The rms values of both φ and ψ tend to be on the high side for pilot acceptability. If the control budget were less restrictive the rms value of φ could be reduced substantially. However, the large rms ψ is the result of the aircraft weathercocking in response to the very low bandwidth side gusts. Nothing can be done to reduce the deterministic ψ response if crabbed approaches are intended. In view of the severity of the disturbance environment, the rms values of φ and ψ, however, may be acceptable.

Design target values for the rms values of $A_{1_{SAS}}$, $A_{1_{AFCS}}$, $\dot{A}_{1_{AFCS}}$, and δ_r have been given previously in Table 28. It is observed that the rms values for these control variables are all well within the design target values.

Inspection of Table 41 further reveals that the response in localizer deviation and localizer deviation rate to steady wind is zero because of the integral by-pass. There are small responses in bank angle and localizer deviation, and modest responses in ψ and β to the deterministic wind shear. None of these responses are so large that the probability of flying through the Cat II window or pilot acceptance would be appreciably compromised.

This indicates that the advanced lateral-directional coupler design may be considered to be fairly satisfactory.

C. APPROACH OUTCOME PROBABILITIES AND RELATED MEASURES OF PERFORMANCE AND SAFETY

The performance data of the previous subsection can be used to calculate approach outcome probabilities and the combined measure of performance and safety, the accident exposure multiplier. The approach outcome probability is merely the probability that the aircraft will have acceptable deviations from the glide slope, localizer and possibly airspeed references at passage of the decision altitude. The limits upon "acceptable" are here taken to be those of the Cat II window shown in Fig. 10.

Use of the accident exposure multiplier as a combined measure of performance and safety has been justified in Ref. 1. The accident exposure multiplier is a factor which, when applied to the probability of an accident (say, of a given type) on any one approach continued from the window, accounts for the additional accident exposure which results from missed approaches. From a different point of view, the accident exposure multiplier is also the expected number of approaches given the arrival of one aircraft in the terminal area. Consequently, this parameter can also be used to correct the ideal runway capacity for the effect of the missed approach rate characteristic of a given measuring system. Hence, in this sense the accident exposure multiplier is also related to performance.

These probabilities and measures have been computed for the straightforward and advanced design systems for the CH-53A, and are given below. The techniques used are those described in Sections V and VII of Ref. 1.

The marginal probabilities of being within each Cat II window limit on any one approach are given in Table 42 for the straightforward design system,* and in Table 43 for the advanced design system.

TABLE 42

MARGINAL PROBABILITIES FOR STRAIGHTFORWARD DESIGN SYSTEM

VARIABLE	MEAN	RMS	MARGINAL PROBABILITY OF BEING WITHIN WINDOW
Glide slope deviation (ft)	3.74	4.003	0.9821
Smoothed airspeed deviation† (ft/sec)	4.64	3.375	0.8707
Localizer deviation (ft)	0.642	6.643	~1.000

†Airspeed is smoothed by filtering actual airspeed by $0.1/(s+0.1)$.

TABLE 43

MARGINAL PROBABILITIES FOR ADVANCED DESIGN SYSTEM

VARIABLE	MEAN	RMS	MARGINAL PROBABILITY OF BEING WITHIN WINDOW
Glide slope deviation (ft)	0.300	3.932	0.9976
Smoothed airspeed deviation‡ (ft/sec)	4.77	3.485	0.8642
Localizer deviation (ft)	0.642	6.643	~1.000

‡Airspeed is smoothed by filtering actual airspeed by $0.1/(s+0.1)$.

*This system consists of the straightforward design longitudinal system and the advanced lateral-directional system.

Table 44, which is the grand culmination of the analysis, presents the approach outcome probabilities and related measures of performance and safety for the straightforward and advanced design systems. The probabilities and measures have been computed both inclusive and exclusive of the airspeed deviation effects because, as mentioned earlier, it may be argued that the Cat II airspeed deviation limits are probably not crucial in vehicles capable of hover. This is because lift changes due to airspeed changes can always be compensated for by using direct lift control. As for the results themselves, in Table 44 both system designs have acceptably low probabilities of being outside the window on any one approach, regardless of the airspeed deviation consideration. This in turn means that the probability of a missed approach on any one approach, the expected number of missed approaches per arrival, and the accident exposure multiplier are also acceptably small. Not surprisingly, the advanced system is somewhat superior to the straightforward system in terms of any of the measures. This is because the mean values of the variables arising from the winds and wind shears are more effectively suppressed or eliminated entirely by the advanced system.

This concludes the discussion of the performance of the single-rotor helicopter on approaches to a decision height of 100 ft.

TABLE 44

APPROACH OUTCOME PROBABILITIES AND RELATED MEASURES OF PERFORMANCE AND SAFETY

SYSTEM	PROBABILITY OF		EXPECTED NUMBER OF	
	BEING OUTSIDE WINDOW, P_W	MISSED APPROACH,* $P_{MA} = P_W P_D$	MISSED APPROACHES PER ARRIVAL, $P_{MA}/(1-P_{MA})$	APPROACHES PER ARRIVAL (ACCIDENT EXPOSURE MULTIPLIER), $1/(1-P_{MA})$
Straightforward Design				
(Evaluation based upon GSD and LOC only)	0.0179	0.0170	0.0173	1.0173
(Evaluation based upon GSD, LOC and AS)	0.1449	0.1377	0.1597	1.1597
Advanced Design				
(Evaluation based upon GSD and LOC only)	0.0024	0.0023	0.0024	1.0024
(Evaluation based upon GSD, LOC and AS)	0.1379	0.1310	0.1507	1.1507

*It is assumed that P_D, the pilot centered probability that an approach is discontinued if outside the window at the decision altitude, has a value of 0.95.

SECTION IV

ANALYSIS OF LANDING FROM THE DECISION ALTITUDE THROUGH FLARE AND TOUCHDOWN FOR A SINGLE ROTOR HELICOPTER REPRESENTATIVE OF A STOL AIRCRAFT

In this section, analytical techniques are applied to represent, through systems analysis, the landing performance of a particular aircraft and measuring system combination. The main objective of this section is to illustrate the manner in which the stated problem may be treated by analysis in distinction to simulation.

The CH-53A helicopter, longitudinal and lateral approach couplers, measuring system model and disturbance environment described at the beginning of Section III will be used here. The basic longitudinal flight profile for this phase of the approach, flare and touchdown will consist of a decelerating approach and a one-step flare. Some additions to the basic approach coupler design are needed to accomplish these maneuvers. The additions mainly affect the command structure (in distinction to the loop structure) of the system already described in Section III. The fact that a decelerating approach and a change in the reference glide slope characterize the flight profile causes some complication in representing wind shear effects because these effects are basically functions of absolute altitude. A quasi-linearization approach is used to resolve this complication.

At this preliminary stage of the analytical process description, it may seem to the reader that the approach taken is likely only to be applicable for simple flight profiles such as the decelerating approach plus one-step flare. While it is true that the specific development which follows is restricted to this special case, the analytical techniques used are useful for most practical landing flight profiles. In particular, it appears quite likely that the flight profile consisting of glide slope tracking (or for that matter glide slope "extension") from the decision altitude to the flare initiation altitude followed by an exponential flare can be modeled by the appropriate application of the same techniques. The exponential flare in that case would play a role analogous to that of the one-step flare used here.

The following subsection will describe in detail the decelerating approach and one-step flare, the additions to the automatic control system which are necessary for execution of this maneuver, and the equations describing the command and disturbance environment. Then the results of exercising the analytical model will be presented and finally the conclusions to be drawn from the analysis are described.

A. DESCRIPTION OF THE MODEL FOR THE DECELERATING APPROACH AND ONE-STEP FLARE

This model consists of the description of the CH-53A helicopter, the approach couplers, and the disturbance environment given in Section III plus additional equations describing the effective command environment and control system modifications necessary for completing the landing maneuver.

1. Decelerating Approach and One-Step Flare

The aircraft is presumed to have arrived at the decision altitude (100 ft) with certain glide slope, localizer and airspeed deviations with respect to the reference glide path (−6 deg) and reference airspeed. These deviations form the initial conditions on the analytical model. Initial conditions on all other perturbation variables are assumed to be zero. Just after passage of the decision altitude, a large step input in longitudinal cyclic pitch is applied which causes the aircraft to pitch up, and the lift vector to tilt rearward, decelerating the aircraft. This step command is also scaled and washed out and fed to collective pitch. This is for the purpose of reducing lift via collective pitch in a way which approximately compensates for the increase in lift resulting from the increase in angle of attack.

The aircraft continues to decelerate and descend along the reference −6 deg glide path until a preselected flare initiation altitude (here taken as 50 ft) is reached. At this altitude, the reference glide path is changed to −3 deg. In order that this transition be made quickly, a feedforward command is also applied in addition to selection of the new reference glide path. The aircraft captures the new reference glide path and continues on to touchdown decelerating all the while. In the nominal case, the initial airspeed at the decision altitude is 101 ft/sec. The deceleration causes

the airspeed to decrease in a nearly exponential manner. The airspeed at touchdown in the nominal case is approximately 40 ft/sec. In the absence of winds, and since the aircraft is on a reference glide path of −3 deg, the vertical velocity at touchdown is approximately −2.0 ft/sec.

The geometry for this scenario is shown in Fig. 18 along with the assumed dimensions for the measuring system site.

2. Additions to the Basic Approach Coupler Designs

The longitudinal approach coupler (modified for the deceleration and flare) is shown in Fig. 19. (The original configuration is shown in Fig. 13). Feedforward paths to longitudinal cyclic pitch, B_{1_c}, and collective pitch, δ_{cc}, have been provided for the step input, $B_{1_{cc}}$, which is applied at the decision altitude. In the path to collective pitch this step input is washed out at a rate comparable to the rate of airspeed response. The washout has been included in the airspeed-to-collective pitch crossfeed path also, since it is part of the ideal crossfeed. (The washout was omitted in the crossfeed path of the Fig. 13 design for the sake of simplicity.)

The reader will notice in Fig. 19 that it is now glide slope deviation being fed back rather than altitude perturbation, h. This is because a specific choice of feedback must be made before the equations describing the command and disturbance environment are obtained. A feedforward path to collective pitch, δ_{cc}, is also provided through C_2 in Fig. 19. This is for speeding up capture of the second glide slope segment. Transition to the second glide slope segment is initiated at 50 ft altitude. The nominal effective glide slope command (in actual fact, this arises from the second segment of the constant glide slope), $d_{c_{ff}}$, can be estimated. Its first derivative, $\dot{d}_{c_{ff}}$, can then be used to complement the effective glide slope command, d_c, so that the glide slope response of the system in the transition is not unduly slowed down by the low pass filter, G_{h_c}. The filter C_2 is complementary to G_{h_c} in order to accomplish this. That is, C_2 satisfies:

$$G_{h_c} + sC_2 = 1 \qquad (28)$$

The transfer function for C_2 is given in Table 34.

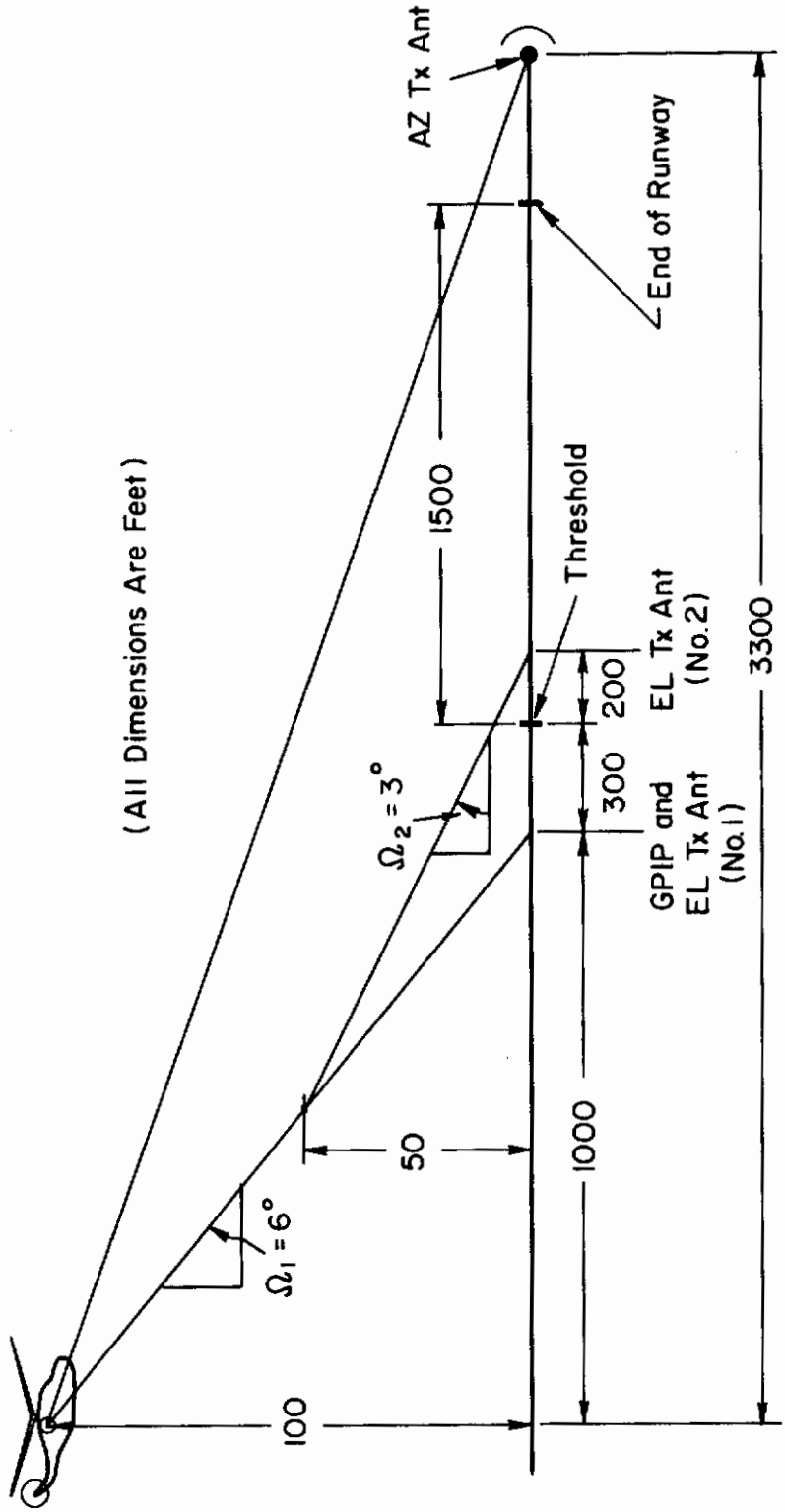

Figure 18. Assumed Geometry of Glide Path and Measurement System Site; Short-Runway Case (All Dimensions Are Feet)

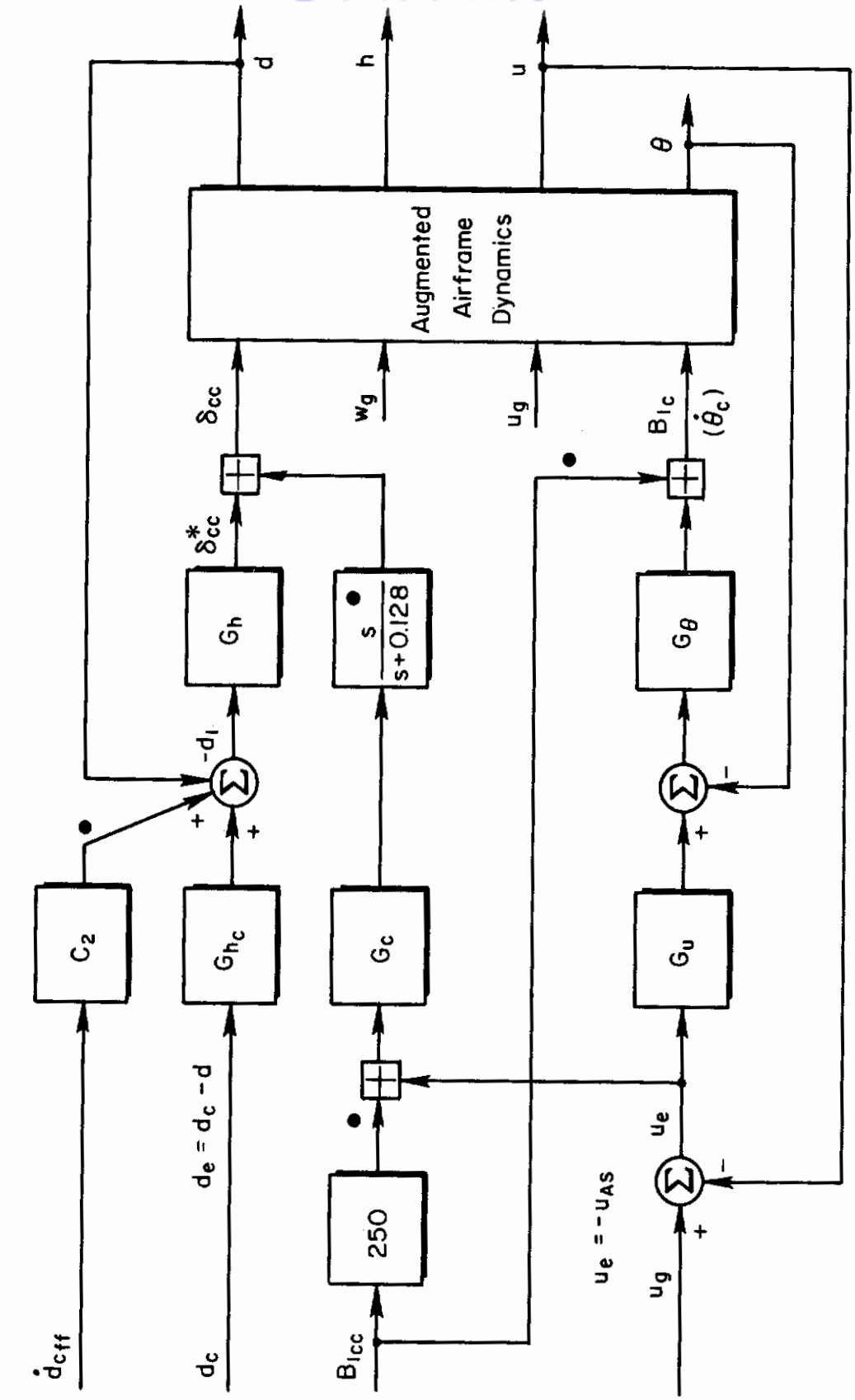

Figure 19. Modification to the Advanced Longitudinal Coupler for Execution of the Decelerating Approach and One-Step Flare

No modifications to the lateral-directional approach coupler have been made. However, it has been assumed that linear (i.e., range compensated) measures of both glide slope and localizer deviation are available.

3. Description of the Command and Disturbance Environment

The approach used to develop the command and disturbance environment consists of superimposing the nominal description which applies along the unperturbed, -6 deg, reference path, and the effects of the dominant low frequency modes of motion of the aircraft which account for the large deviations of the aircraft from the nominal reference path. The large deviations arise in airspeed because of the decelerating maneuver, the one-step flare and the wind shear; and in glide slope deviation because of the one-step flare.

Consider now the description of these effects. The wind shear model used is

$$\dot{u}_s(t) = \mp R\dot{h}_{abs} \doteq \pm R(V_{T_o} + u) \sin \Omega_1 \mp R\dot{d}_{cc} \qquad (29)^*$$

from the start of the problem at the decision altitude until touchdown. u_s is the wind shear velocity component. R is the magnitude of the shear rate with altitude, here taken as 0.135 ([ft/sec u_s]/[ft h_{abs}]). Only a single shear segment is used for the sake of simplicity. Next, the effects of the decelerating approach upon $\dot{u}_s$ must be considered. Therefore, the Laplace transform of u(t) is:

$$u(s) = \frac{u_w}{s} + \frac{u}{u_s}(s)u_s + \frac{u}{B_{1_{cc}}}(s)B_{1_{cc}} + \frac{u}{d_{cc}}(s)d_{cc} \qquad (30)$$

u_w/s is the steady wind component of u. The succeeding terms in Eq. 30 include the effects of wind shear, deceleration input and actual glide slope command, respectively. Each of the transfer functions, in turn, may be simply approximated. The approximate expressions are:

*A plus or minus sign is chosen, dependent upon the sense of the wind shear desired. $\pm R > 0$ means an increasing tailwind component.

$$\frac{u}{u_s}(s) \doteq \frac{0.128}{s + 0.128} \tag{31}$$

$$\frac{u}{B_{1_{cc}}}(s) \doteq \frac{41.2}{s + 0.128} \tag{32}$$

$$\frac{u}{d_{cc}}(s) \doteq \frac{0.0214\ s(s + 0.502)}{s + 0.128} \tag{33}$$

These approximate expressions have been obtained from the exact transfer functions computed in connection with Section III. The mode which remains in these approximations is the closed-loop speed subsidence mode.

The $B_{1_{cc}}$ input for Eq. 30 is a step applied at t = 0 (at the decision altitude), $b_{1_{cc}}/s = (-0.191)/s$. The magnitude is 0.191 rad (11.0 deg). This results in an approximate nose-up maximum pitch attitude perturbation of approximately 14 deg and a steady state reduction in airspeed of 61.5 ft/sec. In the case of a strong headwind component, one-half this value of $b_{1_{cc}}$ is used.

The next step is to obtain an expression for the actual glide slope command, d_{cc}. This is

$$\dot{d}_{cc} \doteq \begin{cases} 0 & , \ h > 50 \text{ ft} \\ (V_{T_o} + u)(\sin \Omega_1 - \sin \Omega_2), & 50 \geq h \geq 0 \text{ ft} \end{cases} \tag{34}$$

$$d_{cc}(0) = 0$$

The nominal effective glide slope command for feedforward through C_2 is closely related to the above expression. It is assumed that groundspeed ($\doteq V_{T_o} + u$) is not known in the aircraft so that airspeed is used instead. The nominal effective glide slope command is given by:

$$\dot{d}_{cff} = \begin{cases} 0 & , \ h > 50 \text{ ft} \\ (V_{T_o} + u - u_w - u_s)(\sin \Omega_1 - \sin \Omega_2), & 50 \geq h \geq 0 \text{ ft} \end{cases} \tag{35}$$

$$d_{cff}(0) = 0$$

Equations 34 and 35 involve the factor $(\sin \Omega_1 - \sin \Omega_2)$, which might be regarded as a time-varying coefficient which takes on the value 0 for $h > 50$ ft and $(\sin \Omega_1 - \sin \Omega_2)$ for $50 \geq h \geq 0$ ft.

Let

$$\Omega = \begin{cases} 0 & , \quad h \geq 50 \text{ ft} \\ \sin \Omega_1 - \sin \Omega_2, & 50 \geq h \geq 0 \text{ ft} \end{cases} \tag{36}$$

then

$$\dot{d}_{cc} = (V_{T_o} + u)\Omega \quad , \; d_{cc}(0) = 0 \tag{37}$$

and

$$\dot{d}_{cff} = (V_{T_o} + u - u_w - u_s)\Omega, \; d_{cff}(0) = 0 \tag{38}$$

At this point the assumption that the time-varying character of Ω is unimportant is made. Then the characteristic polynomial for Eqs. 29 through 33, 37 and 38 is*

$$(1 + 0.0214\Omega)s^2 + (0.128 + 0.0107\Omega)s \pm 0.128R(\Omega - \sin \Omega_1)$$

$$\doteq (s + 0.128)(s \pm R[\Omega - \Omega_1])$$

where the approximation follows by virtue of the magnitudes of the quantities involved. The maximum magnitude of $R[\Omega - \Omega_1]$ is 0.0135 rad/sec which implies a time constant of 74 sec for this mode. Since the nominal interval of time from the decision altitude to touchdown is 22 sec, $(s \pm R[\Omega - \Omega_1])$ is further approximated by s. This latter approximation renders the questionable validity of neglecting the time-varying nature of Ω a moot point. By making approximations similar to those used for the characteristic polynomial it is possible to obtain expressions for the variables $\dot{d}_{cc}$, $\dot{d}_{cff}$ and $\dot{u}_s$. Each of these variables is expressed as a sum of time functions.

$$\dot{d}_{cc} = \Omega \mathcal{L}^{-1}\left[\frac{V_{T_o} + u_w}{s} + \frac{41.2\, b_{1cc}}{s(s + 0.128)}\right] \tag{39}$$

$$d_{cc}(0) = 0$$

*Equations 29, 37 and 38 must first be Laplace transformed of course.

$$\dot{d}_{cff} = \Omega \mathcal{L}^{-1}\left[\frac{V_{T_o}}{s} + \frac{41.2\, b_{1_{cc}}}{s(s + 0.128)}\right]$$
$$d_{cff}(0) = 0 \qquad (40)$$

$$\dot{u}_s = \pm R(\Omega_1 - \Omega)\mathcal{L}^{-1}\left[\frac{V_{T_o} + u_w}{s} + \frac{41.2\, b_{1_{cc}}}{s(s + 0.128)}\right]$$
$$u_s(0) = 0 \qquad (41)$$

The above time functions are integrated where appropriate and then are used to force the system of Fig. 19. Notice that u_s enters the u_g forcing point in that figure as does u_w, the steady wind component. The steady wind component is also part of the initial condition on the perturbation velocity, u.

To this point, the lateral-directional equations have not been considered. This is now easily accomplished since the crosswind shear effect may simply be scaled from u_s, the longitudinal wind shear. Here, the wind shear and crosswind shear rates have been assumed equal so that $v_s = u_s$. The v_s time function is used to force the system of Fig. 15. Notice that v_s enters the v_g forcing point in that figure, as does v_w, the steady crosswind component. The lateral-directional control system is proofed against steady crosswinds so that the effect of the v_w component is to produce a steady v component which exactly equals v_w. Therefore, the initial condition on v is v_w, and since a crabbed approach is used, this produces an initial condition on ψ given by $(-v_w/V_{T_o})$.

Because only elementary time functions and initial conditions are involved, it was convenient to compute the required system responses in terms of Laplace transforms and then invert the transforms to obtain the time histories for the responses. It was necessary to carry out this process in two stages because of the change in the value of Ω which occurs at h_{abs} = 50 ft. Therefore the responses were first evaluated for the time interval between h_{abs} = 100 ft and h_{abs} = 50 ft on the approach. The time for which h_{abs} = 50 ft was also determined. This is essential for generating the input time functions for the second stage. This stage covers the time interval between h_{abs} = 50 ft and touchdown (h_{abs} = 0 ft). The additional system response components which arise from the portions of the input time functions dependent upon Ω are added to the response components arising from inputs dependent upon Ω_1 and the initial conditions.

4. Kinematic Equations

The outputs of the system shown in Figs. 19 and 15 are combined in the kinematic equations in order to obtain the vehicle coordinates with respect to the runway. The equations are:

$$h_{abs} = h_{abs}(0) - [(V_{T_o} + u_w) \sin \Omega_1]t + h \tag{42}$$

$$\begin{aligned} \dot{x}_{abs} &= (V_{T_o} + u) \cos \Omega_1 + \dot{d} \sin \Omega_1 \\ x_{abs}(0) &= x_o \end{aligned} \tag{43}$$

$$\begin{aligned} \dot{y}_{abs} &\doteq \dot{y} \\ y_{abs}(0) &= y_o \end{aligned} \tag{44}$$

Equations 42 and 43 are valid linear approximations for the kinematics. Equation 44, however, implicitly neglects the large changes in airspeed and groundspeed which result from the decelerating approach. The lateral-directional responses will be somewhat inaccurate because of this, but will still be indicative of actual performance.

B. RESULTS OF EXERCISING THE ANALYTICAL MODEL FOR THE DECELERATING APPROACH AND ONE-STEP FLARE

This subsection summarizes the results of exercising the analytical model for three near worst-case combinations of initial conditions and the atmospheric environment and one nominal case.

1. Parameters and Initial Conditions for Cases Considered

Four combinations of initial conditions and atmospheric disturbances were considered. These correspond qualitatively to the four cases considered for the DC-8 automatic landing system in Section II. The relative positions of the touchdown points are the same as in Fig. 9. The specific conditions for the cases are summarized in Table 45.

TABLE 45

CONDITIONS FOR CASES COMPUTED
DECELERATING ONE-STEP FLARE IN A SINGLE ROTOR HELICOPTER

CASE	INITIAL CONDITIONS AT WINDOW	WIND CROSSWIND AND SHEARS	DECELERATION INPUT MAGNITUDE $^{b}_{1cc}$	QUALITATIVE DESCRIPTION
0 (nominal)	$\Delta u_{AS} = d = 0$ $y = \psi = 0$	$u_w = u_s = 0$ $v_w = v_s = 0$	11.0 deg	Nominal, no winds or shears
1	$\Delta u_{AS} = -8.45$ ft/sec $d = -12.0$ ft $y = \psi = 0$	$u_w = -42.2$ ft/sec $v_w = v_s = 0$ $\pm R = 0.135$ 1/sec	5.5 deg	Low, slow at window; decreasing headwind
2	$\Delta u_{AS} = d = 0$ $y = -24.0$ ft $\psi = 0.243$ rad	$u_w = u_s = 0$ $v_w = -24.5$ ft/sec $\pm R = -0.135$ 1/sec	11.0 deg	Left of runway ℄ at window; increasing crosswind from right
3	$\Delta u_{AS} = 8.45$ ft/sec $d = 12.0$ ft $y = \psi = 0$	$u_w = 16.9$ ft/sec $v_w = v_s = 0$ $\pm R = -0.135$ 1/sec	11.0 deg	High, fast at window; decreasing tail wind

2. Trajectories and Touchdown Coordinates

Table 46 summarizes the touchdown coordinates, sink rate, groundspeed, airspeed, and time of touchdown.

TABLE 46

TOUCHDOWN COORDINATES

Case	x_{abs}* (ft)	y_{abs} (ft)	$-\dot{h}_{abs}$ (ft/sec)	Groundspeed (ft/sec)	Airspeed (ft/sec)	t† (sec)
0	−75.0	0	2.42	44.0	44.0	22.0
1	−20.0	0	2.66	43.8	86.0	39.0
2	−75.0	2.8	2.42	44.0	44.0	22.0
3	−230.0	0	4.22	66.9	50.0	11.8

*Measured in the direction of flight from the intersection of the second (−3 deg) glide slope segment with the runway.

†t = 0 is at passage of the decision altitude.

The approach and flare trajectory results are considered next. Figure 20 shows the ideal geometric reference path in space. This path lies in the vertical plane through the runway centerline. The decision altitude, flare initiation altitude and touchdown points along this ideal trajectory are denoted by circular symbols. These symbols will be reproduced on subsequent figures showing actual trajectories for purposes of reference.

The actual trajectory for the nominal case (Case 0) is shown in Fig. 21. No initial condition offsets at the window, or winds or wind shear are present. Notice that the CH-53A helicopter tracks the initial segment of the glide slope quite closely, but that a small transient is present. This transient is the result of the deceleration maneuver, and it arises in particular from the fact that the change in lift from the pitch-up is only approximately compensated for by the crossfeed to the collective pitch (i.e., direct-lift) control.

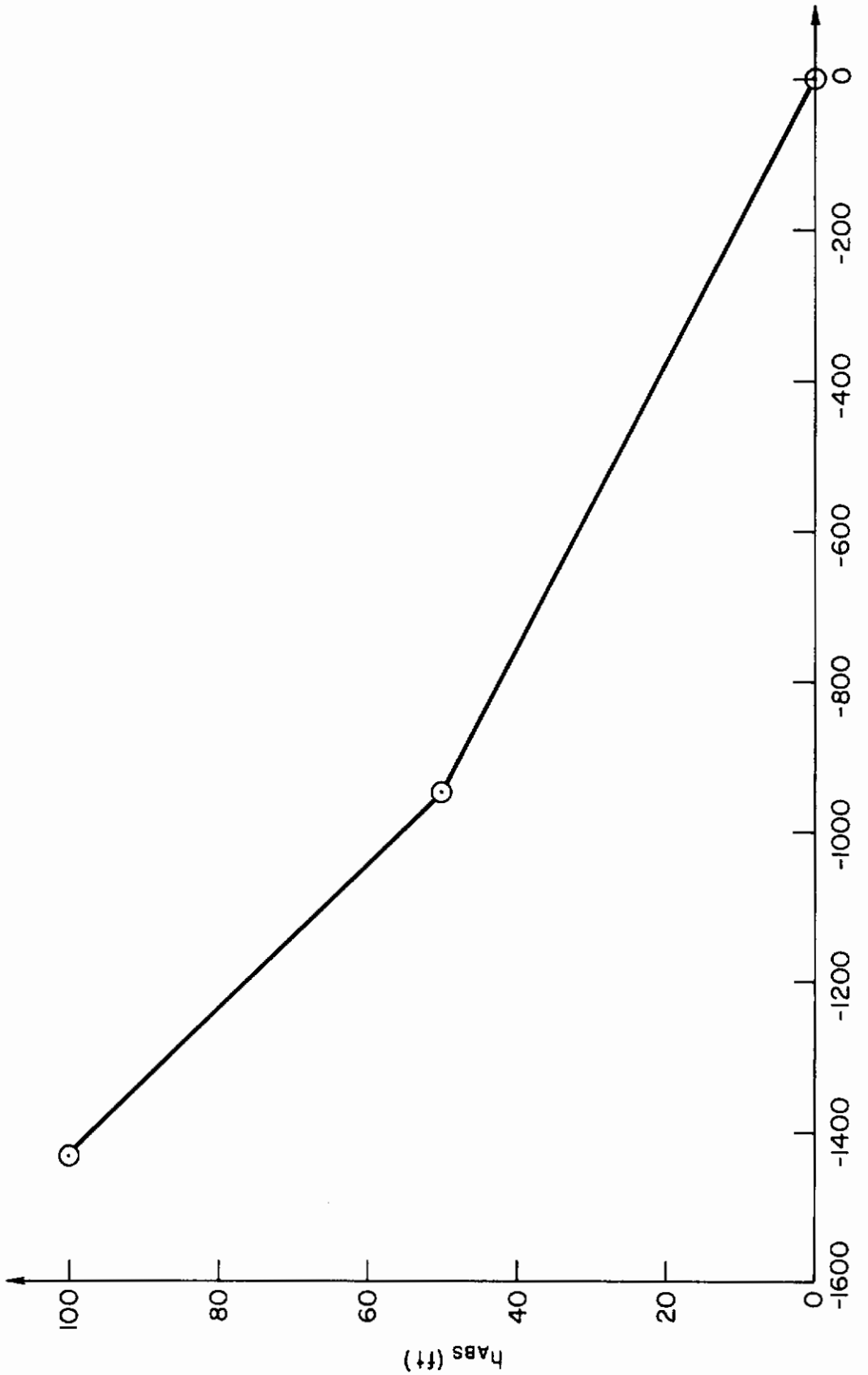

Figure 20. Ideal Geometric Approach and Flare Trajectory

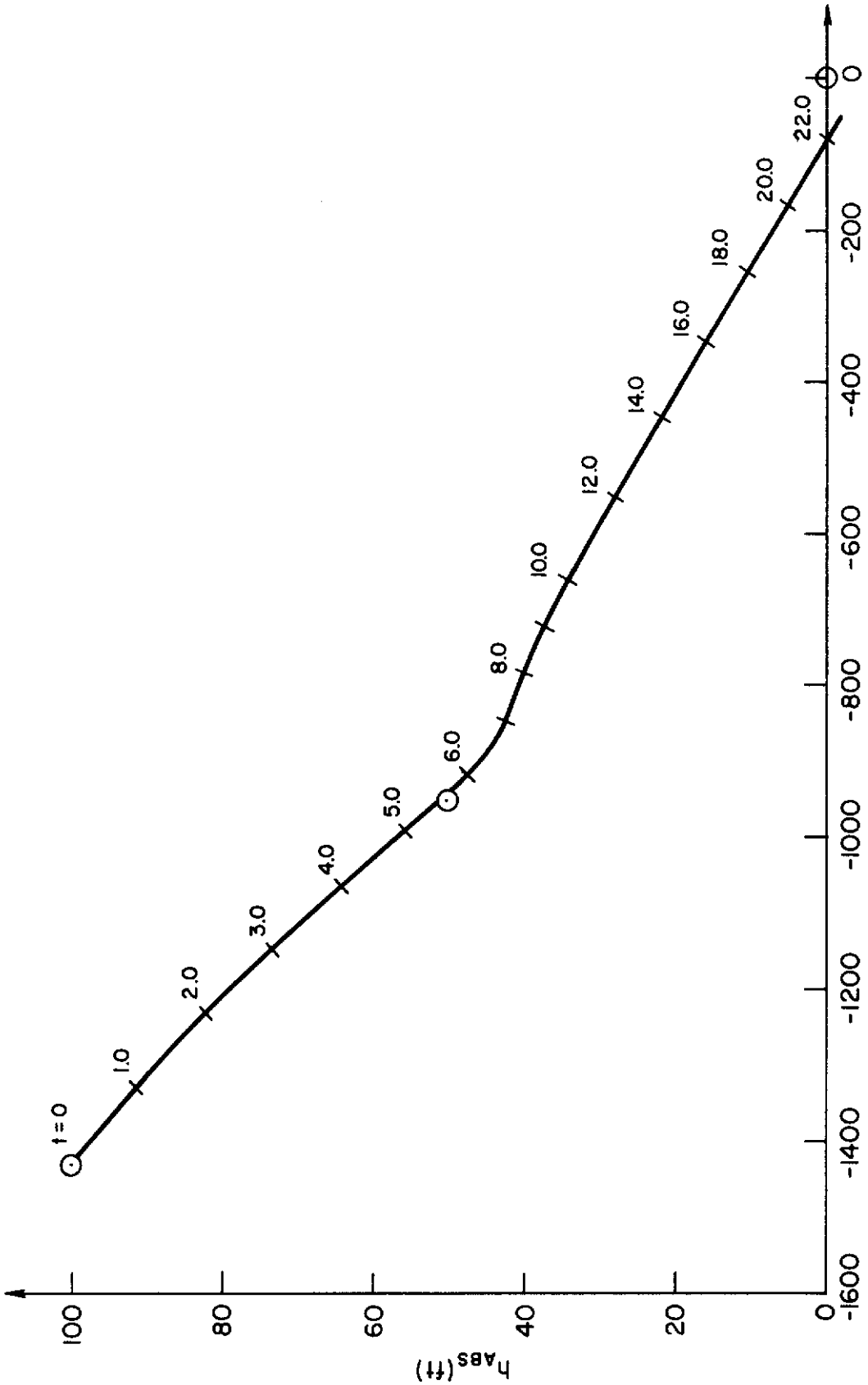

Figure 21. Actual Approach and Flare Trajectory, Case 0 (Nominal) and Case 2

Transition to the second glide slope segment is initiated at approximately t = 5.5 sec. There are short and long term transients in response to the glide slope transition. The short term transient results in the path-following mode. The long term transient is the result of the integral bypass action. While not shown, it is true that the glide slope response is asymptotic to the extended geometric reference trajectory. Touchdown for the nominal case is 75 ft short of the reference touchdown point. Sink rate at touchdown is 2.42 ft/sec, which is slightly greater than the reference value of 2.33 ft/sec. All in all, the longitudinal trajectory is well controlled, and is within ±4 ft of the ideal geometric reference trajectory throughout the deceleration, flare and touchdown.

The actual trajectory for Case 1 is shown in Fig. 22. The Case 1 conditions are low and slow at the decision altitude on a glidepath parallel to the first segment of the ideal geometric reference trajectory with a decreasing headwind present. Early in this trajectory a glide slope recapture transient occurs when the glide slope offset (initial condition) is removed suddenly at t = 0. This transient is almost entirely in the path mode. (It should be mentioned here that the transient response to a step change in glide slope command, d_c, would be much less rapid than this response to an initial glide slope offset. This is because d_c is first prefiltered by

$$G_c = \frac{(0.333)^2}{s^2 + 2(0.7)0.333s + (0.333)^2} \qquad (45)$$

before being applied to the closed-loop system whereas the initial glide slope offset is effectively applied directly as a step.)

Progress along the approach is much slower in this case because of the headwind. This is the case even though the deceleration has been reduced by one-half in this case to avoid reaching zero groundspeed and zero rate of descent at some altitude above the runway.

Initiation of the glide slope transition occurs at t = 14.4 sec. A very substantial overshoot occurs. This is because the glide slope transition command <u>feedforward</u>, d_{cff} (please refer to Fig. 19), is computed on the

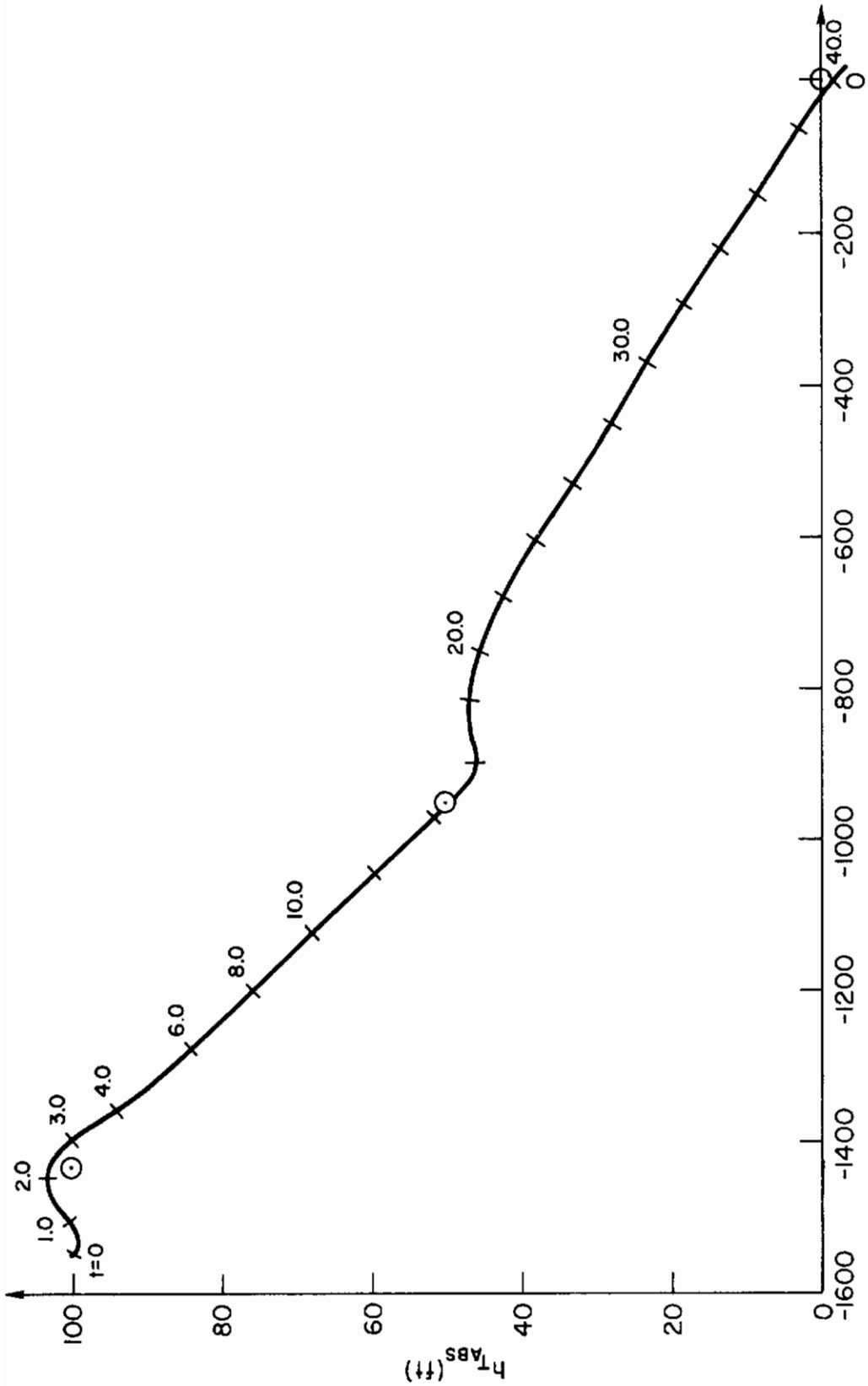

Figure 22. Actual Approach and Flare Trajectory, Case 1 (Low, Slow at Window; Decreasing Headwind)

basis of airspeed as an approximation to the correct quantity, groundspeed. This is to simulate what can reasonably be done on board the aircraft. Not too surprisingly, the headwind component which is approximately one-half of the airspeed at that point, causes a fairly substantial error. Nevertheless, the aircraft remains within ±6 ft of the ideal geometric reference trajectory. The touchdown is 20 ft short of the reference point and the sink rate, 2.66 ft/sec, is somewhat greater than the reference value of 2.33 ft/sec.

The actual trajectory for Case 3 is shown is Fig. 23. The Case 3 conditions are high and fast at the decision altitude on a glide path parallel to the first segment of the ideal reference trajectory with a decreasing tailwind present. Early in this trajectory a glide slope recapture transient occurs when the glide slope offset (initial condition) is removed suddenly at t = 0. This transient is almost entirely in the path mode. Because of the tailwind the groundspeed is high. However, even so, there is sufficient time to complete the critical glide slope recapture before initiation of the glide slope transition command at t = 3.2 sec. The transient response to the glide slope transition command is not sufficient to prevent substantial undershoot in this case. This is for two reasons. The first is that airspeed is used to approximate groundspeed in computing the glide slope feedforward command, d_{cff}. The result is that d_{cff} is substantially underestimated in the critical fly-up direction. The second reason is the high groundspeed arising from the tailwind component. The high groundspeed causes "things to happen so fast" that correction via the absolute glide slope command, d_c, is insufficient because of system dynamic lag. Even so, the system maintains the ideal geometric reference trajectory over the last segment within +0, −12 ft. The resulting touchdown is 230 ft short of the reference point. Sink rate at touchdown is high, 4.22 ft/sec, with respect to the reference value 2.33 ft/sec. High groundspeed at touchdown, 66.9 ft/sec, is the major factor in the high sink rate at touchdown.

Next, the lateral-directional dimensions of the trajectory will be considered. Figure 24 shows the actual trajectory for the only off-nominal case examined, Case 2. The initial conditions for Case 2 are for the aircraft displaced to the left of the extended runway centerline at the decision altitude on a path parallel to the runway centerline. An increasing crosswind is assumed blowing from the pilot's right. The lateral offset was restricted

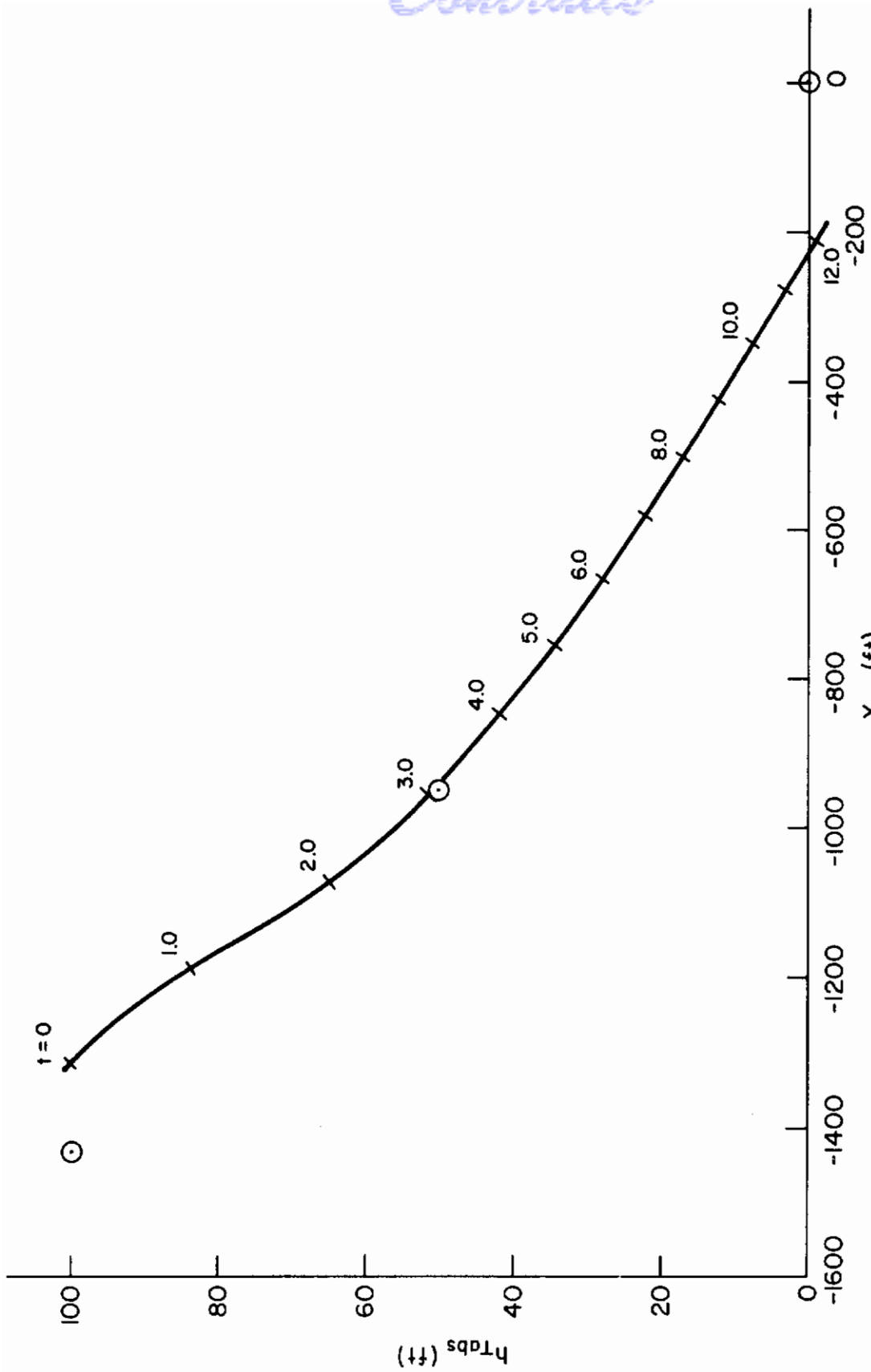

Figure 23. Actual Approach and Flare Trajectory; Case 3 (High, Fast at Window; Decreasing Tailwind)

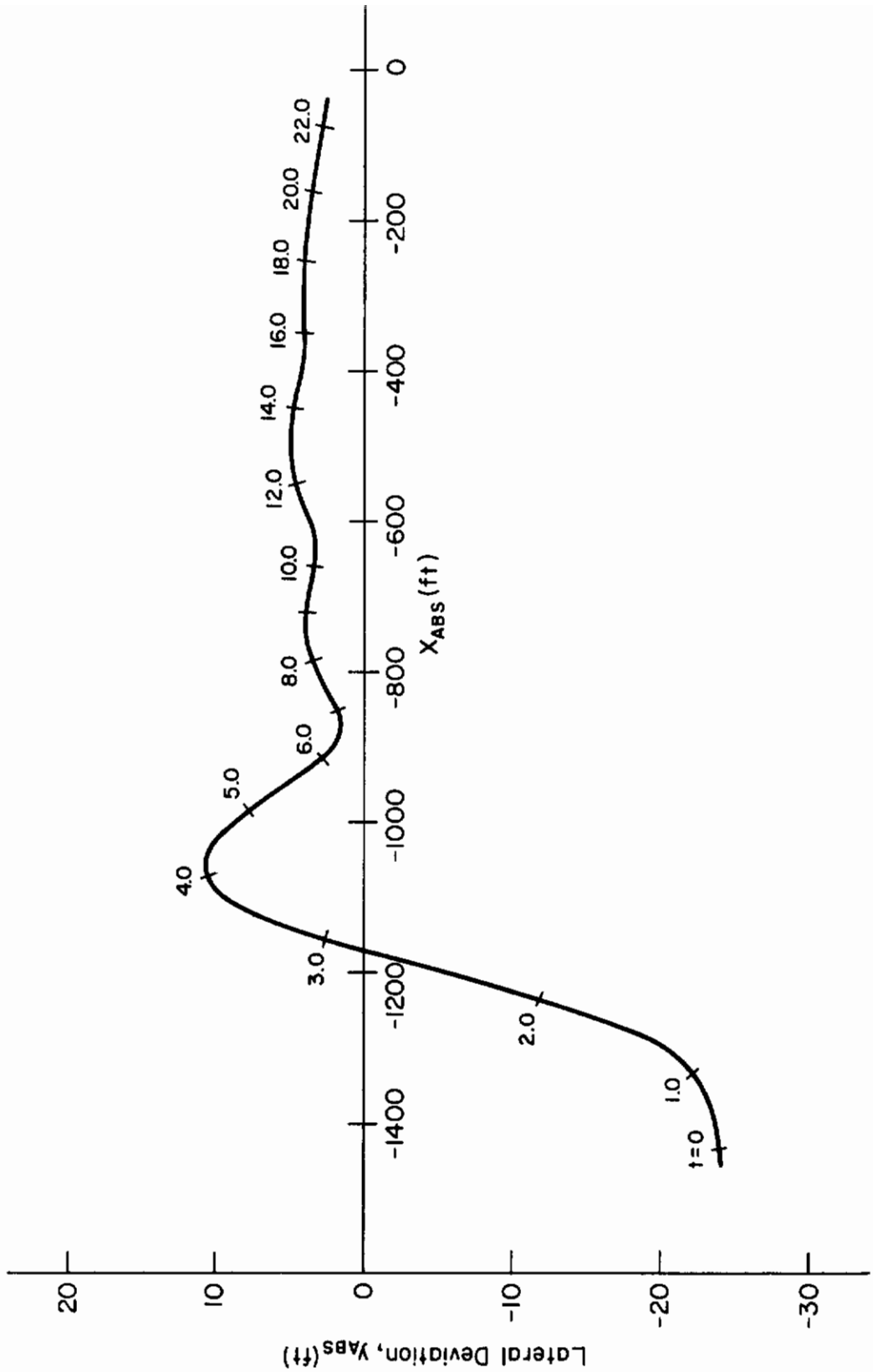

Figure 24. Lateral Approach Trajectory, Case 2
(Left of Runway ℄ at Window; Increasing Crosswind from Right)

to $y_o = -24$ ft so that the maximum bank angle would not exceed 25 deg. (It is appropriate to remark here that examining the transient response to so large an offset is inappropriate for a high gain tracking system such as this one. Such excursions should actually be exceedingly rare since the previous results presented in Section III indicate a mean deviation at the decision altitude in y of only -0.625 ft and an rms value of 1.46 ft.) The localizer recapture transient which results from removal of the initial offset (initial condition) suddenly at t = 0 is characterized by one overshoot in the rapid portion of the transient and a slow portion which is the result of crosswind shear action and the integral bypass effects. The aircraft touches down 3.0 ft to the left of the runway centerline. $\dot{y}$ at touchdown is +0.25 ft/sec.

Table 47 summarizes the CH-53A landing requirements felt to be realistic and safe at the outset of this program. All touchdowns for the cases completed are within the prescribed limits except that airspeed at touchdown is (intentionally) low in all cases except Case 3. Low airspeed at touchdown is hardly a crucial matter in a vehicle such as the CH-53A which is capable of hover.

TABLE 47

CH-53A LANDING REQUIREMENTS (REF. 19)

Acceptable Parameter Ranges	Parameter
$\lvert X_{TD_{max}} - X_{TD_{min}} \rvert \leq 300$ ft	Touchdown spread
$0 \leq \dot{h}_{TD} \leq 5$ ft/sec	Sink rate
$0 < \theta_{TD} < 5$ deg	Pitch attitude to avoid tail strikes and nose wheel first landings
$59.5 \leq AS \leq 93.5$ ft/sec ($35 < AS < 55$ kt)	Airspeed (AS)
$\lvert y_{TD} \rvert \leq 27$ ft	Lateral Deviation
$\lvert \dot{y}_{TD} \rvert \leq 8$ ft/sec	Crosstrack velocity
$\lvert \beta_{TD} \rvert \leq 4$ deg	Inertial sideslip at touchdown. (Landing gear side load considerations)
$\lvert \varphi_{TD} \rvert \leq 5$ deg	Bank angle

Figures 25 through 27 present comparative time histories for the absolute altitude, pitch attitude and airspeed perturbation responses for the single rotor helicopter landings. The noteworthy observations to be made in connection with these figures are as follows:

- The peak pitch attitude excursion from trim occurs for Case 3 and is +15.5 deg. This results from the deceleration maneuver.
- The pitch attitude at touchdown is +5.43 deg for Case 3. This, in a minor way, exceeds the prescribed limit (+5.0 deg) given in Table 47.

All longitudinal responses are smooth and of reasonable magnitudes for pilot acceptance.

Figures 28 through 30 present the time histories in absolute lateral deviation, heading exclusive of initial crab angle, and bank angle. These responses are generally acceptable, but may be criticized for having too little damping. (This is most evident in the bank angle response [Fig. 30] subsequent to t = 7.0 sec). Subsequent investigation has shown that this would not have been a problem had the integral bypass, G_c, in Fig. 16 been located just after the next downstream summing junction instead of before it.

There is one more noteworthy observation to make in connection with Fig. 29. This is that aircraft heading at touchdown is 6.7 + 13.8 = 20.5 deg because of the combined effects of steady crosswind and crosswind shear. Since $\dot{y}_{TD}$ = +0.25 ft/sec and $(V_{T_o} + u)$ = 44 ft/sec,

$$\beta_{TD} = \frac{0.25}{44.0} 57.3 - 20.5 = -20.2 \text{ deg}$$

This far exceeds the allowable value of 4.0 deg in Table 47. However, no attempt has been made to decrab the aircraft in this study. Addition of such a feature or crosswind landing gear could alleviate this problem. With the exceptions mentioned above, the lateral-directional responses are smooth and of reasonable magnitudes for pilot acceptance.

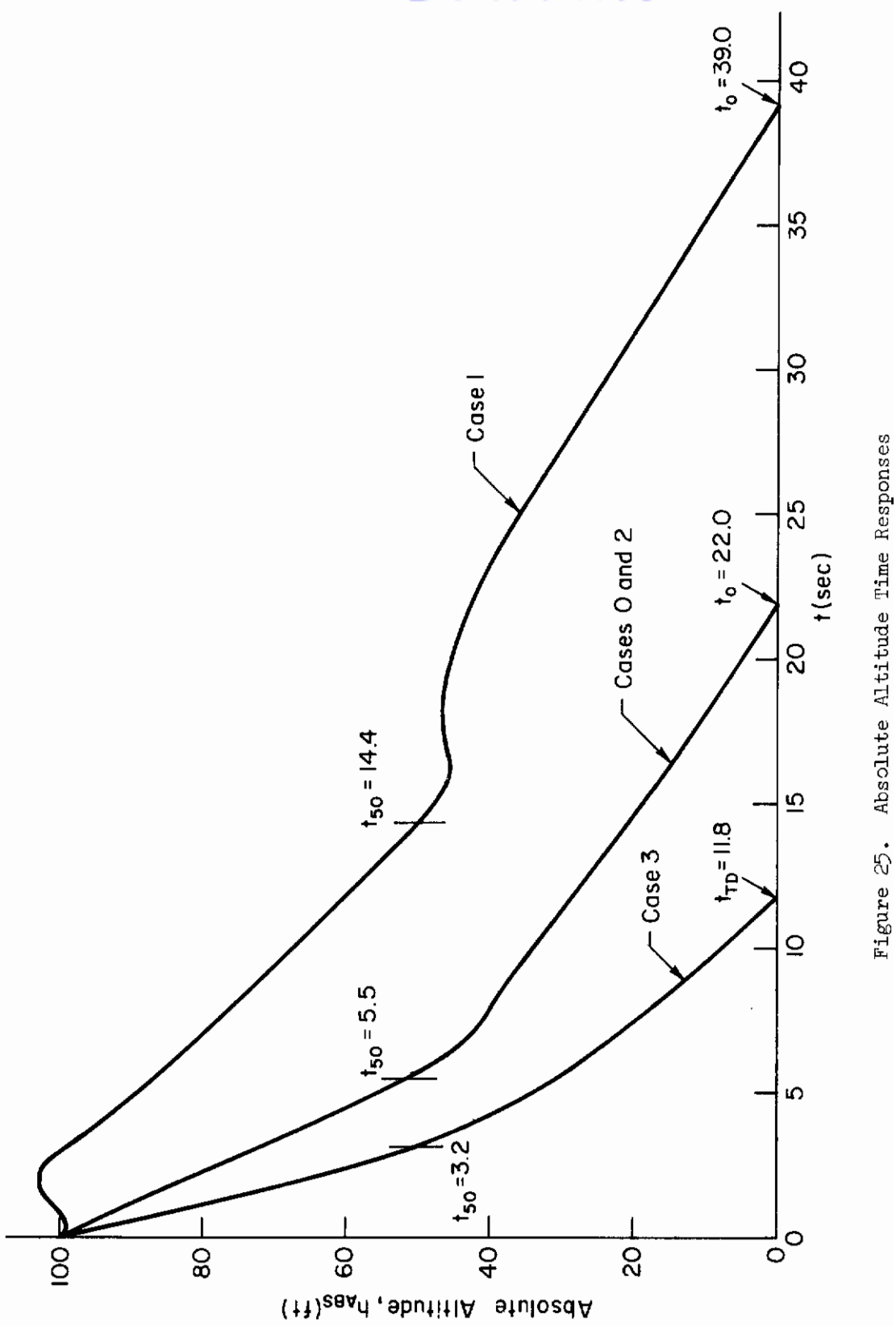

Figure 25. Absolute Altitude Time Responses

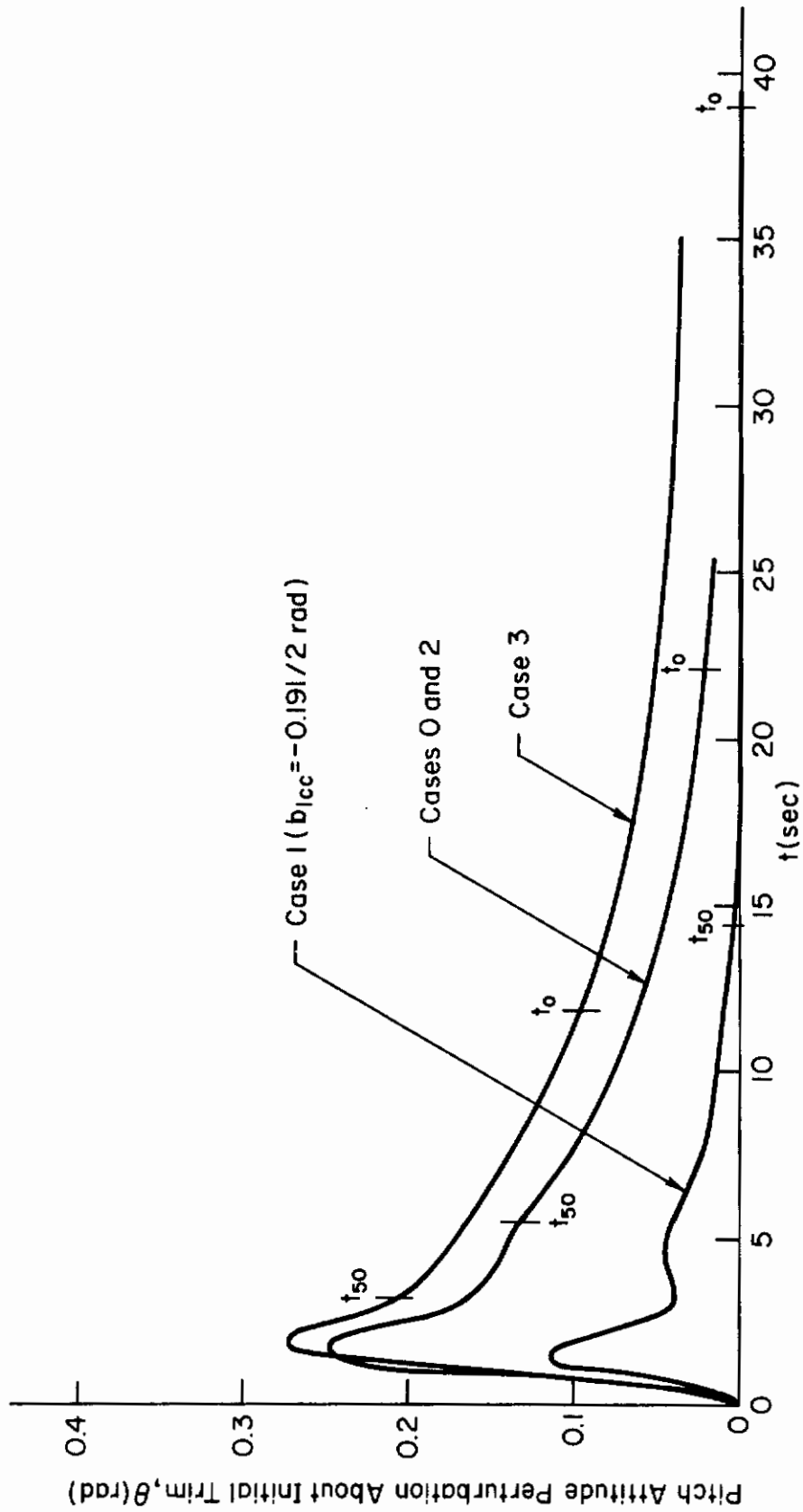

Figure 26. Pitch Attitude Perturbation Response

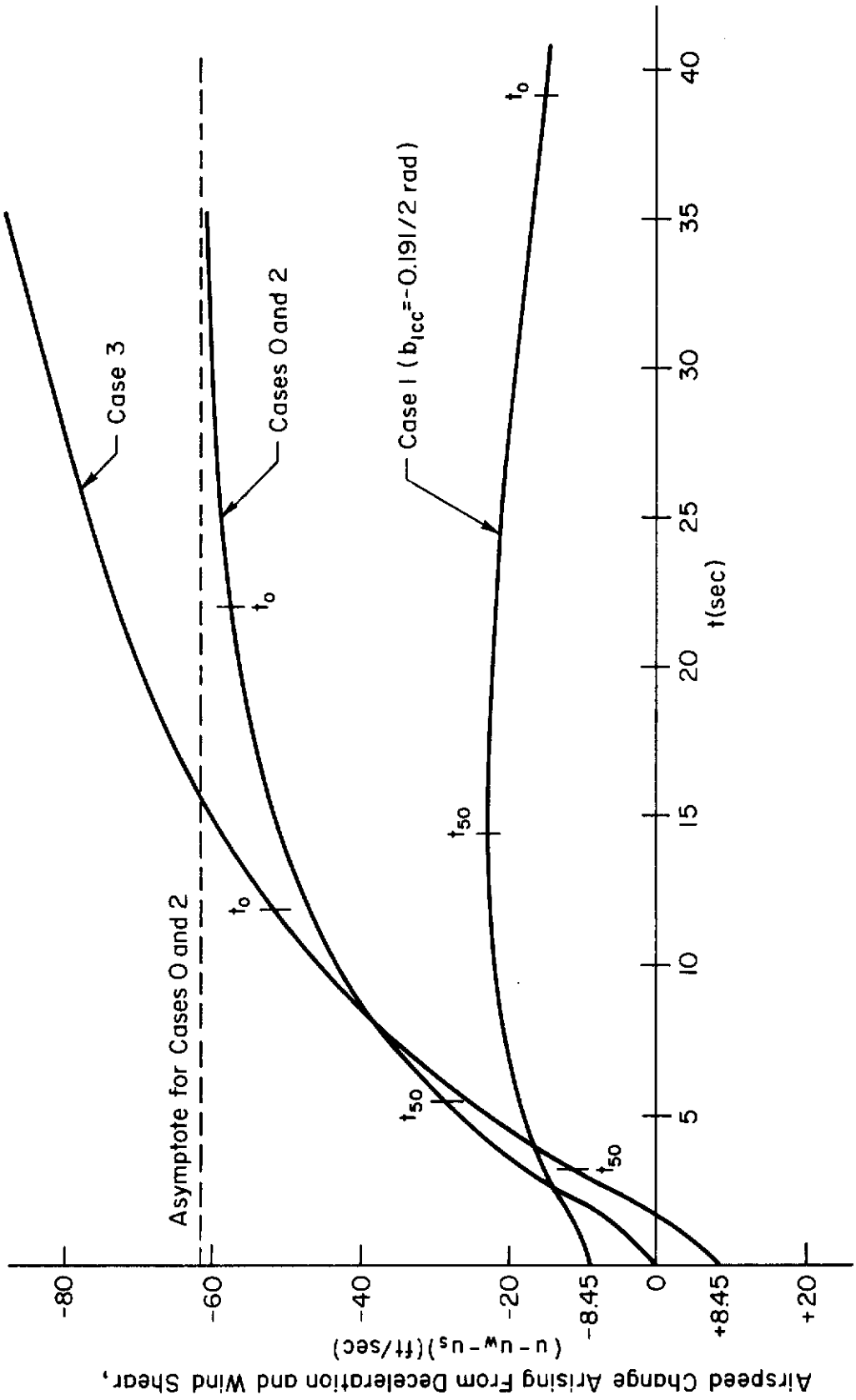

Figure 27. Airspeed Perturbation Response to the Deceleration Command and Wind Shears

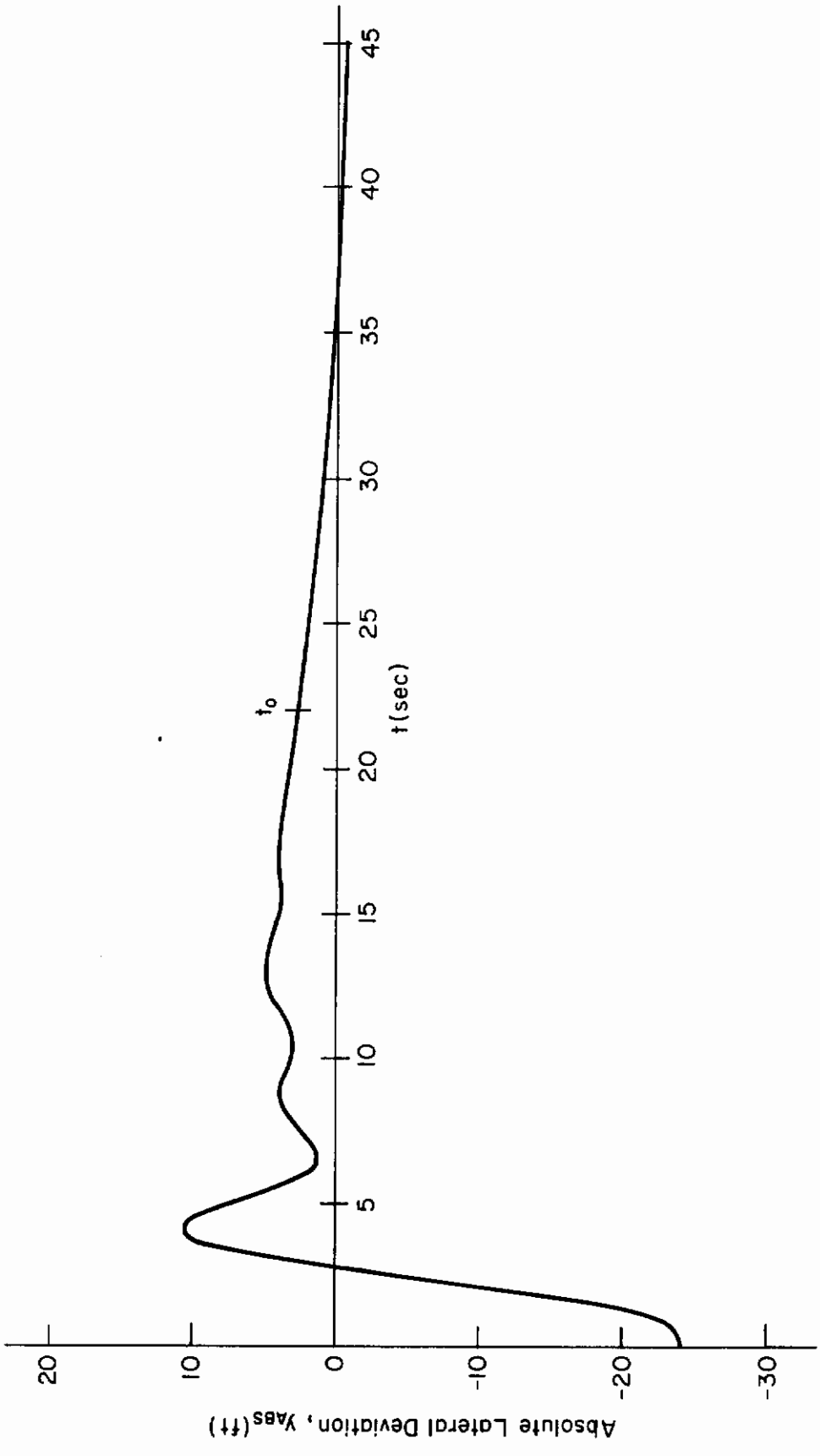

Figure 28. Absolute Lateral Deviation Response (Case 2)

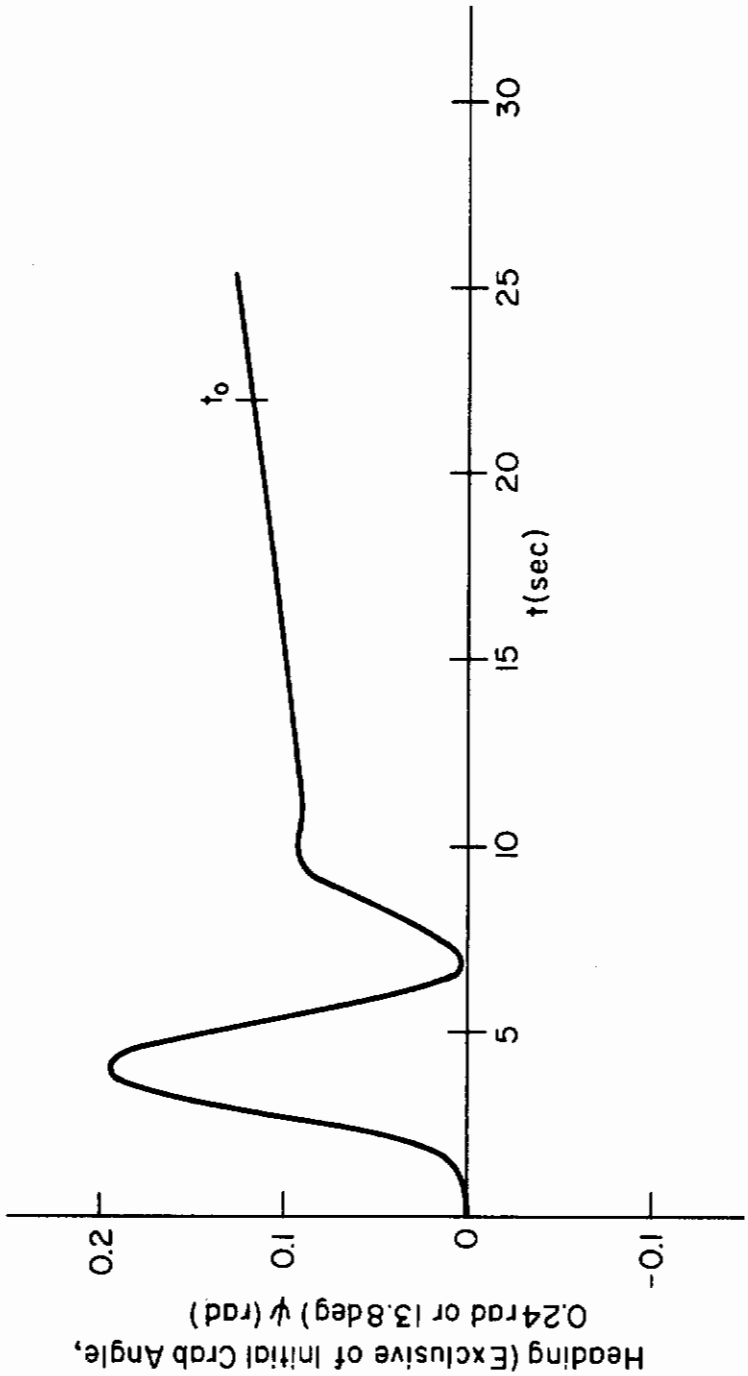

Figure 29. Heading Response Exclusive of the Initial Crab Angle (Case 2)

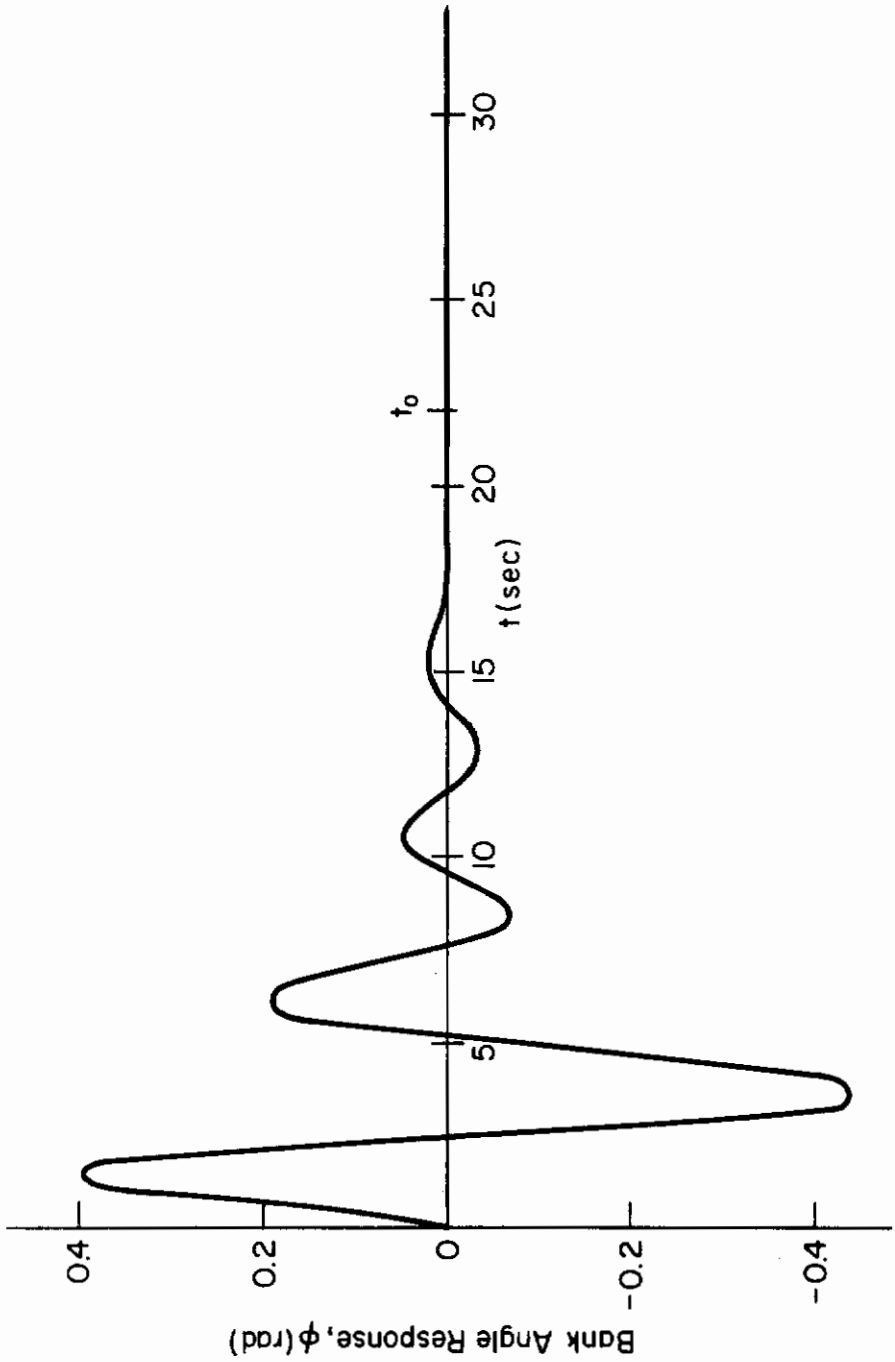

Figure 30. Bank Angle Response (Case 2)

C. ADDITION OF STOCHASTIC INPUT EFFECTS

The response of the CH-53A system to deterministic inputs and initial conditions have been obtained for the decelerating approach, one-step flare and touchdown. The next item of interest is the effect of the stochastic inputs in producing variability about the deterministic trajectories. From estimates of the variability and the deterministic trajectories, one can then gauge the ranges for responses of the actual system.

Modeling of the system and stochastic input environment presents particular problems. Namely, one can usually conceive a model which is sufficiently comprehensive that one may be reasonably confident of the results obtained. On the other hand, however, the comprehensiveness of the model itself may be inimical to obtaining the needed results in an economical and timely manner. This latter consideration rules out Monte Carlo type analyses based upon a time domain simulation model for example. There are other alternatives which are more reasonable. One method would involve solving the covariance equation for a linear (possibly time-varying) model of the aircraft, measuring system and kinematics for the nominal interval of time between passage of the decision altitude and touchdown. A second method (which is more approximate, however) is to use a linear, time-invariant model of the aircraft, measuring system and kinematics and solve for those steady-state covariances which are of interest. Both methods share the following deficiencies:

- It is not clear at the present time how stochastic gusts should be modeled when used in concert with a deterministic wind shear model. (This problem was discussed previously in Section II.)

- Special statistical techniques are required to convert the linear model statistical results into statistics for conditions at touchdown. This is because the "presence" of the runway boundary can only be represented in a nonlinear model. The special statistical techniques required produce approximate results using the linear model.

The second method has the additional deficiency that the steady-state covariance may substantially misestimate the covariance at the nominal touchdown time. However, if one replaces the power at low frequencies in the stochastic gust power spectral densities with deterministic wind and wind shear components

having the same energy spectral density for the nominal time interval between passage of the decision altitude and touchdown, one might, on an intuitive basis, expect the two methods to produce similar results.

Here, the second method will be used, but without the refinement suggested in the preceding paragraph. The principal reason for this choice is economy of computation. This is because the second method allows use of the rms quantities already computed (Tables 37 and 40).

The remaining portion of the problem is to convert the longitudinal rms quantities into appropriate statistics for the longitudinal touchdown dispersion. (The lateral-directional touchdown dispersion about the mean is described by a Gaussian probability density function having the rms value for y given in Table 40 because the lateral-directional model of the problem is an entirely linear one.) It has been demonstrated previously in Ref. 1 that the covariance between glide slope deviation response and the airspeed deviations is negligible in comparison to the variance of either of those quantities. Hence glide slope deviation will be the only significant contributor to longitudinal touchdown dispersion.

First consider a simple-minded approach for converting the glide slope deviation statistics into longitudinal touchdown dispersion statistics. This consists of converting the probability density function for glide slope deviation, d, into the probability density function for longitudinal touchdown dispersion about the mean touchdown point. The probability density function for the glide slope deviation from the mean is Gaussian having the rms value for d given in Table 37. The distance, Δx, between the touchdown point and the mean touchdown point can usually be expressed as a continuous single-valued function of d_r the distance in the d-direction of the runway level from the mean trajectory. Let this function be:

$$\Delta x = f(d_r) \tag{48}$$

Three functional relationships for Eq. 48 are implied by the plots in Figs. 21 through 23. Then, if probability density function for the glide slope deviation, d, is

$$\rho(d) = \frac{e^{-d^2/2\sigma_d^2}}{\sqrt{2\pi}\,\sigma_d} \tag{49}$$

it is well known (e.g., Ref. 20) that the probability density function for the touchdown dispersion, Δx, is:

$$\rho(\Delta x) = \rho(d)/f'(d) \tag{50}$$

Since the mean trajectory is nearly a straight path for an altitude of 20 ft or more above the runway level in Figs. 21 through 23, it is convenient to approximate Eq. 48 by a linear equation

$$\Delta x \doteq d_r/\sin(-\gamma_{TD}) \doteq -d_r/\gamma_{TD} \tag{51}$$

where γ_{TD} is the mean flight path angle at touchdown. Equation 50 may then be written:

$$\rho(\Delta x) = \frac{e^{-(\Delta x)^2/2(\sigma_d/-\gamma_{TD})^2}}{\sqrt{2\pi}\,(\sigma_d/-\gamma_{TD})} \tag{52}$$

The effective rms value of touchdown dispersion about the mean is :

$$\sigma_{\Delta x} = \sigma_d/-\gamma_{TD} \tag{53}$$

Values for $\sigma_{\Delta x}$ for the cases examined are given in Table 48

TABLE 48

LONGITUDINAL TOUCHDOWN DISPERSIONS
ABOUT THE MEAN

Case	$\sigma_{\Delta x}$ (ft)
0	61.3
1	51.3
2	61.3
3	54.0

Next, consider justification of this "simple-minded" approach. The point that this approach fails to consider is that a touchdown is defined to occur the first time on any one approach that the joint event of "altitude equal to zero" and "sink rate greater than zero" occur. The simple-minded approach counts as a touchdown only in the event "altitude equal to zero." It turns out, however, that the probability density functions for the event "altitude equal to zero" and for the joint event "altitude equal to zero" and "sink rate greater than zero" are identical when the power spectral densities of altitude perturbation and sink rate perturbation are proper rational functions of frequency as in this problem. This is because the covariance of a zero-mean, Gaussian variable and its first time derivative is zero when both have power spectral densities which are proper rational functions of frequency. This in turn means that the expected value of the sink rate perturbation for any particular given altitude perturbation is zero. In other words, the perturbation sink rate for a given altitude perturbation is equally likely to be positive or negative. It then follows that the probability density functions are the same as stated above.

This means that the only approximation made in this simple-minded approach arises because no distinction is made between the first time and subsequent times that the joint event "altitude equal to zero" and "sink rate greater than zero" might occur for a single ensemble member. Stated another way, the simple-minded approach does not account for the fact that a single trajectory can vary with time about the mean trajectory. It is this property which makes it possible for the joint event to occur more than once for a single ensemble member.

The expected multiplicity in the occurrence of the joint event "altitude equal to zero" and "sink rate greater than zero" can be calculated by extending Rice's static level crossing frequency expression (Ref. 21) for the case of a moving level. The resulting expression for the expected number of occurrences of the joint event per second for a single ensemble member (assuming Eq. 51 holds) is

$$N_{TD} = \frac{\overline{\dot{h}_{abs}}}{\gamma_{TD}} \left[1 - F\left(\frac{\overline{\dot{h}_{abs}}}{\sigma_{\dot{h}}} \right) + \frac{\sigma_{\dot{h}} e^{-(\overline{\dot{h}_{abs}})^2/2\sigma_{\dot{h}}^2}}{\sqrt{2\pi}\,(-\overline{\dot{h}_{abs}})} \right] \times \frac{e^{-(\overline{\dot{h}_{abs}}/\gamma_{TD})^2 (t-t_o)^2/2(\sigma_h/-\gamma_{TD})^2}}{\sqrt{2\pi}\,(\sigma_h/-\gamma_{TD})} \tag{54}$$

where $F(\overline{\dot{h}_{abs}}/\sigma_{\dot{h}})$ is the distribution function

$$F(Z) = \int_{-\infty}^{Z} \frac{e^{-z^2/2}}{\sqrt{2\pi}}\, dz \tag{55}$$

and $\overline{\dot{h}_{abs}}$ and t_o denote values of the respective variables at touchdown for the mean trajectory. If N_{TD} is integrated over all time, the result is the expected number of occurrences of the joint event per ensemble member.

$$\int_{-\infty}^{\infty} N_{TD}\, dt = 1 - F\left(\frac{\overline{\dot{h}_{abs}}}{\sigma_{\dot{h}}} \right) + \frac{\sigma_{\dot{h}} e^{-(\overline{\dot{h}_{abs}})^2/2\sigma_{\dot{h}}^2}}{\sqrt{2\pi}\,(-\overline{\dot{h}_{abs}})} \tag{56}$$

The last two terms in Eq. 56 represent the expected number of second and subsequent occurrences of the joint event per ensemble member when $\overline{\dot{h}_{abs}} \leq 0$ and $\gamma_{TD} \leq 0$. Hopefully the sum of the last two terms will turn out to be very much smaller than unity, indicating that second and subsequent occurrences are so infrequent as to be negligible. This would mean that the approximation in Eq. 52 is an accurate one. The sum of the last two terms in Eq. 56 is given in Table 49. This sum is called the joint event excess fraction. The joint event excess fraction is very small with respect to unity only for Case 3. This is the result of the larger negative value of $(\overline{\dot{h}_{abs}})/\sigma_{\dot{h}}$ ratio for that case. The large value of the ratio indicates relative dominance of the mean sink rate with respect to the stochastic variability in sink rate. (When this ratio is $(-\infty)$ the joint event excess fraction is zero. When the ratio is zero the joint event excess fraction is infinite. In the latter case, Eq. 54 reduces

Revised 16 Feb. 1972

TABLE 49

JOINT EVENT EXCESS FRACTION

Case	Excess Fraction
0	0.127
1	0.099
2	0.127
3	0.020

to Rice's static level crossing expression for the level zero. In the former case, Eq. 54 reduces to an impulsive level crossing rate at time $t = t_o$. These, of course, are the correct limiting case results.)

For Cases 0, 1 and 2, about one-tenth of all the joint events are second or subsequent occurrences of the joint event. This may raise some doubt as to the complete validity of the approximation in Eq. 52 for these cases. While this may be so, the dispersions estimated using this approach may nevertheless be indicative of actual performance in the immediate region about the nominal touchdown point. That this may be so is suggested by the fact that the probability of <u>any</u> occurrence of the joint event outside of the $\pm 2\ \sigma_{\Delta x}$ interval about the nominal touchdown point is only 0.0456. Furthermore, an upper bound upon the probability that a second or subsequent occurrence of the joint event takes place in the interval $|\Delta x| \leq 2\ \sigma_{\Delta x}$ <u>and</u> the first occurrence takes in $\Delta x \leq -2\ \sigma_{\Delta x}$, is 0.0228. This indicates that while the approximate technique employed may not result in the exact probability density function for touchdown dispersion, it does provide the means for obtaining an upper bound on the probability of having an unacceptable deviation on any one landing which is not overly conservative. Furthermore, it appears to provide an accurate approximation to the probability density function for the touchdown dispersion which is not overly distorted by the second and subsequent occurrences of the joint event. That may be so is suggested by the expected wavelength of the stochastic motion about the mean trajectory. This is given by the expression, $2\pi V_{T_o} \sigma_h / \sigma_{\dot{h}}$. The numerical value of the wavelength is 766.4 ft, or approximately 12 $\sigma_{\Delta x}$. This indicates that the probability density function

Revised 16 Feb. 1972

approximation for Δx should be very little distorted by second and subsequent occurrences of the joint event for $|\Delta x| \leq 2\,\sigma_{\Delta x}$.

Still another interesting check upon Eq. 52 is available. If the expression for N_{TD}, Eq. 54, is normalized by dividing through by $\int_{-\infty}^{\infty} N_{TD}dt$ as given in Eq. 56 in order to eliminate the effect of second and subsequent joint event occurrences, and the u degree of freedom is neglected in the relationship between h and d so that

$$\dot{h} = \dot{d}\cos\gamma_o + u\sin\gamma_o \doteq \dot{d} \tag{57}$$

then Eq. 52 is

$$\rho(\Delta x) \doteq \frac{e^{-(\Delta x)^2/2(\sigma_h/-\gamma_{TD})^2}}{\sqrt{2\pi}\,(\sigma_h/-\gamma_{TD})} \tag{58}$$

and Eq. 56 is:

$$\frac{N_{TD}}{\int_{-\infty}^{\infty} N_{TD}dt} = \frac{\overline{\dot{h}_{abs}}}{\gamma_{TD}} \frac{e^{-(\overline{\dot{h}_{abs}}/\gamma_{TD})^2(t-t_o)^2/2(\sigma_h/-\gamma_{TD})^2}}{(\sigma_h/-\gamma_{TD})} \tag{59}$$

Then it turns out that

$$\rho(\Delta x)\frac{d(\Delta x)}{dt} \doteq \frac{N_{TD}}{\int_{-\infty}^{\infty} N_{TD}dt}$$

because

$$(\Delta x) \doteq (\dot{h}_{abs}/\gamma_{TD})(t - t_o) \tag{60}$$

when the u degree of freedom is neglected.

This concludes the summary on analysis of the CH-53A helicopter automatic landing system performance from the decision altitude, through deceleration and flare, to touchdown.

SECTION V

SUMMARY

The investigation reported here had three main facets, all of which addressed the central purpose of developing methods by which requirements for the Air Force Advanced Landing System may be formulated.

The first task of the investigation was to develop a time domain simulation model sufficiently detailed in description of the measuring site, radio beam characteristics, airborne system and aircraft that a broad spectrum of automatic landing system characteristics can be simulated with confidence. The simulation is for the portion of the approach and landing from passage of the decision altitude through flare, decrab, touchdown and rollout. This simulation was exercised using the DC-8 transport aircraft as an example.

The second facet of the investigation was to apply the systems analysis procedure for instrument approach reported in Ref. 1 to a representative STOL vehicle. Application was for the CH-53A single-rotor helicopter operating below the speed for minimum power. The purpose of this example application was to determine if vehicles characterized by high lift curve slope or having direct lift control, placed any unique requirements upon the measuring system. No unique measuring system requirements were discovered for this class of vehicle.

The last facet of the investigation was to develop a procedure for analyzing the approach and landing from passage of the decision altitude through touchdown. The analytical procedure was to be by means other than explicit time domain simulation of the process. This analytical procedure was applied to determine the performance of the CH-53A helicopter in executing an automatic deceleration maneuver and a one-step flare. The analytical procedure consists of dividing the problem into phases each of which can be described by a linear, constant coefficient model. The system responses were then obtained for each phase and superposed in an appropriate manner. A key feature of the procedure was to represent the effects of gross vehicle deviations from trim (e.g., deceleration, flare) by simple approximations for the purpose of determining

the effect of these deviations upon the effective input environment (e.g., wind shear, glide slope deviation command). This, in turn, indicated that further simplifying approximations could be made, without effectively compromising the validity of the results. These latter approximations introduced sufficient simplification into the analytical model that computations could be carried out as routinely as for any servo analysis problem.

A. POSITIVE RESULTS

The time domain simulation results have served to emphasize the importance of a properly designed airborne control system to complement the ground based and airborne components of a measuring system of given characteristics. This is because the likely quality of future measuring systems will be such that the dominant source of glide path errors will be atmospheric disturbances. In particular, close attention must be given to eliminating static errors in regulating the aircraft to the reference glide path by means providing washouts of inner-loop feedback quantities and integrals of outer-loop errors where appropriate. Dynamic errors can often be substantially reduced by combining equivalent feedback signals from two or more sensors in a way which discriminates against the noise contained in each.

The CH -53A helicopter, discussed in Section III of the report, provides an example of the ultimate performance which might be obtained from the combination of a high quality measuring system and an appropriately designed airborne system.

Measuring system requirements for flare guidance are essentially that of requiring two glide slope transmitter sites or one glide slope transmitter plus DME (distance measuring equipment) so that a curved reference trajectory in space may be defined. Use of two glide slope transmitter sites plus DME offers greater flexibility. Use of DME offers ground speed information. This could have been used to very good advantage in improving the performance of the DC-8 and CH-53A systems.

Aircraft having high effective lift curve slope, direct lift control or both (e.g., STOL's) do not place any unique requirements upon the ground-based portion of the measuring system beyond those necessary to accommodate steeper

approach paths. Unique requirements upon the airborne approach coupler, however, can be generated by aircraft having these characteristics.

B. NEGATIVE RESULTS

The principle negative finding is that the technique of representing atmospheric disturbances, and in particular wind shears and stochastic gusts, by a combination of a deterministic wind shear plus the Dryden form stochastic gust model is likely to be inappropriate for landing systems analyses. This is for three reasons.

- There is virtually no evidence that the Dryden form stochastic gust model is representative of turbulence at very low altitudes.
- The landing process takes place in a relatively short space of time. There is, however, no reason to believe that a correspondingly short sample from a stochastic gust time history will have the same statistical properties as the infinite length sample from which it was drawn. In fact, it can be established that it will not.
- Representation of the wind shear by a deterministic model would seem redundant when the Dryden form stochastic gust model is also used. This is because the wind shear is represented statistically in the low frequency portion of Dryden form power spectral density.

The matters of appropriate turbulence models at very low altitudes and of techniques for combining deterministic and stochastic models of atmospheric disturbances are deserving of research attention.

The second negative finding revolves around the multiplicity in the occurrence of the joint event "altitude equal to zero" and "sink rate greater than zero" in the analytical treatment of the landing process. While the arguments in favor of neglecting this have been presented, the practical significance of the typically rather large joint event excess fractions remains to be discovered.

REFERENCES

1. Graham, D., W. F. Clement and L. G. Hofmann, Investigation of Measuring System Requirements for Instrument Low Visibility Approach, AFFDL-TR-70-102, Feb. 1971.

2. Croxton, F. E. and D. J. Cowden, Applied General Statistics, Prentice-Hall, New York, 1939, p. 251.

3. Shah, K. V., W. F. Clement and L. G. Hofmann, User's Manual for Digital Landing Simulation Program, (forthcoming)

4. Anonymous, Microwave Scanning Landing Guidance System (LGS), Radio Technical Commission for Aeronautics Special Committee 117, Paper 189-70/SC117SFDT-27, Sept. 5, 1970.

5. Neuman, F. and J. D. Foster, Investigation of a Digital Automatic Aircraft Landing System in Turbulence, NASA TN D-6066, Oct. 1970.

6. Johnson, W. A. and R. H. Hoh, Determination of ILS Category II Decision Height Window Requirements, Systems Technology, Inc. Tech. Rept. 182-4, Jan. 1971.

7. Anonymous, Automatic Landing Systems, FAA AC No. 20-57, 29 Jan. 1968. (This has been superseded by FAA AC No. 20-57A, 12 Jan. 1971.)

8. Anonymous, DC-8 Flight Manual, United Air Lines, 1 Sept. 1964.

9. Skelton, G. B., Investigation of the Effects of Gusts on V/STOL Craft in Transition and Hover, AFFDL-TR-68-85, Oct. 1968.

10. Anonymous, Military Specification Flying Qualities of Piloted Airplanes, United States Air Force, MIL-F-8785B (ASG), 7 Aug. 1969.

11. Chalk, C. R., T. P. Neal, T. M. Harris, F. E. Pritchard, and R. J. Woodcock, Background Information and User Guide for MIL-F-8785B(ASG), "Military Specification - Flying Qualities of Piloted Airplanes," AFFDL-TR-69-72, Aug. 1969.

12. Carter, E. S., Simulation Information for CH-53A JANAIR Study, letter from Sikorsky Aircraft Division to Systems Technology, Inc., Reference SE-2915, 14 Nov. 1968.

13. Clement, W. F., and L. G. Hofmann, A Systems Analysis of Manual Control Techniques and Display Arrangements for Instrument Landing Approaches in Helicopters, Vol. I: Speed and Height Regulation, Systems Technology, Inc. Tech. Rept. 183-1, July 1969.

14. Personal communication between W. F. Clement and R. Monteleone, Sikorsky, 24 July 1970.

15. Personal communication between L. G. Hofmann and R. Monteleone, Sikorsky, 29 July 1970.

16. Anonymous, Standard Performance Criteria for Autopilot/Coupler Equipment, Paper 31-63/DO-118, Radio Technical Commission for Aeronautics SC-79, Washington, D. C., 14 March 1963.

17. Anonymous, TACLAND/AILS, Approach/Flare Controller, AIL, a division of Cutler-Hammer, Final Rept. No. 8160-1, Jan. 1970.

18. Johnson, W. A., and D. T. McRuer, Development of Category II Approach System Model, Systems Technology, Inc., Tech. Rept. 182-1, Dec. 1969.

19. Systems Technology, Inc., S. O. 198 progress report dated 9 Sept. 1970.

20. Lanning, J. H., R. H. Battin, Random Processes in Automatic Control, McGraw-Hill, 1956.

21. Rice. S. O. "Mathematical Analysis of Random Noise, Part III," Selected Papers on Noise and Stochastic Processes, (N. Wax ed.) Dover, 1954.

Unclassified
Security Classification

DOCUMENT CONTROL DATA - R & D

(Security classification of title, body of abstract and indexing annotation must be entered when the overall report is classified)

1. ORIGINATING ACTIVITY (Corporate author) Systems Technology, Inc. 13766 South Hawthorne Boulevard Hawthorne, California 90250	2a. REPORT SECURITY CLASSIFICATION Unclassified 2b. GROUP NA

3. REPORT TITLE

Investigation of Measuring System Requirements for Instrument Low Visibility Landing

4. DESCRIPTIVE NOTES (Type of report and inclusive dates)

Final, May 1970 to September 1971

5. AUTHOR(S) (First name, middle initial, last name)

Hofmann, Lee Gregor
Clement, Warren F.
Graham, Dunstan
Blodgett, Richard E.
Shah, Kishor V.

6. REPORT DATE December 1971	7a. TOTAL NO. OF PAGES 134	7b. NO. OF REFS 21
8a. CONTRACT OR GRANT NO. F33615-70-C-1621 b. PROJECT NO. 404L c. Work Unit 002 d.	9a. ORIGINATOR'S REPORT NUMBER(S) STI-TR-198-1 9b. OTHER REPORT NO(S) (Any other numbers that may be assigned this report)	

10. DISTRIBUTION STATEMENT

Distribution of this document is unlimited.

11. SUPPLEMENTARY NOTES NA	12. SPONSORING MILITARY ACTIVITY Air Force Flight Dynamics Laboratory Aeronautical System Division Wright-Patterson Air Force Base, Ohio

13. ABSTRACT

Two methods for determining measuring system requirements for instrument low visibility landing are described. These methods have been applied for analysis of two automatic landing systems using microwave scanning beam landing guidance. Results obtained from these analyses are presented and discussed in detail.

The first method is by means of a detailed time domain simulation which includes the airplane, its control system, the guidance system as well as atmospheric wind, windshear and turbulence inputs, and guidance system fluctuation noise. Application of this method is demonstrated with an automatic landing and rollout system and the DC-8 aircraft for the portion of the approach and landing from the Category II-B decision altitude to a ground rolling velocity of less than 50 ft/sec.

The second method is analytical. A linearized description of the measuring system, kinematics, airplane and its control system is used to investigate the influence of the atmospheric wind, and windshear inputs. Stochastic components of system responses arising from atmospheric turbulence inputs and guidance system fluctuation noise are then added to the deterministic responses to complete the model. Application of this method is demonstrated with a high performance automatic landing system and the CH-53A helicopter. The analysis is carried out in two stages. System performance in terms of delivering the aircraft within the approach "window" at the Category II-B decision altitude is first evaluated. Then the approach and landing from the Category II-B decision altitude is evaluated in terms of the touchdown footprint parameters for a decelerating, one-step flare landing maneuver.

DD FORM 1 NOV 65 1473

Unclassified
Security Classification

14. KEY WORDS	LINK A		LINK B		LINK C	
	ROLE	WT	ROLE	WT	ROLE	WT
Low-visibility approach and landing Instrument approach Automatically controlled approach and landing Scanning beam measuring system Radio landing guidance						

☆U.S.Government Printing Office: 1972 — 759-083/445